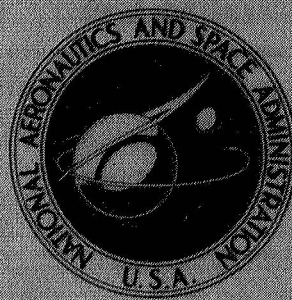


NASA TECHNICAL
MEMORANDUM



NASA TM X-3130

NASA TM X-3130

CASE FILE
COPY

EXPERIMENTAL AERODYNAMIC CHARACTERISTICS
FOR A CYLINDRICAL BODY OF REVOLUTION
WITH SIDE STRAKES AND VARIOUS NOSES
AT ANGLES OF ATTACK FROM 0° TO 58°
AND MACH NUMBERS FROM 0.6 TO 2.0

Leland H. Jorgensen and Edgar R. Nelson

Ames Research Center

Moffett Field, Calif. 94035



1. Report No. TM X-3130		2. Government Accession No.		3. Recipient's Catalog No.	
4. Title and Subtitle EXPERIMENTAL AERODYNAMIC CHARACTERISTICS FOR A CYLINDRICAL BODY OF REVOLUTION WITH SIDE STRAKES AND VARIOUS NOSES AT ANGLES OF ATTACK FROM 0° TO 58° AND MACH NUMBERS FROM 0.6 TO 2.0				5. Report Date March 1975	
				6. Performing Organization Code	
7. Author(s) Leland H. Jorgensen and Edgar R. Nelson				8. Performing Organization Report No. A-5759	
9. Performing Organization Name and Address Ames Research Center, Moffett Field, Calif. 94035				10. Work Unit No. 505-06-81	
				11. Contract or Grant No.	
12. Sponsoring Agency Name and Address National Aeronautics and Space Administration Washington, D. C. 20546				13. Type of Report and Period Covered Technical Memorandum	
				14. Sponsoring Agency Code	
15. Supplementary Notes					
16. Abstract					
<p>For a body of revolution with afterbody side strakes, an experimental investigation was conducted in the Ames 6- by 6-Foot Wind Tunnel to determine the effects on the aerodynamic characteristics of forebody geometry, nose strakes, body side strakes, Reynolds number, Mach number, and angle of attack. Aerodynamic force and moment characteristics were measured for the straked cylindrical afterbody (cylinder fineness ratio of 7) with tangent ogive noses of fineness ratio 2.5 to 5.0. In addition, the straked cylinder afterbody was tested with an ogive nose having a rounded tip and an ogive nose with two different nose strake arrangements.</p> <p>The various configurations were tested at Mach numbers of 0.6, 0.9, 1.2, 1.5, and 2.0 at angles of attack from 0° to 58°. The Reynolds numbers, based on body base diameter, were 2.2×10^5, 4.3×10^5, and 6.5×10^5 at $M = 0.6$ and 0.9 and 3.8×10^5 at $M = 1.2, 1.5, \text{ and } 2.0$.</p> <p>The data demonstrate that the aerodynamic characteristics for a body of revolution with side strakes can be significantly affected by changes in nose fineness ratio, nose bluntness, Reynolds number, Mach number, and, of course, angle of attack. Removing the strakes from the cylindrical aftersection greatly decreased the lift, but this removal hardly changed the maximum magnitudes of the undesirable side forces that developed at angles of attack greater than about 25° for subsonic Mach numbers.</p>					
17. Key Words (Suggested by Author(s)) High angle-of-attack aerodynamics Body of revolution Body strakes Nose fineness ratio Nose strakes			18. Distribution Statement Unclassified — Unlimited STAR Category — 02		
19. Security Classif. (of this report) Unclassified		20. Security Classif. (of this page) Unclassified		21. No. of Pages 89	22. Price* \$4.75

NOMENCLATURE

All forces and moments are referred to the body axis coordinate system. Because the data are computer plotted, both the conventional symbol and the plot symbol are given.

<u>Symbol</u>	<u>Plot Symbol</u>	<u>Definition</u>
A_r		reference area = body base area = 34.26 cm ² (5.31 in. ²)
C_A	CA	axial-force coefficient, $C_{A_{bal}} - C_{A_{base}}$
$C_{A_{bal}}$		balance axial-force coefficient, $\frac{F_A}{qA_r}$
$C_{A_{base}}$		base-pressure force coefficient, $\frac{(p - p_{base})}{q}$
C_m		pitching-moment coefficient about balance center 4d from body base, $\frac{\text{pitching moment}}{qA_r X}$
C_N	CN	normal-force coefficient, $\frac{F_N}{qA_r}$
C_n	CYN	yawing-moment coefficient about balance center 4d from body base, $\frac{\text{yawing moment}}{qA_r X}$
C_Y	CY	side-force coefficient, $\frac{F_Y}{qA_r}$
d		body base diameter = 6.60 cm (2.60 in.)
F_A, F_N, F_Y		axial, normal, and side force, respectively
l_N		nose length
M	MACH	free-stream Mach number
p		free-stream static pressure
p_{base}		base pressure

q		free-stream dynamic pressure
$\frac{Re}{L}$		unit Reynolds number, million/m
Re	RE	Reynolds number based on d
X		reference length = $d = 6.60$ m (2.60 in.)
$\frac{x_{acN}}{d}$	XACN/D	distance (in diameters) from body base to aerodynamic force center in normal-force plane, $\left(\frac{C_m}{C_N} + \frac{x_m}{X}\right)$
x_m		distance from body base to balance moment reference = $4d = 26.42$ cm (10.40 in.)
α	ALPHA	angle of attack, deg

Configuration Code

<u>Symbol</u>	<u>Plot Symbol</u>	<u>Component</u>	<u>Fineness Ratio</u>
C_1	C1	circular cylinder	7
N_1	N1	tangent ogive nose	3
N_2	N2	tangent ogive nose	3.5
N_3	N3	tangent ogive nose	5
N_4	N4	tangent ogive nose with rounded tip	3
N_5	N5	tangent ogive nose with tip strakes	3
N_6	N6	tangent ogive nose with side strakes	3
N_7	N7	tangent ogive nose	2.5
S	S	side strakes on circular cylinder	

EXPERIMENTAL AERODYNAMIC CHARACTERISTICS FOR A CYLINDRICAL BODY
OF REVOLUTION WITH SIDE STRAKES AND VARIOUS NOSES AT ANGLES
OF ATTACK FROM 0° TO 58° AND MACH NUMBERS FROM 0.6 TO 2.0

Leland H. Jorgensen and Edgar R. Nelson*

Ames Research Center

SUMMARY

For a body of revolution with afterbody side strakes, an experimental investigation was conducted in the Ames 6-by 6-Foot Wind Tunnel to determine the effects on the aerodynamic characteristics of forebody geometry, nose strakes, body side strakes, Reynolds number, Mach number, and angle of attack. Aerodynamic force and moment characteristics were measured for the straked cylindrical afterbody (cylinder fineness ratio of 7) with tangent ogive noses of fineness ratio 2.5 to 5.0. In addition, the straked cylinder afterbody was tested with an ogive nose having a rounded tip and an ogive nose with two different nose strake arrangements.

The various configurations were tested at Mach numbers of 0.6, 0.9, 1.2, 1.5, and 2.0 at angles of attack from 0° to 58°. The Reynolds numbers, based on body base diameter, were 2.2×10^5 , 4.3×10^5 , and 6.5×10^5 at $M = 0.6$ and 0.9 and 3.8×10^5 at $M = 1.2, 1.5, \text{ and } 2.0$.

The data demonstrate that the aerodynamic characteristics for a body of revolution with side strakes can be significantly affected by changes in nose fineness ratio, nose bluntness, Reynolds number, Mach number, and, of course, angle of attack. Removing the strakes from the cylindrical aftersection greatly decreased the lift, but this removal hardly changed the maximum magnitudes of the undesirable side forces that developed at angles of attack greater than about 25° for subsonic Mach numbers.

INTRODUCTION

High angle-of-attack aerodynamics is increasing in importance because of the demand for greater maneuverability of missiles and aircraft (both manned and remotely piloted). Some recent introductory investigations in this field are reported in references 1 to 9. Presently, however, there is great need to enlarge the relatively small data base for basic bodies alone and in combination with strakes, wings, and tails at subsonic, transonic, and supersonic Mach numbers.

To help fill this need, an investigation has been conducted to measure the aerodynamic force and moment characteristics for a cylindrical body of revolution (cylinder fineness ratio of 7) with side strakes and with tangent ogive noses of fineness ratio 2.5 to 5.0. In addition, the cylindrical

*Project engineer, ARO, Inc., Moffett Field, Calif. 94035.

body with strakes has been tested with an ogive nose having a rounded tip and an ogive nose with two different strake arrangements. In reference 8, similar tests were made with no strakes mounted on the cylindrical body.

In both investigations, the cylindrical body was tested with the various noses in the Ames 6- by 6-Foot Wind Tunnel at Mach numbers of 0.6, 0.9, 1.2, 1.5, and 2.0. The Reynolds numbers, based on model base diameter, were 2.2×10^5 , 4.3×10^5 , and 6.5×10^5 at the subsonic Mach numbers and 3.8×10^5 at the supersonic Mach numbers. Six-component static aerodynamic force and moment coefficients were measured for angles of attack from 0° to 58° .

This report presents the basic data that show the effects on the aerodynamic characteristics of nose fineness ratio, nose tip rounding, nose strakes, Reynolds number, and Mach number over the angle-of-attack range. In addition, the effect of removing the strakes from the cylindrical afterbody is illustrated with the aid of comparative data from reference 8 for the body without strakes.

TEST FACILITY

The experimental investigation was conducted in the Ames 6- by 6-Foot Wind Tunnel – a variable pressure, continuous flow, closed-return type facility. The nozzle ahead of the test section consists of an asymmetric sliding block that permits the Mach number to be continuously varied from 0.6 to 2.3. The test section has a perforated floor and ceiling so that the boundary layer can be removed for transonic testing.

MODELS AND BALANCE

Figure 1 shows the model components. All models tested consisted of a combination of one of the seven noses with the circular-cylinder aftersection. The cylinder aftersection (C_1) was 7 diameters long and had small side strakes (S) extending along the entire length. Noses N_1 , N_2 , N_3 , and N_7 were all circular-arc tangent ogives from 2.5 to 5 diameters long. Noses N_4 , N_5 , and N_6 were also circular-arc tangent ogives but with some modifications. N_4 was formed by rounding the tip of a fineness-ratio 3.5 ogive to give a resulting fineness ratio of 3. N_5 was a fineness-ratio-3 ogive with side strakes near the tip, and N_6 was a similar ogive but with side strakes extending over the entire nose length.

All model parts were constructed of stainless steel, and the models were sting mounted through the base on a six-component, strain-gage "Task" balance. The balance force center was located inside the cylindrical body 4 diameters forward of the base.

Figure 2 shows planform views of the configurations tested. The planform views of the same configurations without side strakes along the cylinder are also shown for comparison. Results for these configurations are reported in reference 8. All configurations tested are identified by the code shown in figure 2.

TESTS AND DATA REDUCTION

All configuration arrangements shown in figure 2 were tested at $\alpha = 0^\circ$ to about 58° . Two model support setups were used — one for $\alpha = 0^\circ$ to about 27° and the other for $\alpha = 27^\circ$ to 58° . Photographs of these setups are shown in reference 8. The models were tested at the following Mach numbers and Reynolds numbers:

<u>M</u>	<u>$Re \times 10^{-6}$ (m)</u>	<u>$Re \times 10^{-6}$ (ft)</u>	<u>$Re \times 10^{-5}$ (based on d)</u>
0.6, 0.9	3.28	1.0	2.2
0.6, 0.9	6.56	2.0	4.3
0.6, 0.9	9.84	3.0	6.5
1.2, 1.5, 2.0	5.74	1.75	3.8

Six-component aerodynamic force and moment data were measured at each test condition, and all data were reduced to coefficient form and referred to the body axis coordinate system. The average base pressure from four base pressure tubes (at the sides, top, and bottom of the base) was used to compute the base drag, which was subtracted from the total axial-force balance measurements, so that the data presented are for forces ahead of the body base. Rolling-moment coefficients were generally negligible and are omitted. Normal-force aerodynamic centers were computed from the normal-force and pitching-moment coefficients and are presented in lieu of the pitching-moment coefficients.

RESULTS AND DISCUSSION

Experimental results (figs. 3–27) show the effects on the aerodynamic characteristics of nose fineness ratio, nose tip rounding, nose strakes, removal of strakes from the cylindrical afterbody, Reynolds number, and Mach number. Each effect is discussed briefly with the aid of plots of C_N , x_{acN}/d , C_Y , C_Y/C_N , and C_n versus α for $\alpha = 0^\circ$ to 60° . Plots of C_A versus α are also presented but are not discussed. Because the models were sting supported from the rear, it is likely that the C_A data include effects of support interference.

Effect of Nose Fineness Ratio

Data that show the effect of nose fineness ratio on the aerodynamic characteristics are presented in figures 3 through 7 for $M = 0.6$ to 2.0. The data are for the highest test Reynolds numbers — $Re = 6.5 \times 10^5$ at $M = 0.6$ and 0.9 (figs. 3 and 4) and $Re = 3.8 \times 10^5$ at $M = 1.2, 1.5,$ and 2.0 (figs. 5–7). Comparisons are made for the cylinder (C_1) with side strakes (S) and noses ($N_1, N_2, N_3,$ and N_7) of fineness ratio 3, 3.5, 5, and 2.5, respectively.

An increase in the nose fineness ratio from 2.5 to 5.0 can change the aerodynamic characteristics significantly. As expected, normal-force coefficient generally increases with increase in nose fineness ratio at all Mach numbers, and the aerodynamic force center in the normal-force plane

moves forward. However, at some angles of attack, the changes are negligible, especially at subsonic Mach numbers.

Probably the most interesting result is the effect of nose fineness ratio on the development of side force and yawing moment with an increase in α above about 25° . At $M = 0.6$ and 0.9 (figs. 3 and 4), the side-force and yawing-moment coefficients become rather large for the straked cylinder with the fineness ratio 3.5 and 5.0 noses (configurations N_2C_1S and N_3C_1S). In fact, for some angles of attack, the side forces become as large as about 30 percent of the normal forces (see plots of C_Y/C_N vs. α). When the nose fineness ratio is 3.0 or less (configurations N_1C_1S and N_7C_1S), the side-force and yawing-moment coefficients become essentially zero throughout the α range. In reference 8, similar results are shown for these configurations without the side strakes on the cylindrical afterbody. This side-force phenomenon appears to be associated primarily with subsonic flow. The side-force and yawing-moment coefficients are small at $M = 1.2$ (fig. 5) and completely disappear at $M = 1.5$ (fig. 6) and $M = 2.0$ (fig. 7).

Based on the results from this investigation and from other studies (e.g., refs. 1, 2, 7-9), two conclusions are evident. First, the magnitudes of the maximum side-force and yawing-moment coefficients generally increase with an increase in the nose fineness ratio. Second, the magnitudes appear to decrease with an increase in Mach number up to about $M = 1.2$.

Effect of Nose Tip Rounding

In figures 8 through 12, data are presented for the straked cylinder (C_1S) with the fineness ratio 3.5 ogive nose (N_2) and with the fineness ratio 3.5 ogive nose whose tip was cut back by rounding to give a nose fineness ratio of 3 (N_4). Data for the straked cylinder (C_1S) combined with the fineness ratio 3 sharp ogive nose (N_1) are also shown for comparison.

The effect of nose tip rounding on the variation of C_N and x_{acN}/d with α is generally small at all Mach numbers investigated. The tip rounding is beneficial, however, in decreasing the side-force and yawing moment coefficients that appear at $M = 0.6$ and 0.9 for $\alpha > 25^\circ$. At $M = 0.6$ (fig. 8), the initial development of side force is at a higher α for the blunt nose than for the sharp (cf. C_Y vs. α results for N_4C_1S and N_2C_1S).

Although nose blunting by rounding the tip appears beneficial in reducing side force, decreasing the nose fineness ratio can be even more beneficial in this case. As shown in figures 8 and 9, the side-force and yawing-moment coefficients are smaller for the configuration (N_1C_1S) with the sharp-nosed ogive of fineness ratio 3 than for the configuration (N_4C_1S) with the blunted nose of the same resulting fineness ratio. A similar result is reported in reference 8 for these configurations without the cylinder side strakes.

Effect of Nose Strakes

In figures 13 through 17, data are presented that show the effect of nose strakes on the aerodynamic characteristics. Data are compared for the straked cylinder (C_1S) combined with the fineness ratio 3 ogive nose (N_1) and the straked cylinder combined with the fineness ratio 3 noses with tip and side strakes (N_5 and N_6).

As expected, the nose strakes provide some additional normal force and move the aerodynamic force centers forward. The configuration with the nose strakes extending over the nose length (N_6C_1S) appears to resist the development of side force and yawing moment best at the high angles of attack (see fig. 13). However, for all configurations compared, the side-force and yawing-moment coefficients are small at $M = 0.6$ and essentially zero at the higher Mach numbers. Unfortunately, the nose strakes were not investigated for the body with the fineness ratio 5 nose, the nose that developed the largest side forces.

Effect of Removing Strakes From Cylindrical Afterbody

In figures 18 through 22, data are presented that show the effect on the aerodynamic characteristics of removing the strakes from the sides of the cylindrical afterbody. Results for the straked cylinder with the fineness ratio 5 nose (configuration N_3C_1S) are compared with results for the same configuration without the strakes (N_3C_1). Also, results for the straked cylinder with the fineness ratio 3 nose with tip strakes (N_5C_1S) are compared with results for this configuration without the cylinder strakes (N_5C_1).

As expected, removing the side strakes greatly reduces the normal force and moves the aerodynamic force center forward at all test conditions. Removing the strakes might also be expected to increase the magnitudes of the undesirable side forces and yawing moments that develop at high angles of attack. However, as shown in figure 18 for $M = 0.6$, removing the strakes from configurations N_3C_1S and N_5C_1S resulted in only little change in the maximum magnitudes of C_Y (CY) and C_N (CYN), although the variations of C_Y with α were changed. It thus appears that controlling undesirable side forces and yawing moments at high α might best be accomplished by changing the nose shape (probably by blunting the nose or reducing the fineness ratio as previously discussed).

Effect of Reynolds Number

In figures 23 through 26, the data presented show the effect of Reynolds number for configurations N_1C_1S and N_3C_1S . The Reynolds numbers are 2.2×10^5 , 4.3×10^5 , and 6.5×10^5 based on body base diameter.

For both configurations, there is no significant effect of Reynolds number on the variation of C_N and x_{acN}/d with α at any of the Mach numbers considered. This result is in opposition to the result reported in reference 8 for the same bodies without side strakes at $M = 0.6$. In reference 8, the same increase in Reynolds number from 2.2×10^5 to 6.5×10^5 was accompanied by a decrease in C_N at the higher values of α . Apparently, the crossflow for a body without side strakes is more sensitive to Reynolds number than the crossflow for a body with side strakes.

As for the bodies without side strakes, the effect of Reynolds number on side-force and yawing-moment coefficients appears to be significant only for the configuration (N_3C_1S) with the high fineness ratio nose ($l_N/d = 5$) at $M = 0.6$ (fig. 25). The values of side force relative to normal force (C_Y/C_N) generally decrease with increase in Reynolds number, but there is little effect on the variation of C_N with α .

Effect of Mach Number

In figure 27, the data presented show the effect of Mach number on the aerodynamic characteristics for configuration N_3C_1S (the fineness ratio 5 ogive nose attached to the straked cylinder). For $M = 0.6$ and 0.9 , the Reynolds number is 6.5×10^5 , and for $M = 1.2, 1.5,$ and 2.0 , the Reynolds number is 3.8×10^5 .

The plots of C_Y (CY) and C_n (CYN) as a function of α clearly demonstrate that the side forces, which develop above $\alpha \approx 25^\circ$, are largest at the lowest Mach number, $M = 0.6$. The side forces diminish considerably with an increase in Mach number to $M = 1.2$ and disappear at the higher supersonic Mach numbers.

At the subsonic Mach numbers, the side forces become as large as 25 percent of the normal forces. Similar results are reported in reference 8 for the same configuration without the side strakes.

CONCLUSIONS

1. An increase in nose fineness ratio caused significant changes in the aerodynamic characteristics. Normal-force coefficient generally increased, and the aerodynamic normal-force center moved forward. For noses of fineness ratio greater than 3, large side-force and yawing-moment coefficients developed at subsonic Mach numbers for angles of attack above about 25° .
2. The large side-force and yawing-moment coefficients that developed at subsonic Mach numbers greatly decreased with increase in Mach number to $M = 1.2$ and disappeared at $M = 1.5$ and 2.0 .
3. Nose-tip rounding of a fineness ratio 3.5 ogive nose decreased the side-force and yawing-moment coefficients for the straked body at subsonic Mach numbers. However, the beneficial decrease was not as large as that obtained by merely using a sharp-nosed ogive of the same fineness ratio (fineness ratio 3) as that for the resulting blunted nose.
4. Nose strakes provided some additional normal force and moved the aerodynamic force centers forward. They provided little or no changes to the side forces and yawing moments for the body with the fineness ratio 3 nose. (Unfortunately, they were not investigated for the body with the fineness ratio 5 nose, the nose that developed the largest side forces.)
5. Removing the strakes from the sides of the cylindrical afterbody resulted in little change in the maximum magnitudes of the undesirable side forces and yawing moments that developed at α greater than about 25° . The distribution of C_Y with α , however, was considerably changed.
6. Reynolds number change from 2.2×10^5 to 6.5×10^5 had no significant effect on the variation of normal-force coefficient and aerodynamic center with angle of attack. The effect of

Reynolds number on the side-force and yawing-moment coefficients was significant only for the configuration with the fineness ratio 5 nose at the lowest Mach number, $M = 0.6$.

Ames Research Center
National Aeronautics and Space Administration
Moffett Field, California, September 26, 1974

REFERENCES

1. Pick, George S.: Side Forces on Ogive-Cylinder Bodies at High Angles of Attack in Transonic Flow. *J. Spacecraft and Rockets*, vol. 9, no. 6, pp. 389–390, June 1972.
2. Clark, William H.; Peoples, John R.; and Briggs, M. Michael: Occurrence and Inhibition of Large Yawing Moments During High Incidence Flight of Slender Missile Configurations. *AIAA Paper 72-968*, 1972.
3. Coe, Paul L., Jr.; Chambers, Joseph R.; and Letko, William: Asymmetric Lateral-Directional Characteristics of Pointed Bodies of Revolution at High Angles of Attack. *NASA TN D-7095*, 1972.
4. Jorgensen, Leland H.: Prediction of Static Aerodynamic Characteristics for Space-Shuttle-Like and Other Bodies at Angles of Attack From 0° to 180° . *NASA TN D-6996*, 1973.
5. Jorgensen, Leland H.: Estimation of Aerodynamics for Slender Bodies Alone and With Lifting Surfaces at α 's From 0° to 90° . *AIAA Journal*, vol. II, no. 3, pp. 409–412, March 1973.
6. Jorgensen, Leland H.: A Method for Estimating Static Aerodynamic Characteristics for Slender Bodies of Circular and Noncircular Cross Section Alone and With Lifting Surfaces at Angles of Attack from 0° to 90° . *NASA TN D-7228*, 1973.
7. Fleeman, E. L.; and Nelson, R. C.: Aerodynamic Forces and Moments on a Slender Body With a Jet Plume for Angles of Attack Up to 180 Degrees. *AIAA Paper 74-110*, 1974.
8. Jorgensen, Leland H.; and Nelson, Edgar R.: Experimental Aerodynamic Characteristics for a Cylindrical Body of Revolution With Various Noses at Angles of Attack From 0° to 58° and Mach Numbers From 0.6 to 2.0. *NASA TM X-3128*, 1974.
9. Keener, Earl R.; and Chapman, Gary T.: Onset of Aerodynamic Side Forces at Zero Sideslip on Symmetric Forebodies at High Angles of Attack. *AIAA Paper 74-770*, 1974.

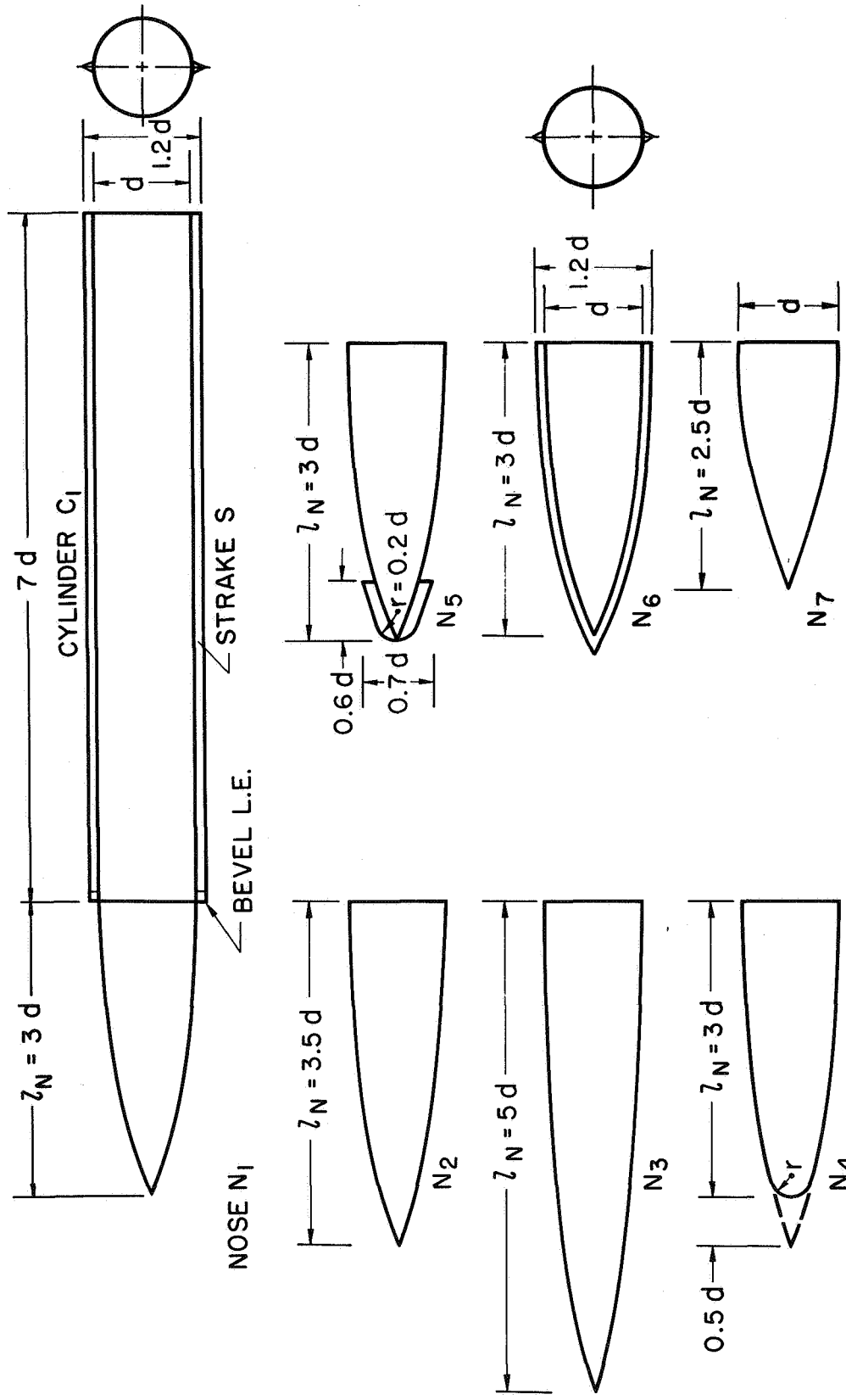
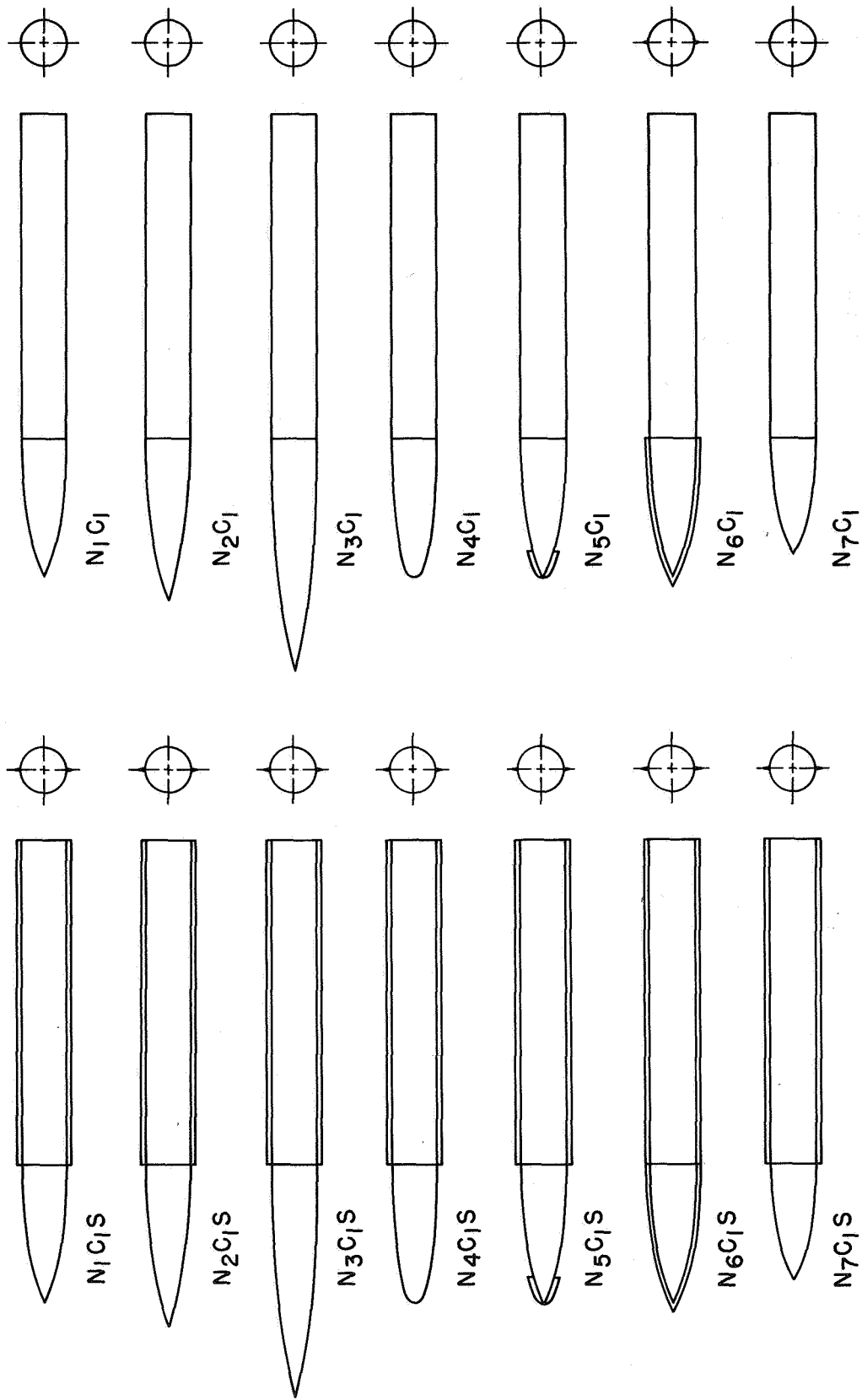


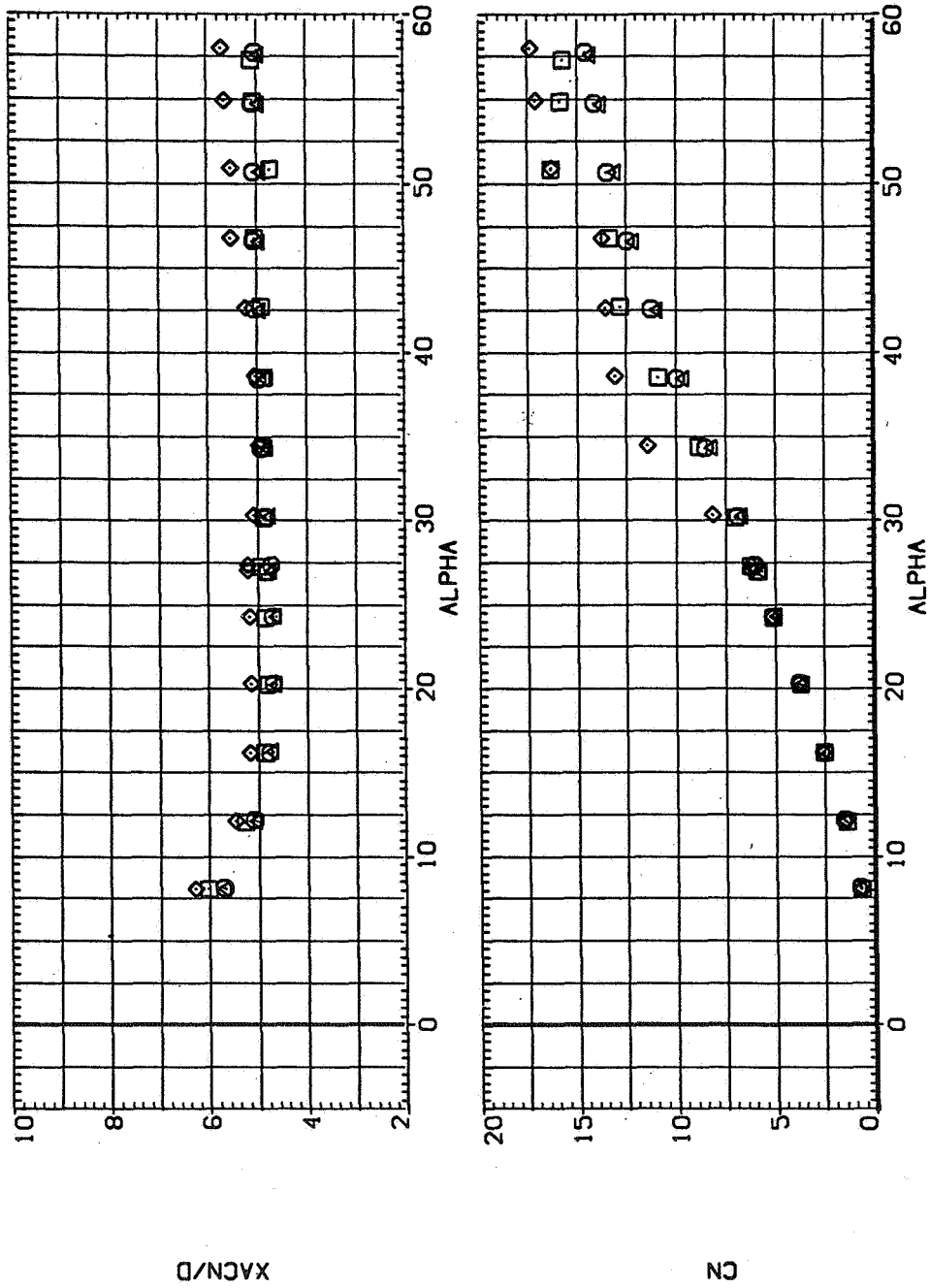
Figure 1.— Model components, $d = 6.6$ cm (2.60 in.).



(a) Configurations for present report. (b) Configurations for reference 8.

Figure 2.— Planform views of configurations tested.

SYMBOL CONFIGURATION DESCRIPTION
 N1 C1 S
 N2 C1 S
 N3 C1 S
 N7 C1 S

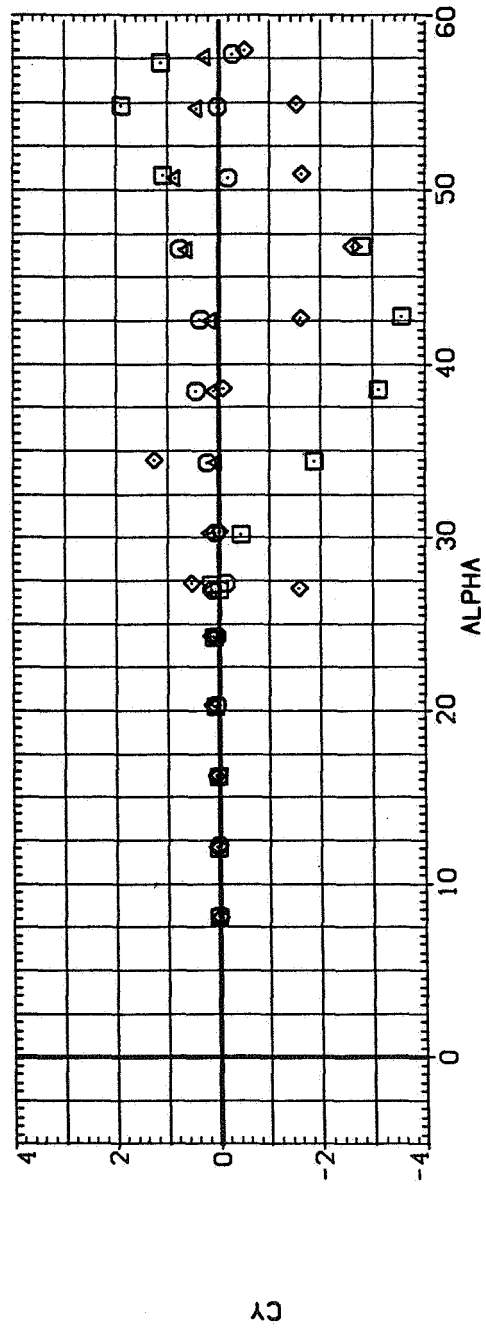
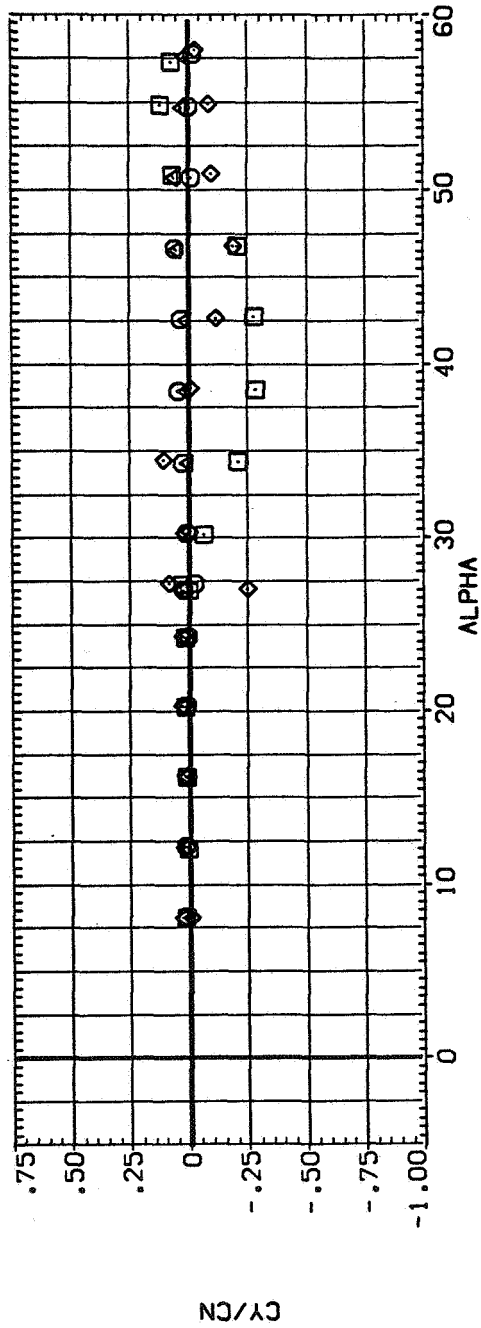


(a) x_{acN}/d and C_N versus α .

Figure 3.— Effect of nose fineness ratio; $M = 0.6$, $Re = 6.5 \times 10^5$.

SYMBOL CONFIGURATION DESCRIPTION

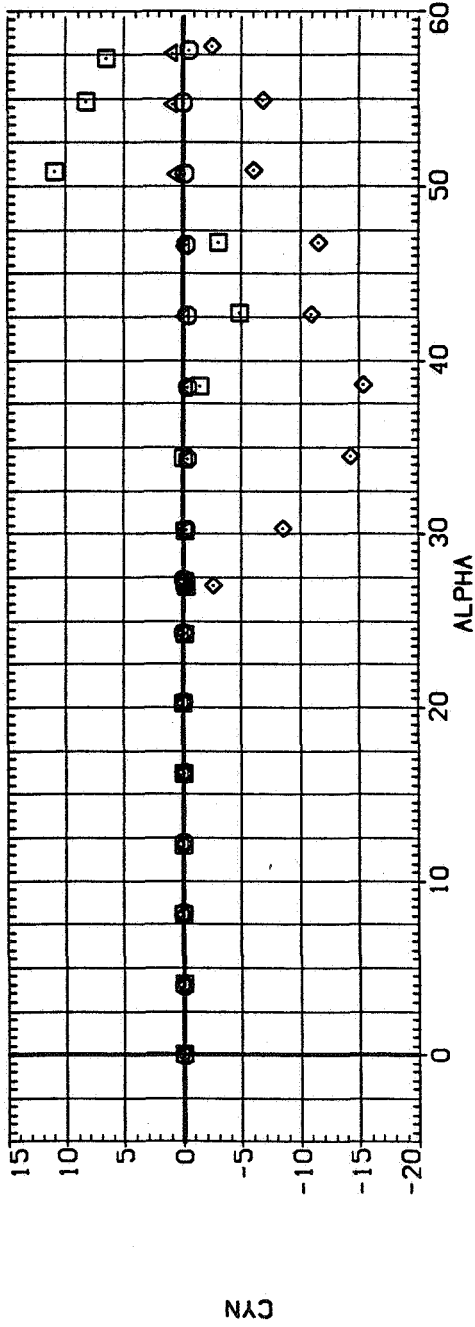
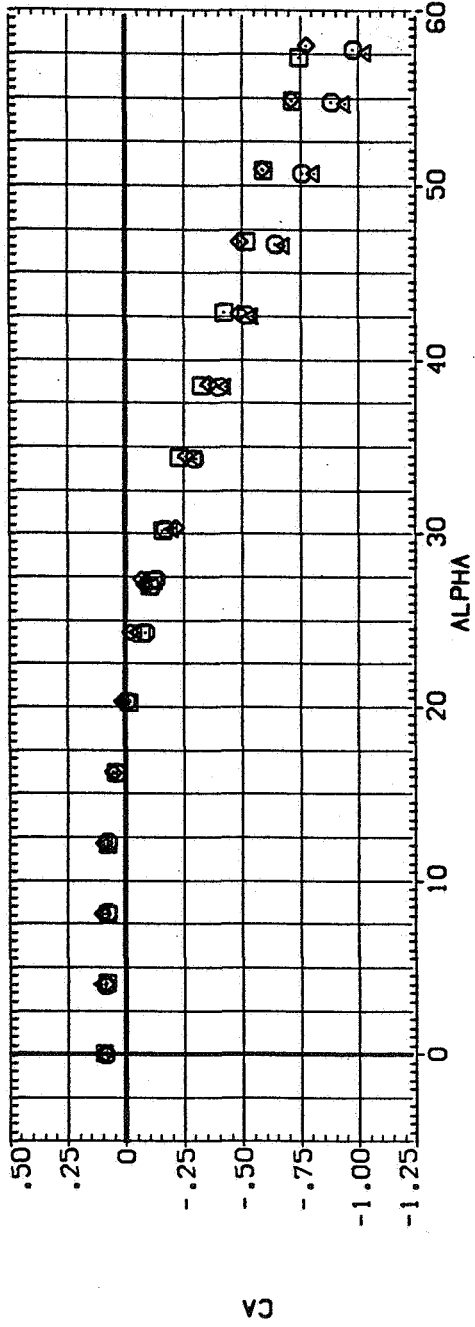
\square N1 C1 S1 S1 S
 \circ N2 C1 S1 S1 S
 \diamond N3 C1 S1 S1 S
 \times N7 C1 S1 S



(b) CY/CN and CY versus α .

Figure 3.— Continued.

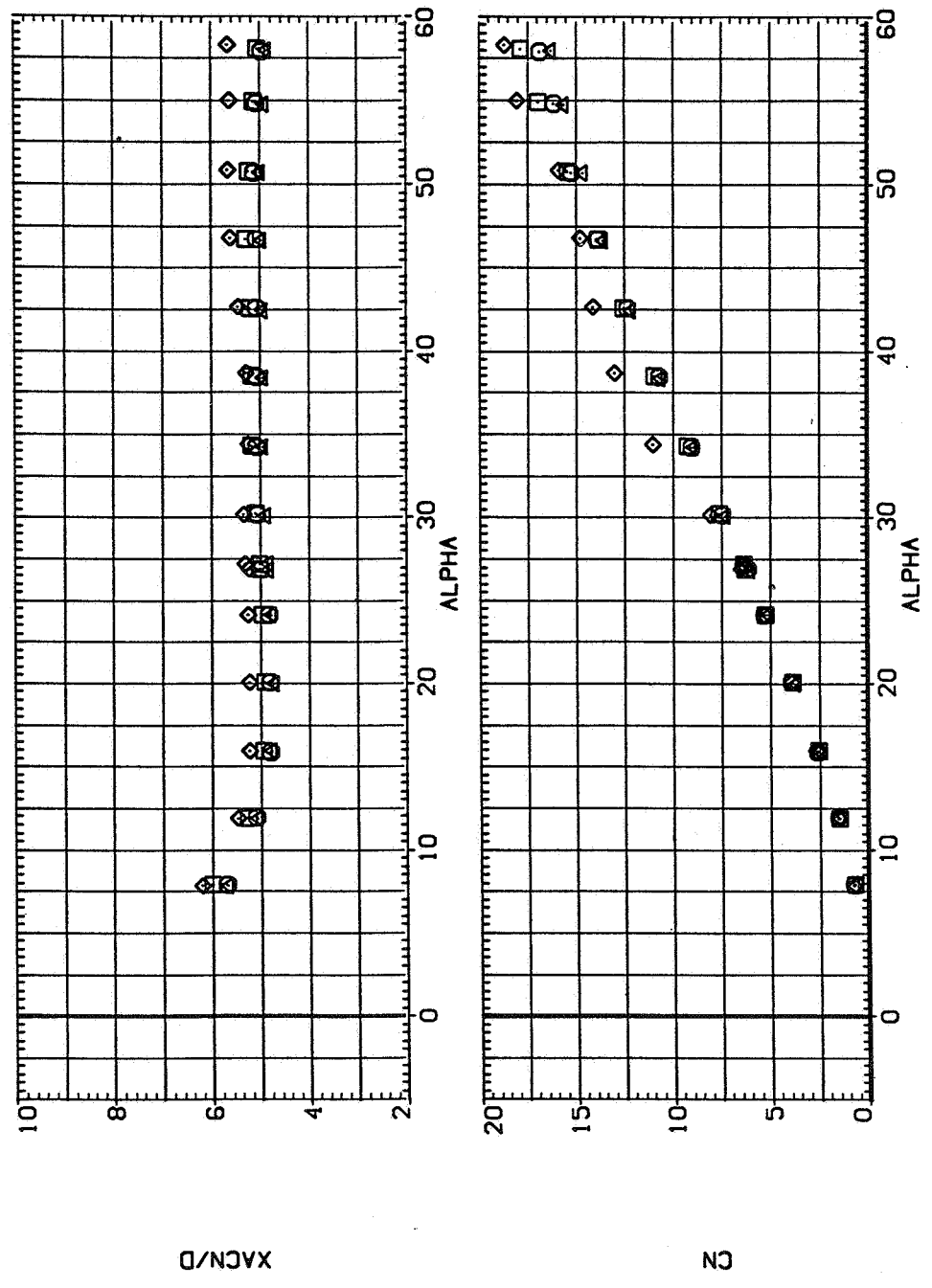
SYMBOL CONFIGURATION DESCRIPTION
 NI CI S
 NI CI S
 NI CI S
 NI CI S



(c) C_A and C_{η} versus α .

Figure 3.— Concluded.

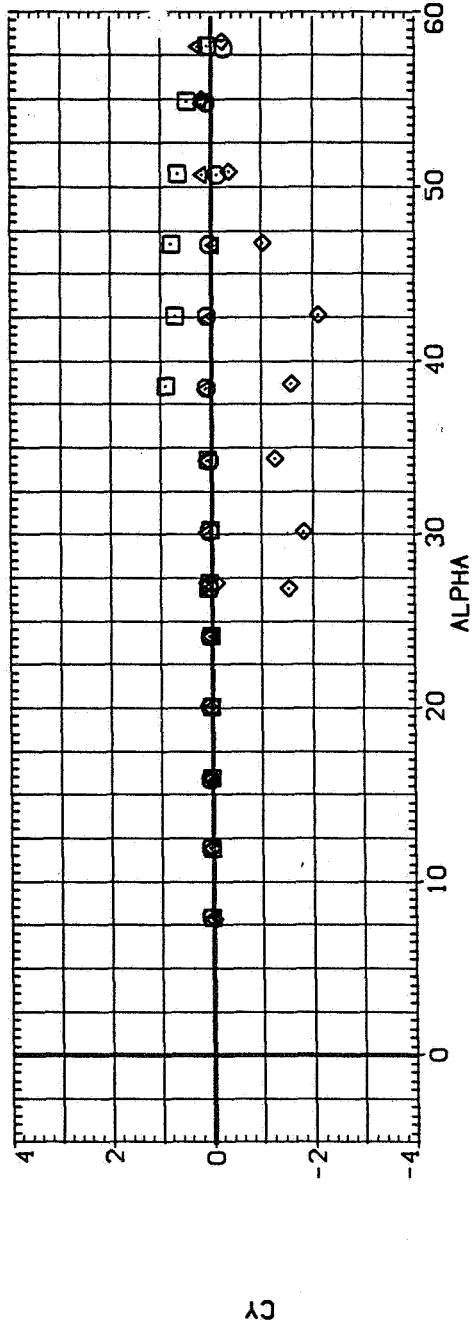
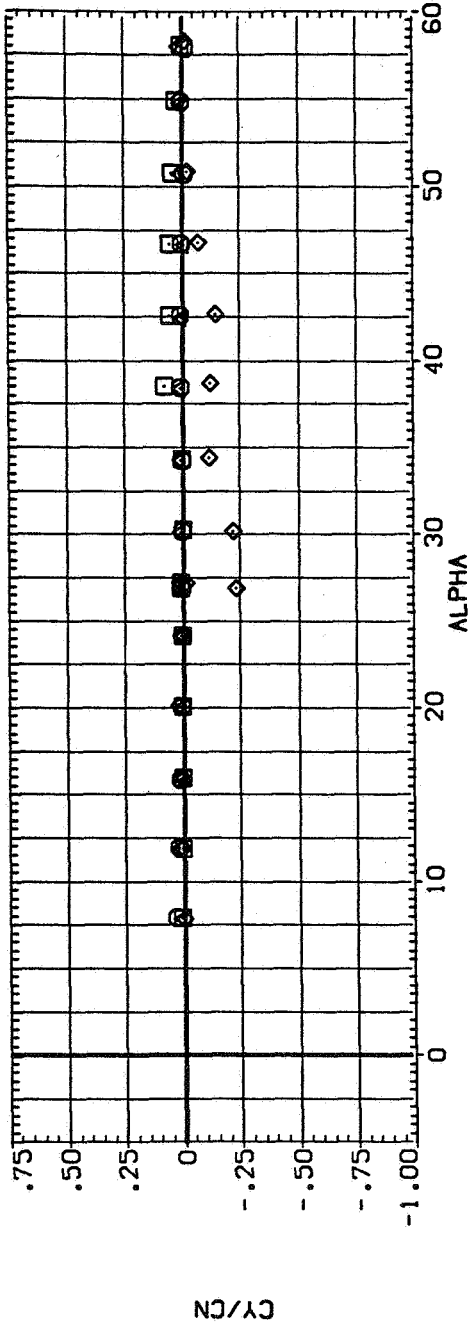
SYMBOL CONFIGURATION DESCRIPTION
 N1 C1 S
 N2 C1 S
 N3 C1 S
 N7 C1 S
 □ X



(a) x_{acN}/d and C_N versus α .

Figure 4.— Effect of nose fineness ratio; $M = 0.9$, $Re = 6.5 \times 10^5$.

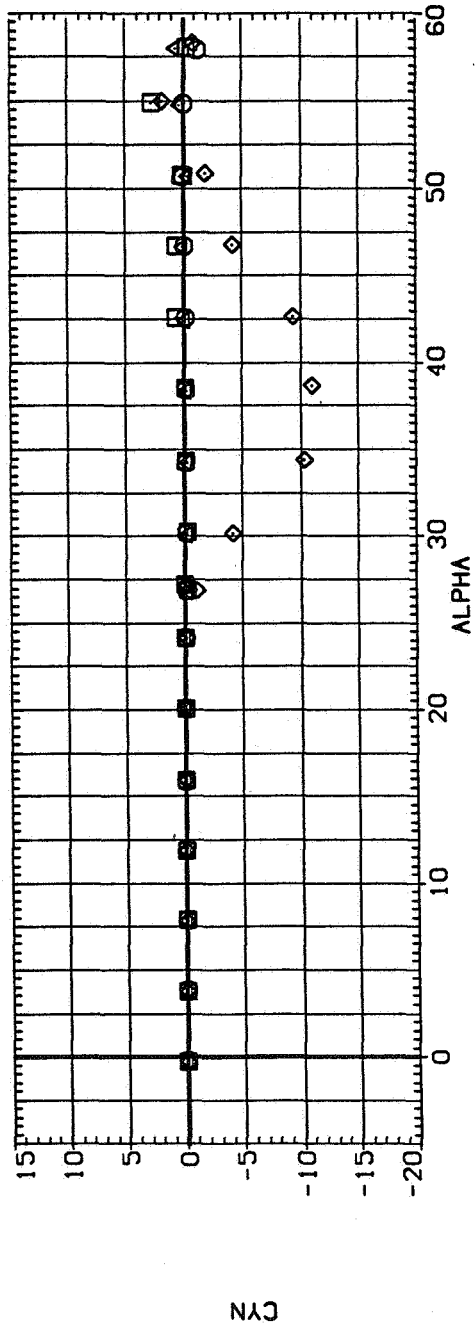
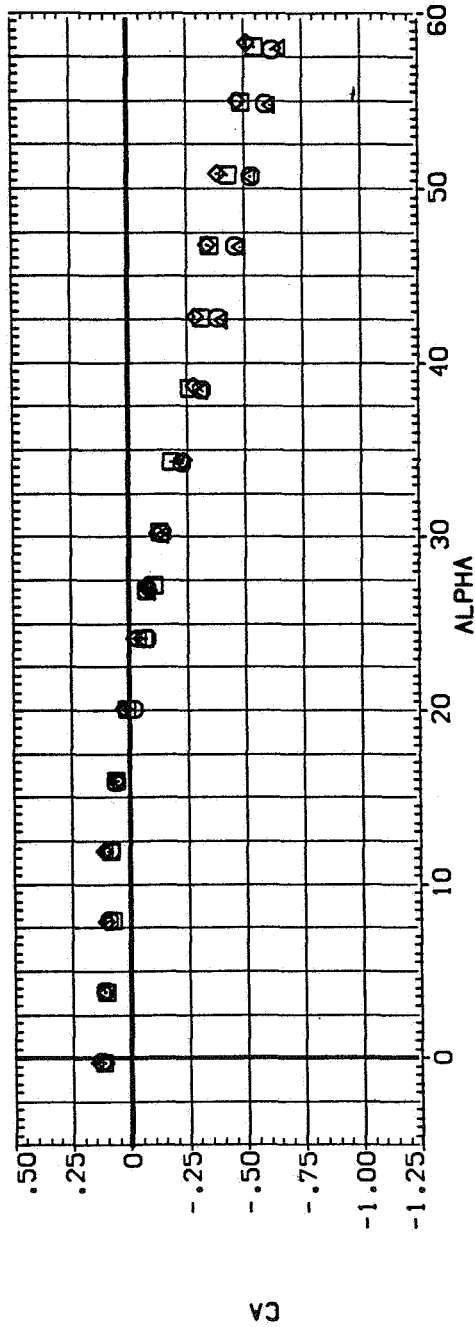
SYMBOL CONFIGURATION DESCRIPTION
 □ N1 C1 S
 ○ N2 C1 S
 △ N3 C1 S
 ◇ N7



(b) C_Y/C_N and C_Y versus α .

Figure 4.-- Continued.

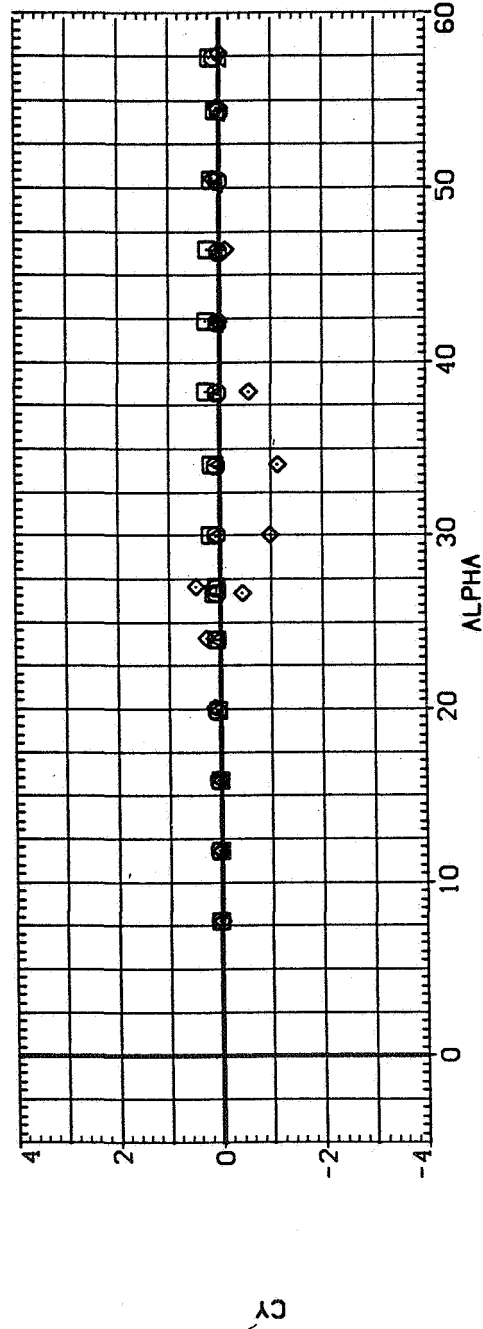
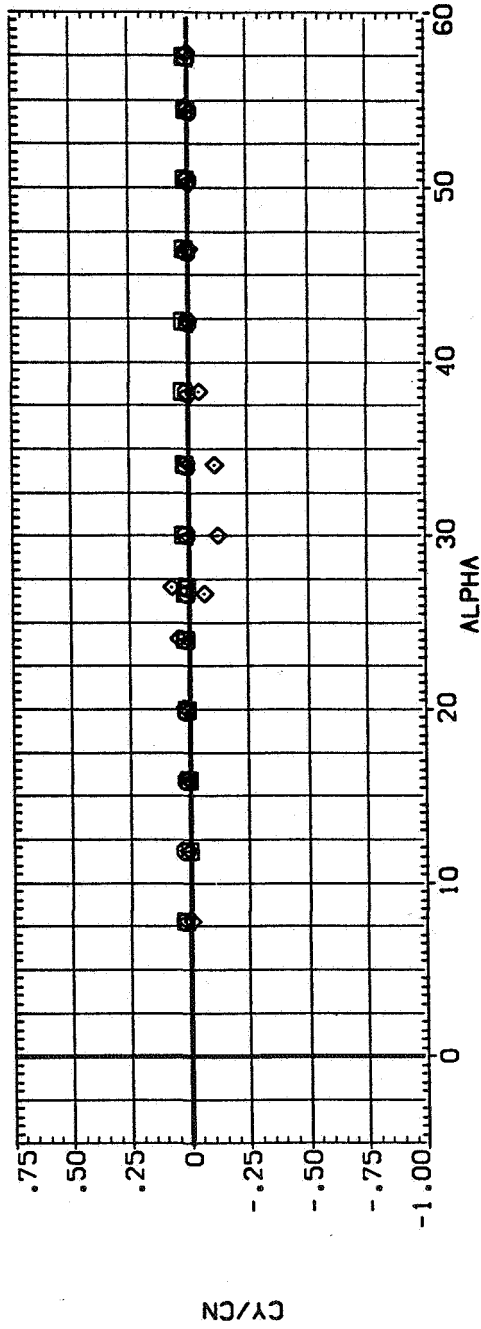
SYMBOL CONFIGURATION DESCRIPTION
 N1 C1 S
 N2 C1 S
 N3 C1 S
 N7 C1 S



(c) C_A and C_n versus α .

Figure 4.- Concluded.

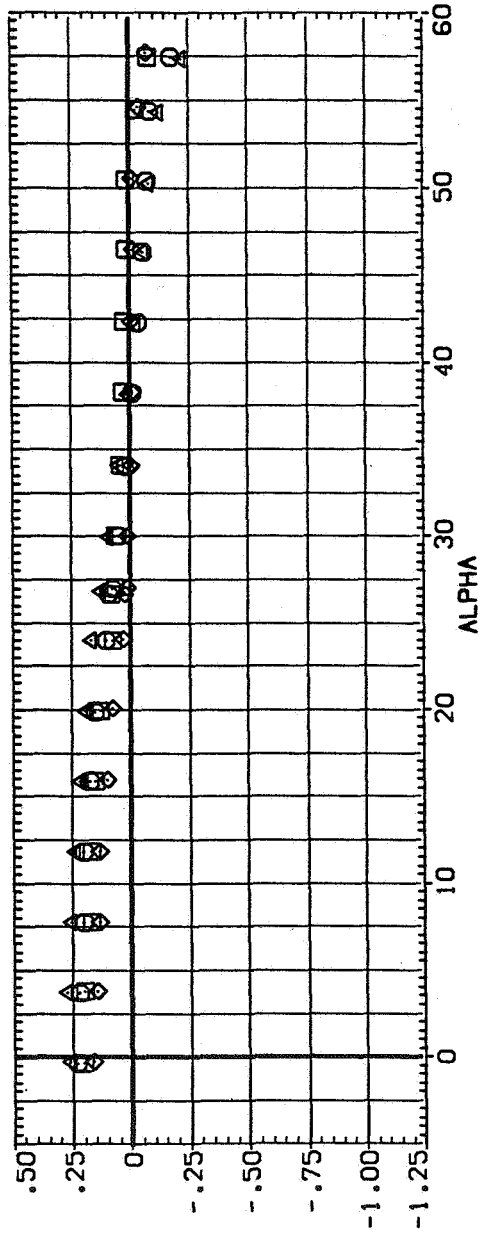
SYMBOL CONFIGURATION DESCRIPTION
 NI CI S
 NI CI S
 NI CI S
 NI CI S



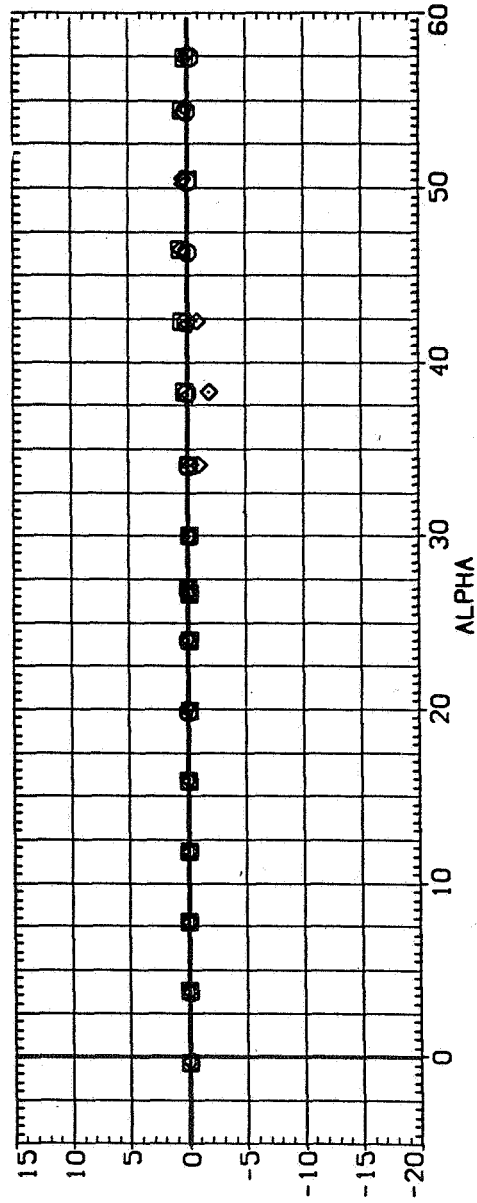
(b) C_Y/C_N and C_Y versus α .

Figure 5.— Continued.

SYMBOL CONFIGURATION DESCRIPTION
 NI Cl S
 N2 Cl S S
 N3 Cl S S
 N7 Cl S



CA



CYN

(c) C_A and C_n versus α .

Figure 5.— Concluded.

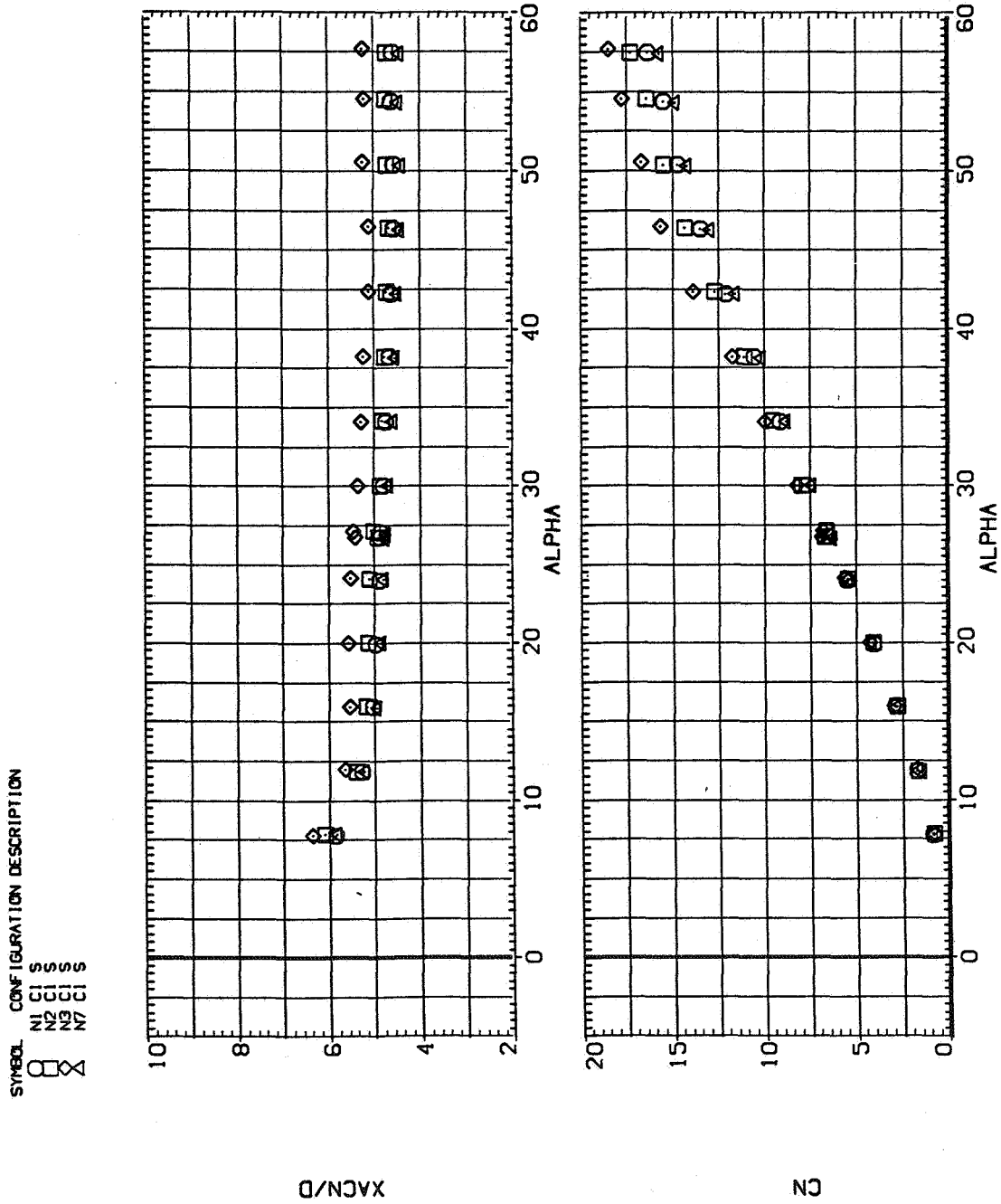
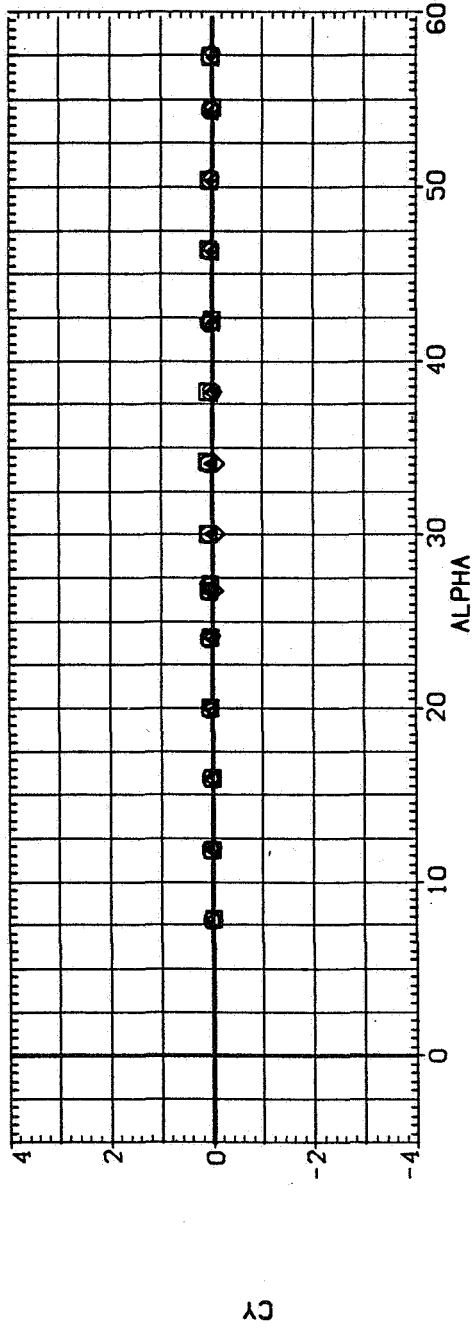
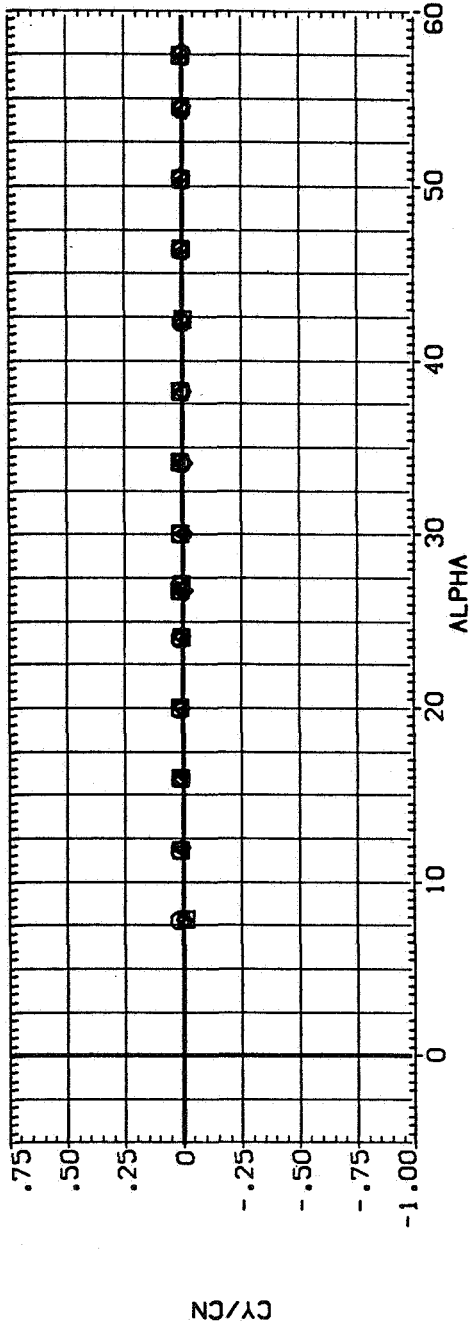


Figure 6.— Effect of nose fineness ratio; $M = 1.5$, $Re = 3.8 \times 10^5$.

SYMBOL CONFIGURATION DESCRIPTION

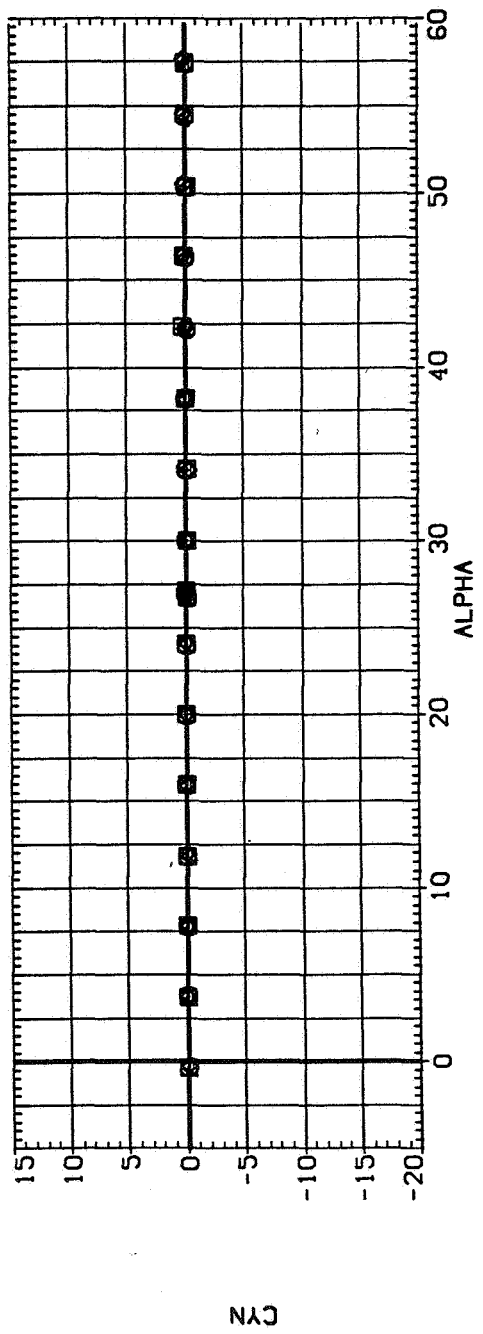
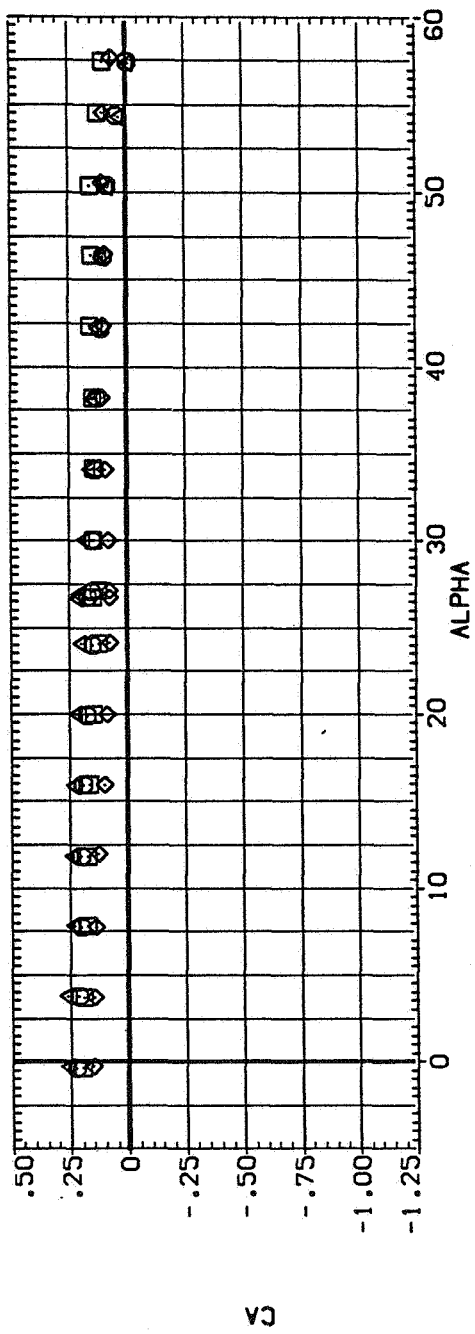
□ N1 C1 S
 □ N2 C1 S
 □ N9 C1 S
 □ N7 C1 S



(b) C_Y/C_N and C_Y versus α .

Figure 6.— Continued.

SYMBOL CONFIGURATION DESCRIPTION
 N1 C1 S
 N2 C1 S
 N3 C1 S
 N7 C1 S

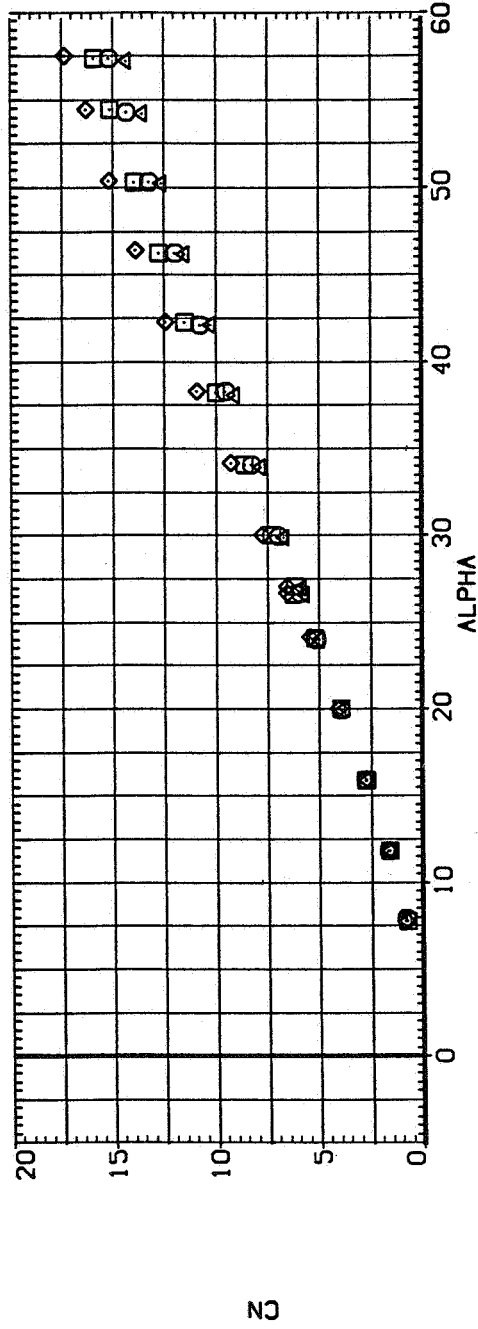
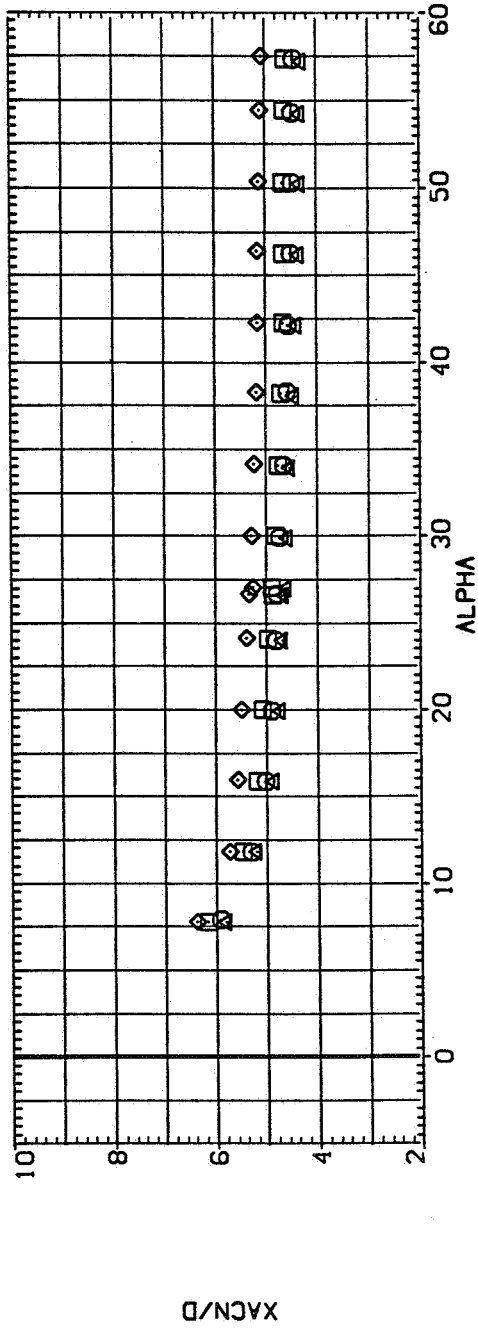


(c) C_A and C_n versus α .

Figure 6.— Concluded.

SYMBOL CONFIGURATION DESCRIPTION

 N1 C1 S
 N2 C1 S
 N3 C1 S
 N7 C1 S

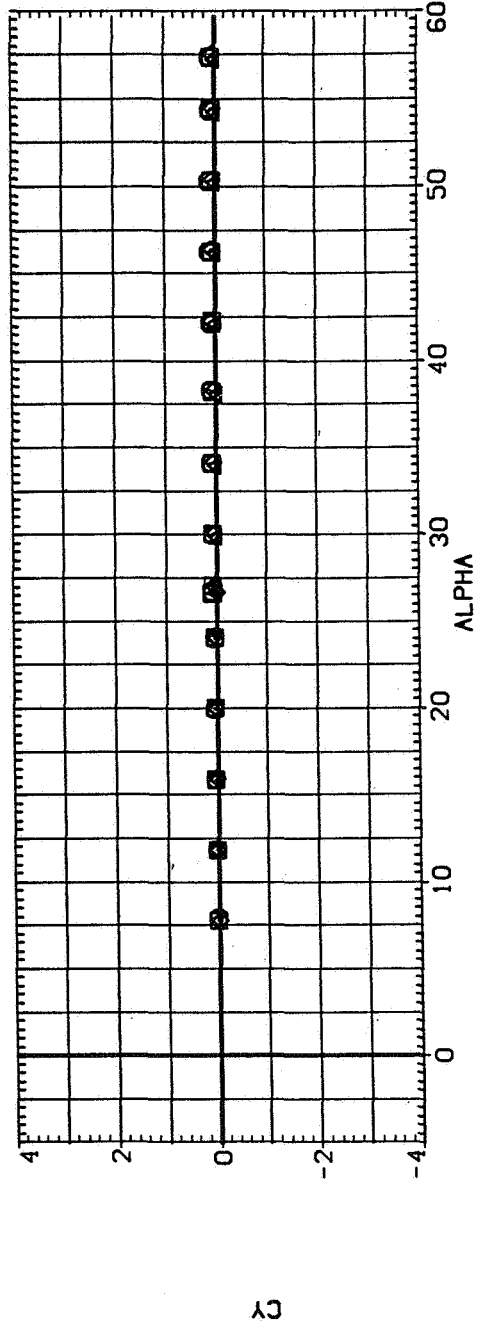
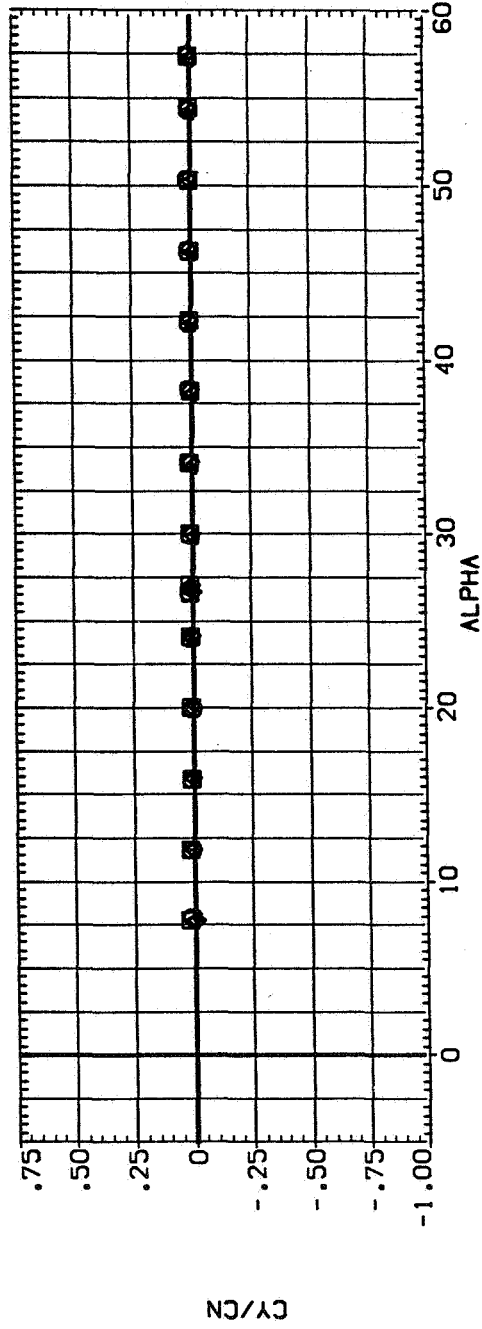


(a) x_{acN}/d and C_N versus α .

Figure 7.— Effect of nose fineness ratio; $M = 2.0$, $Re = 3.8 \times 10^5$.

SYMBOL CONFIGURATION DESCRIPTION

- N1 C1 S
- N2 C1 S
- N3 C1 S
- N7 C1 S

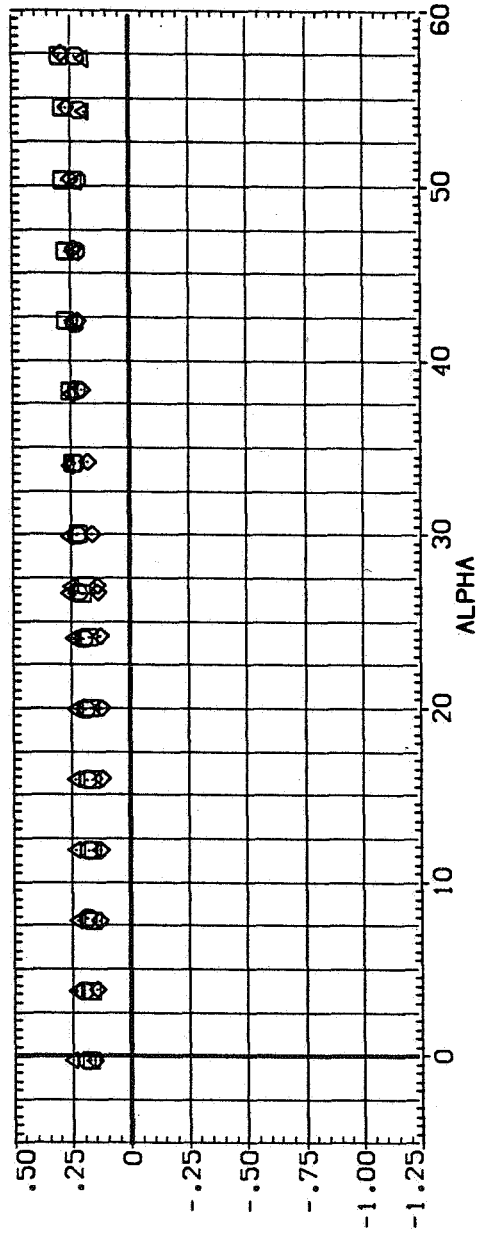


(b) CY/CN and CY versus α .

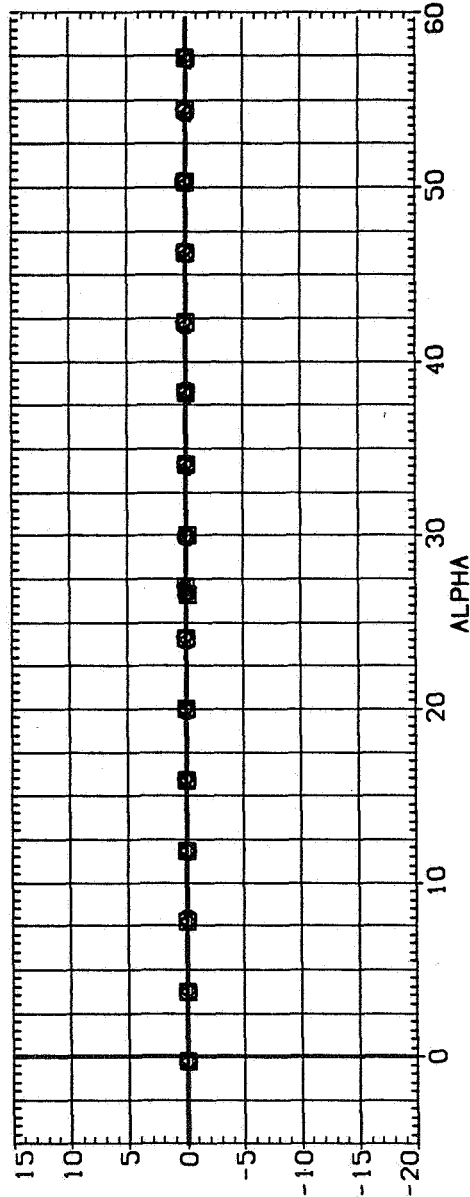
Figure 7.— Continued.

SYMBOL CONFIGURATION DESCRIPTION

N1 C1 S
 N2 C1 S
 N3 C1 S
 N7 C1 S



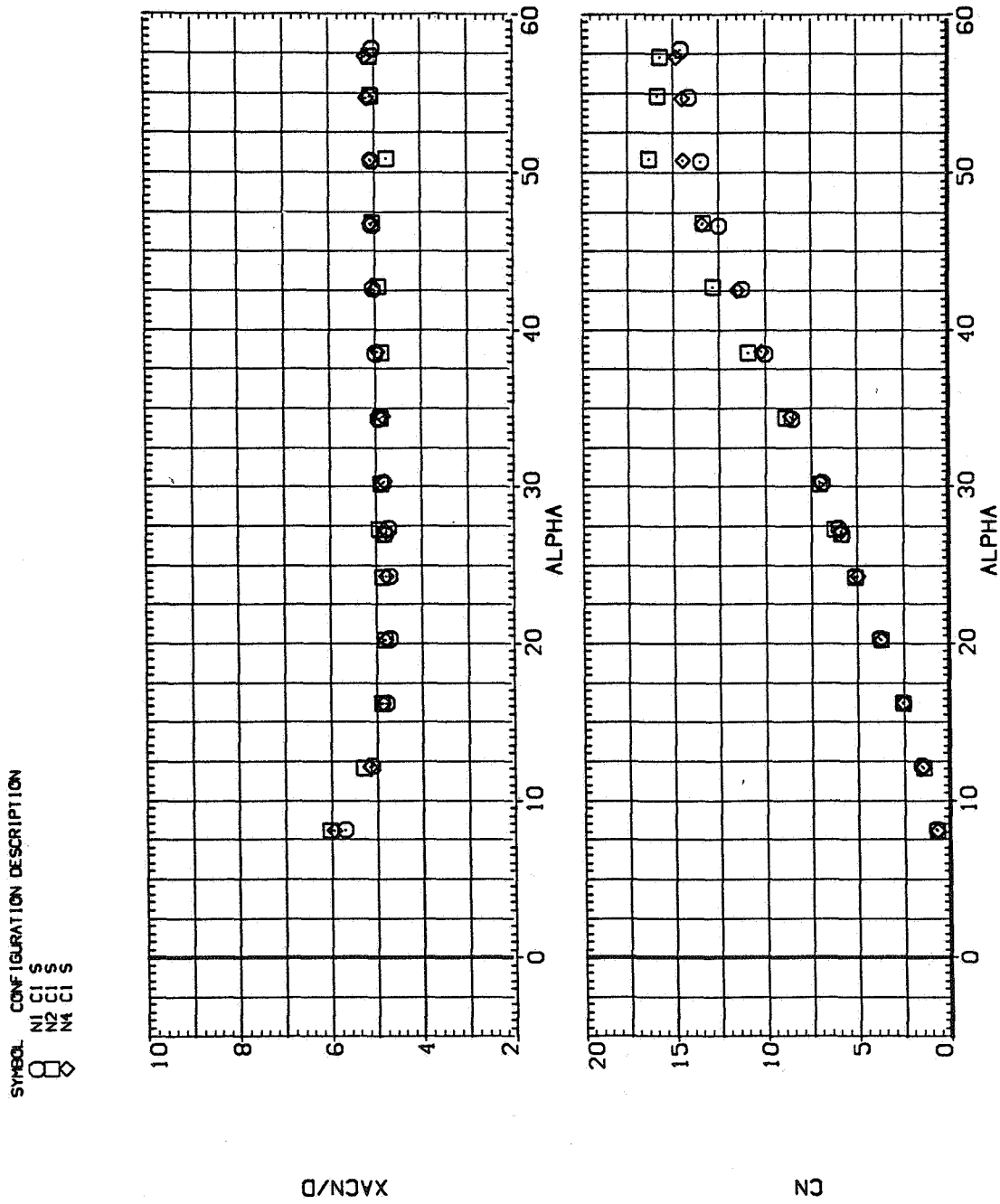
CA



CYN

(c) C_A and C_{η} versus α .

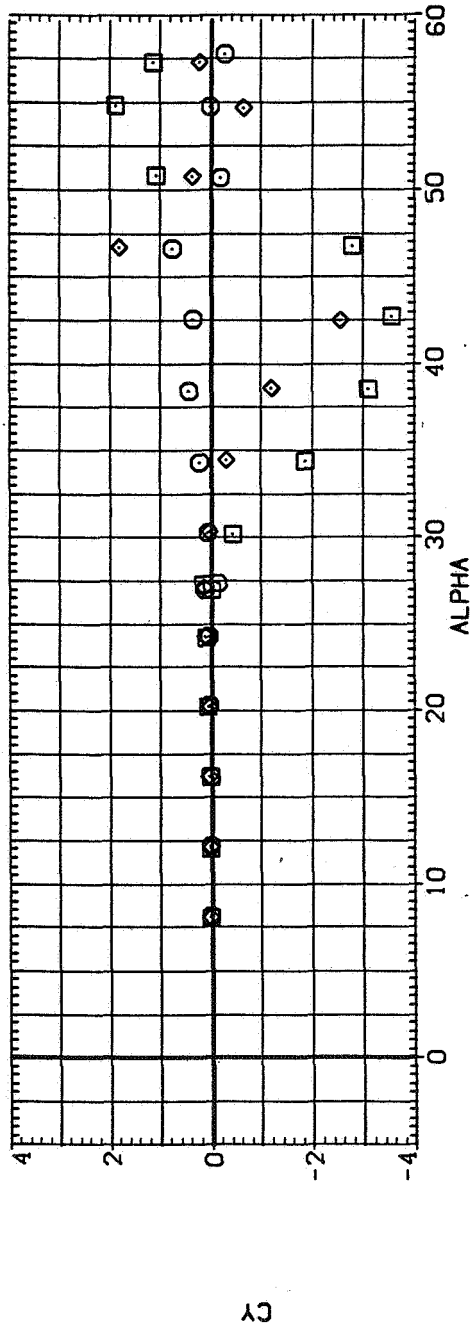
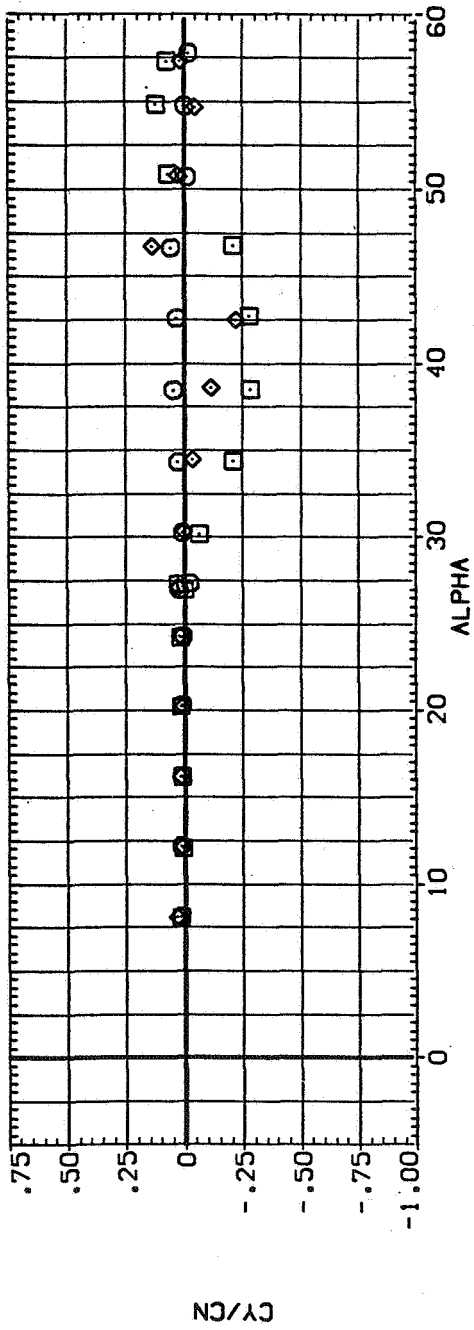
Figure 7.— Concluded.



(a) x_{acN}/d and C_N versus α .

Figure 8.— Effect of nose tip rounding; $M = 0.6, Re = 6.5 \times 10^5$.

SYMBOL CONFIGURATION DESCRIPTION
 N1 Cl S
 N2 Cl S
 N4 Cl S

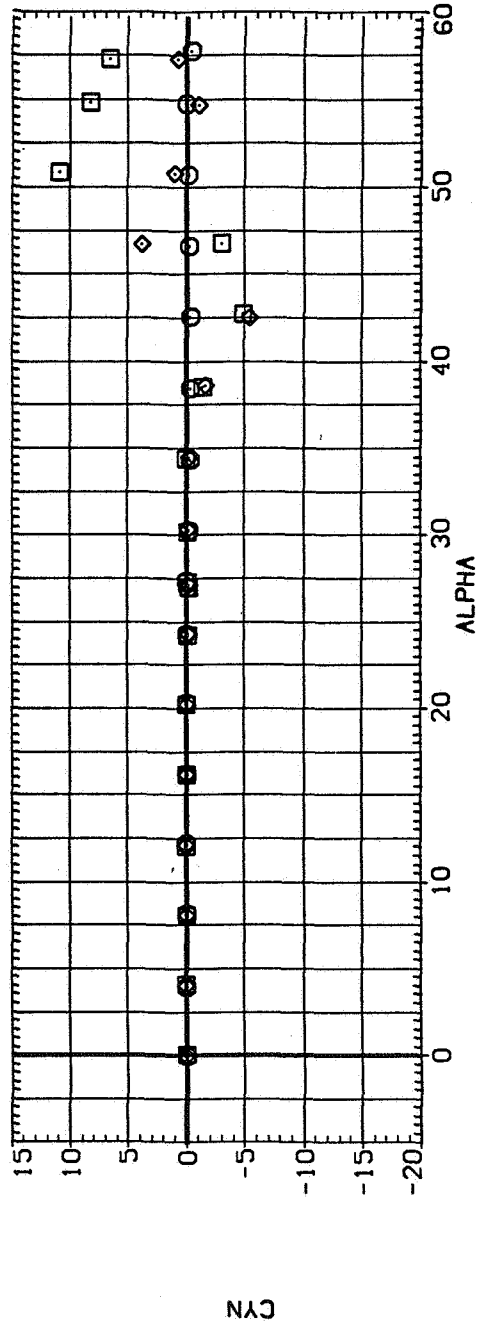
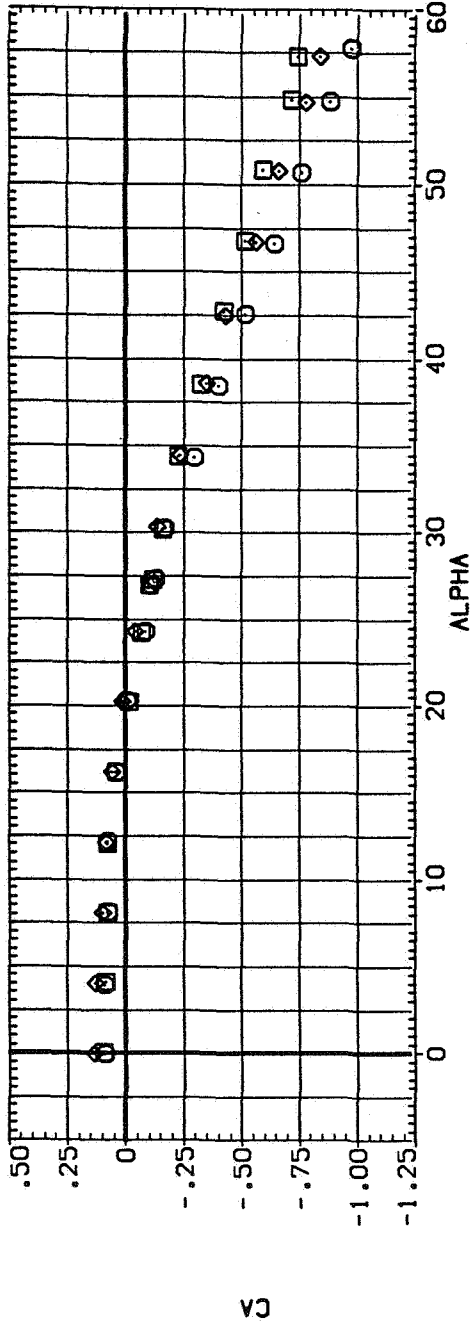


(b) C_Y/C_N and C_Y versus α .

Figure 8.— Continued.

SYMBOL CONFIGURATION DESCRIPTION

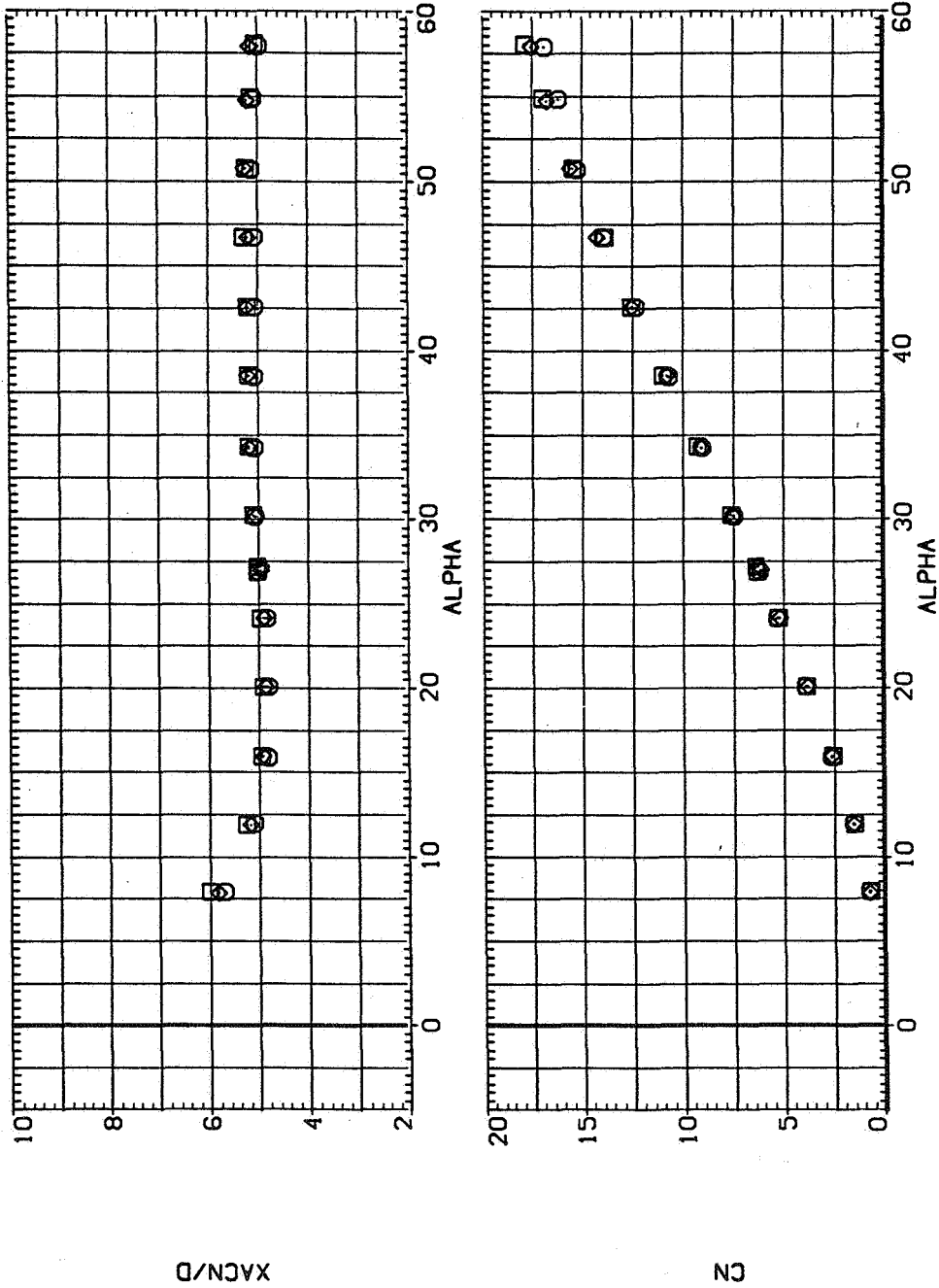
N1 C1 S
 N2 C1 S
 N4 C1 S



(c) C_A and C_n versus α .

Figure 8.— Concluded.

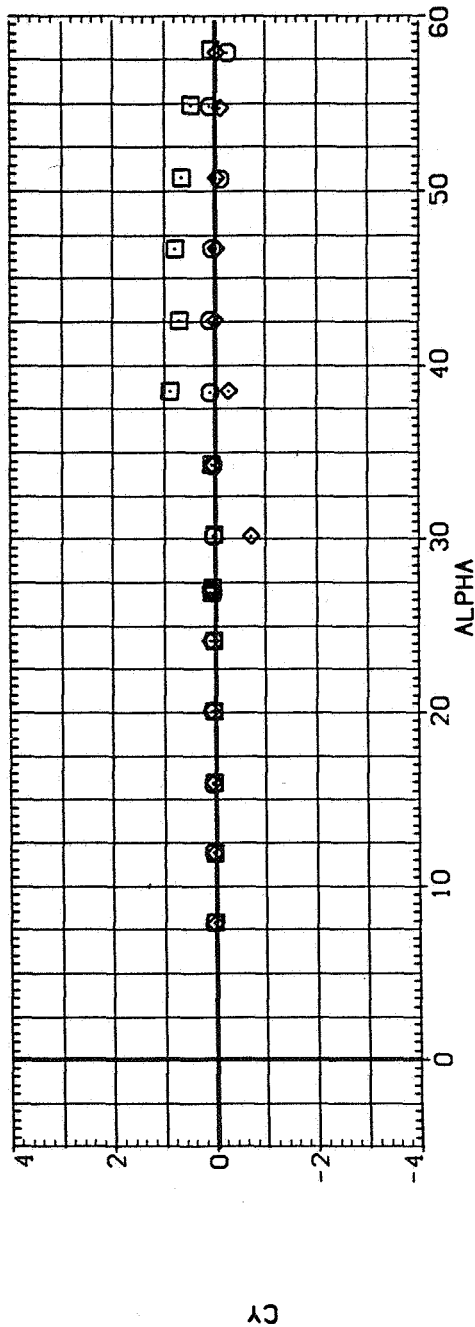
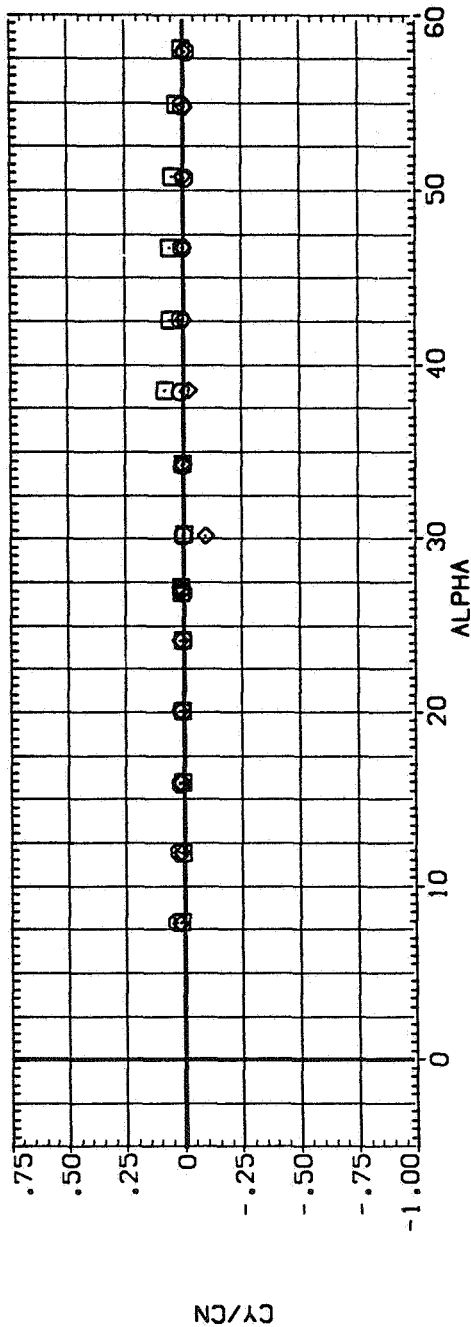
SYMBOL CONFIGURATION DESCRIPTION
 NI C1 S
 N2 C1 S
 N4 C1 S



(a) x_{acN}/d and C_N versus α .

Figure 9.— Effect of nose tip rounding; $M = 0.9$, $Re = 6.5 \times 10^5$.

SYMBOL CONFIGURATION DESCRIPTION
 N1 C1 S
 N2 C1 S
 N4 C1 S

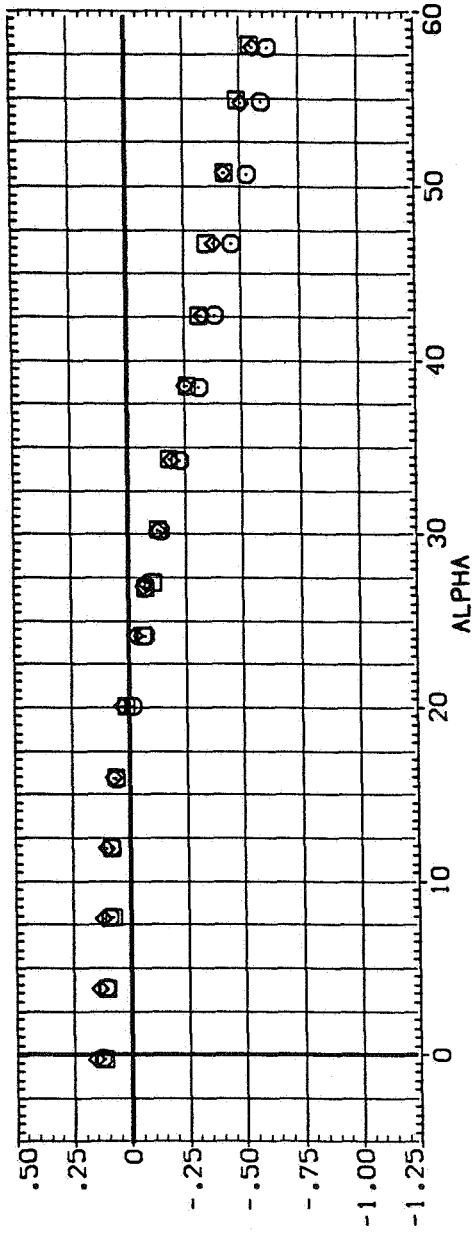


(b) C_Y/C_N and C_Y versus α .

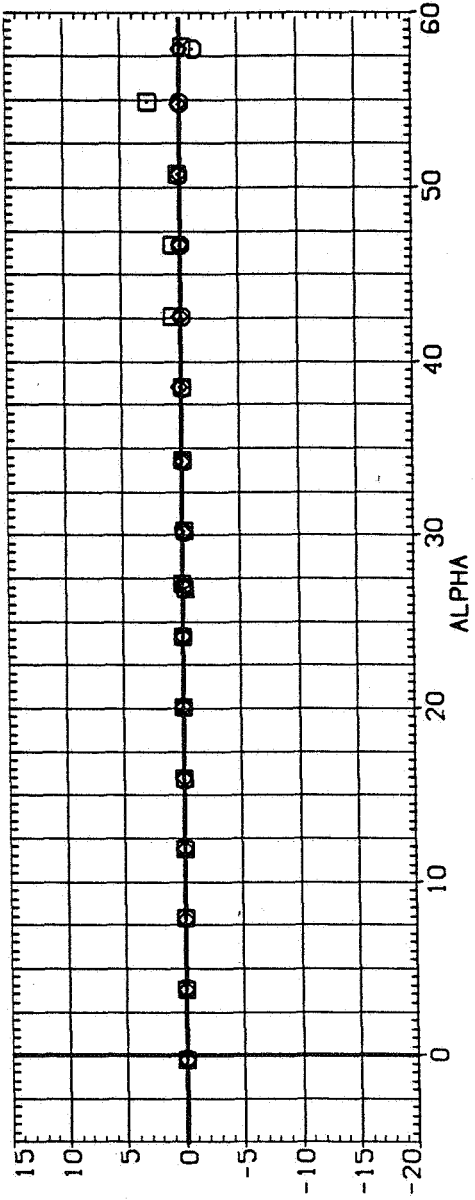
Figure 9. — Continued.

SYMBOL CONFIGURATION DESCRIPTION

NI CI S
 N2 CI S
 N4 CI S



CA

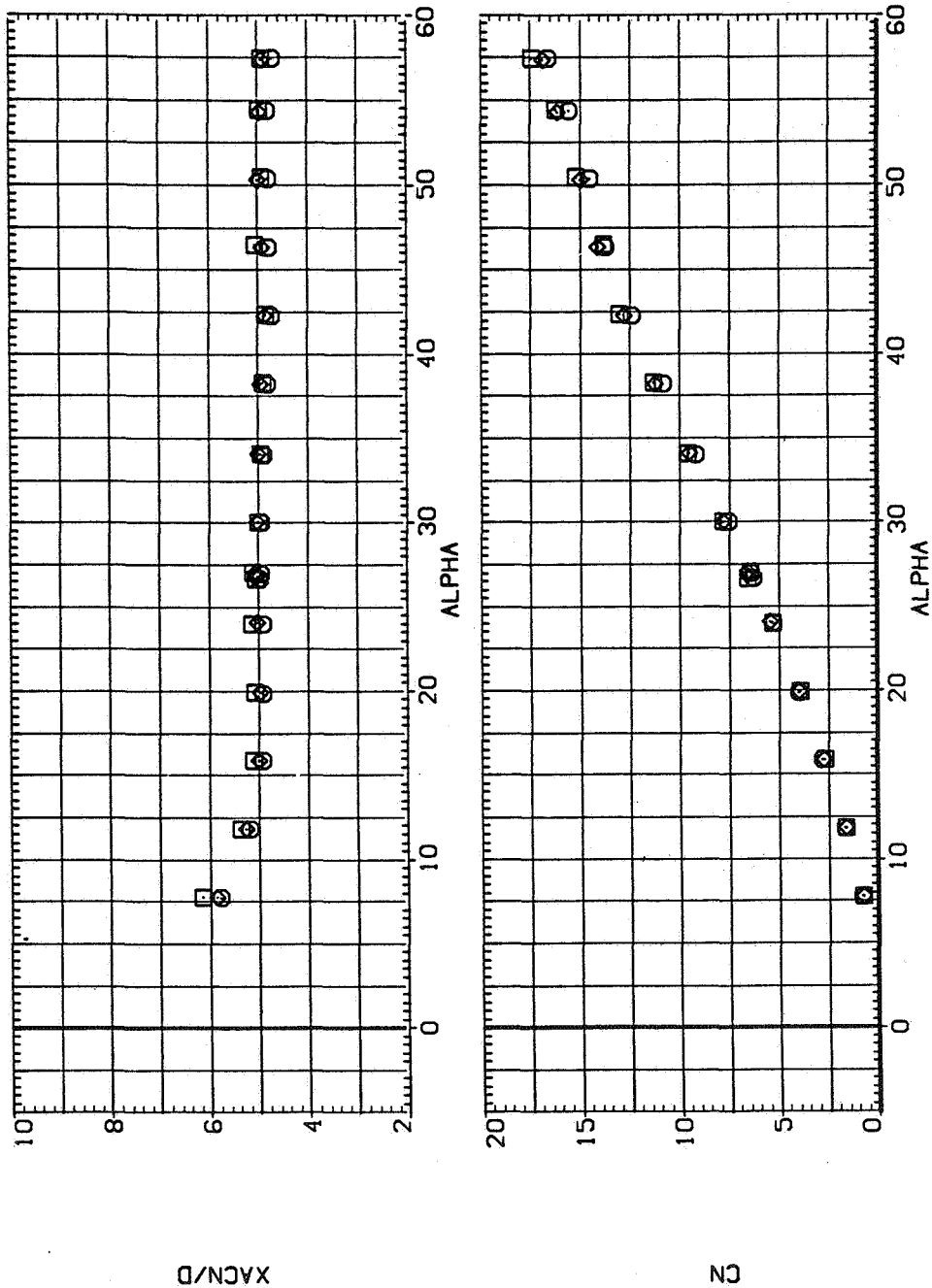


CYN

(c) C_A and C_n versus α .

Figure 9. — Concluded.

SYMBOL CONFIGURATION DESCRIPTION
 NI C1 S
 N2 C1 S
 N4 C1 S

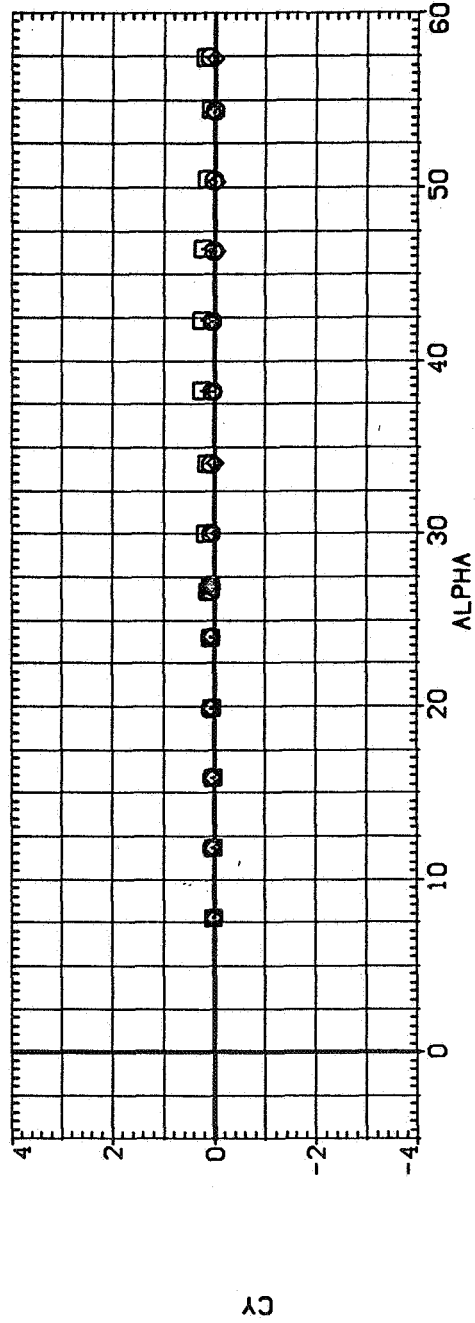
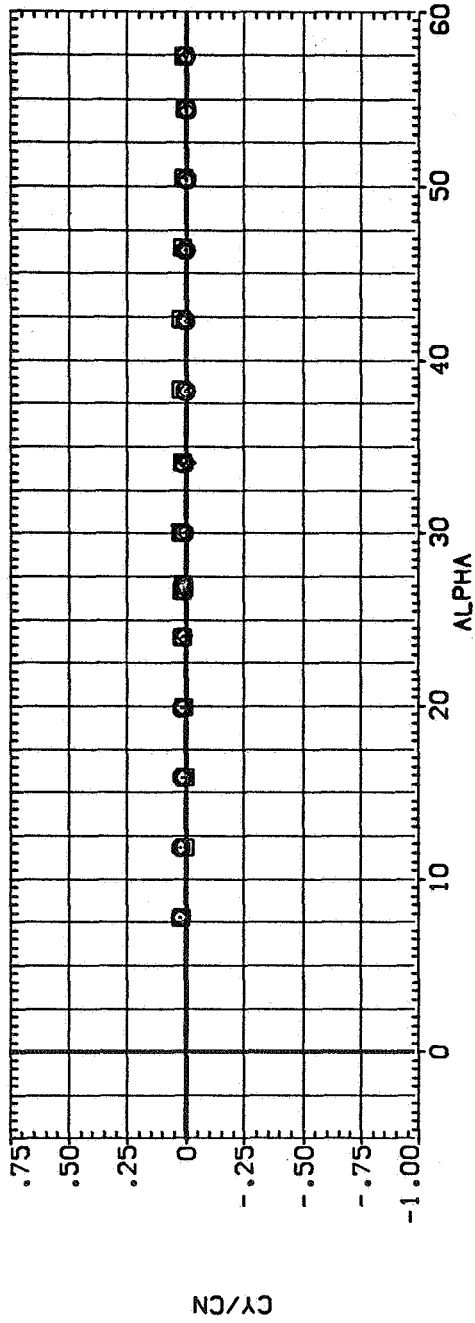


(a) x_{acN}/d and C_N versus α .

Figure 10.— Effect of nose tip rounding; $M = 1.2$, $Re = 3.8 \times 10^5$.

SYMBOL CONFIGURATION DESCRIPTION

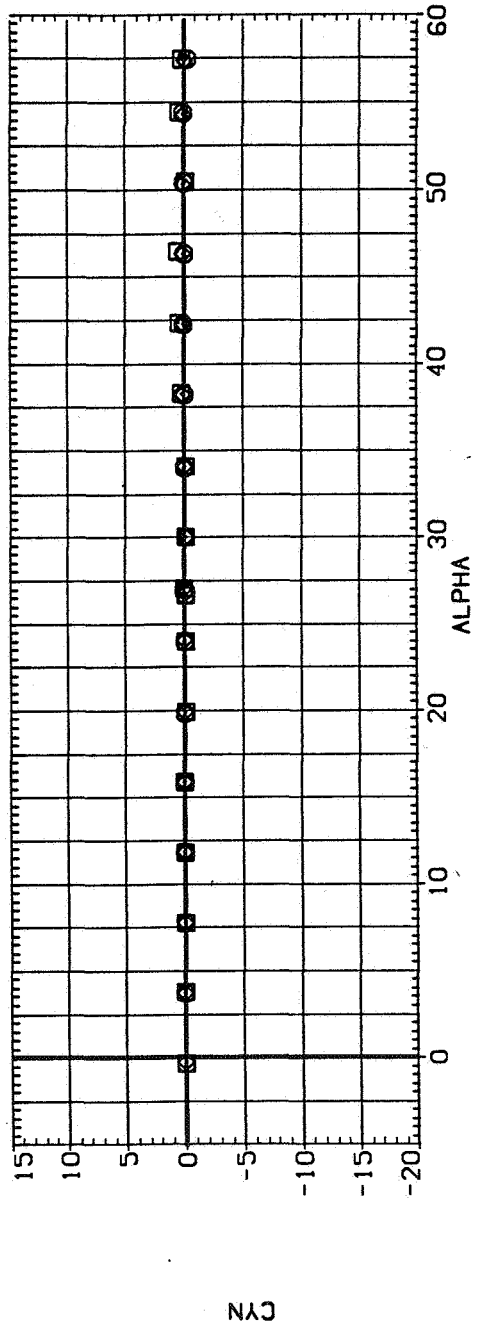
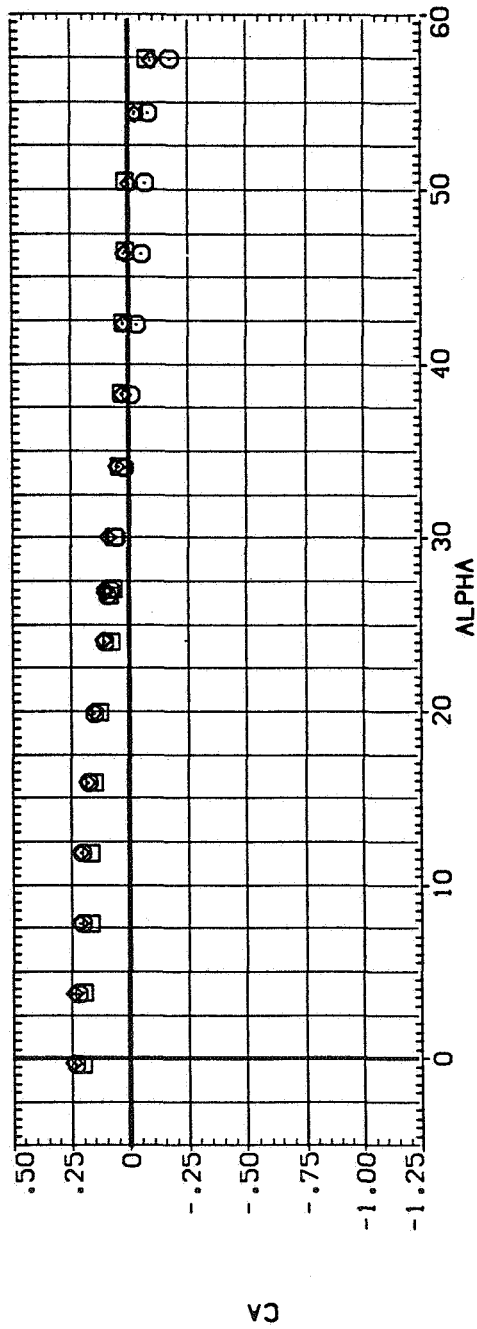
□ N1 C1 S
 ○ N2 C1 S
 ◇ N4 C1 S



(b) C_Y/C_N and C_Y versus α .

Figure 10.— Continued.

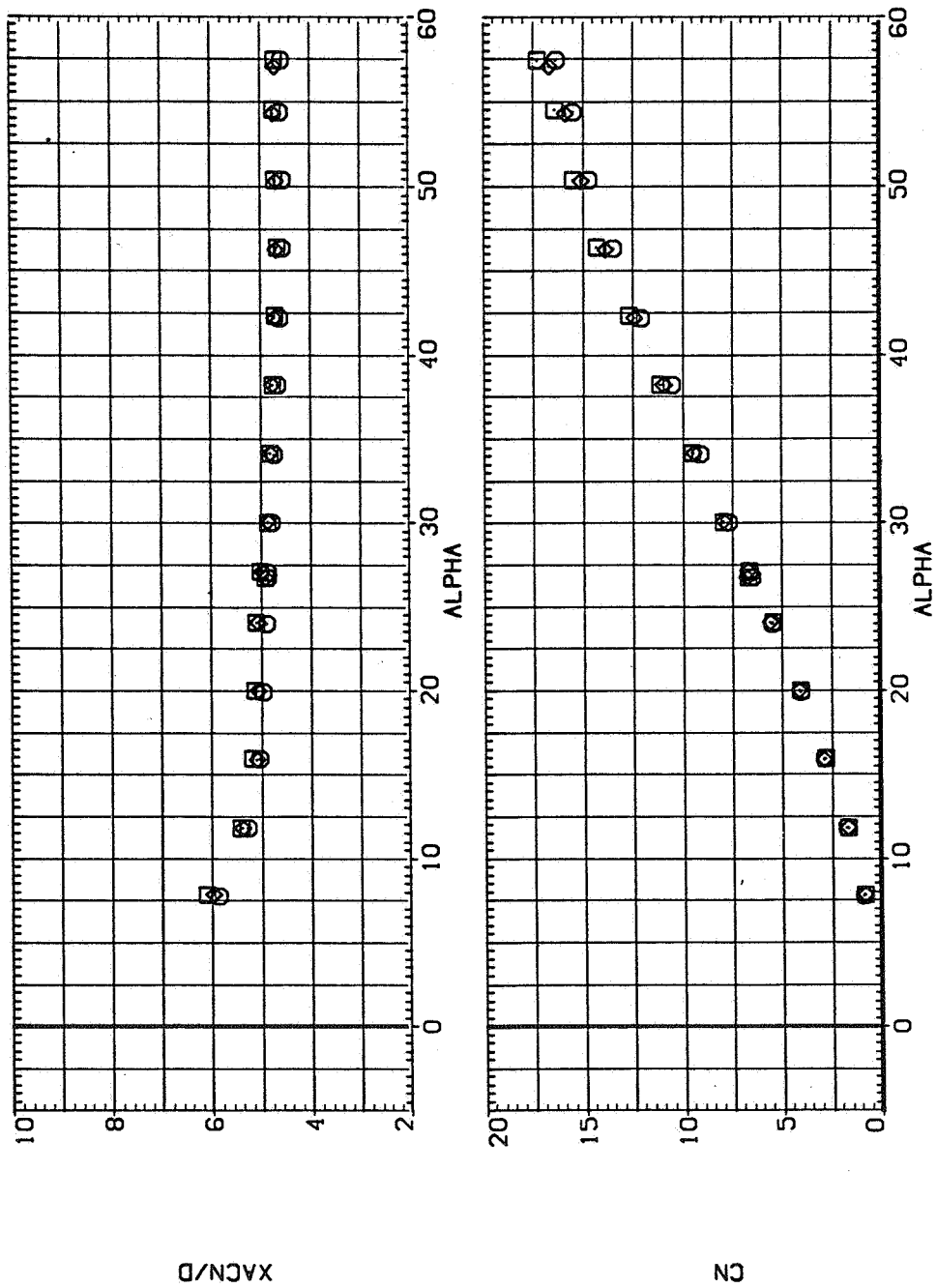
SYMBOL CONFIGURATION DESCRIPTION
 N1 C1 S
 N2 C1 S
 N4 C1 S



(c) C_A and C_n versus α .

Figure 10.— Concluded.

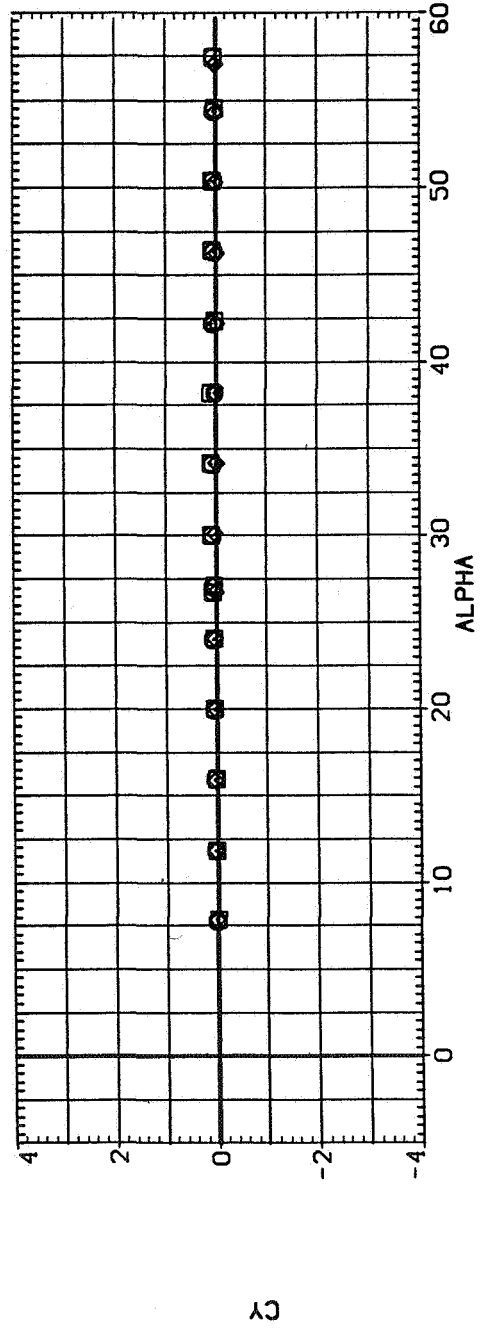
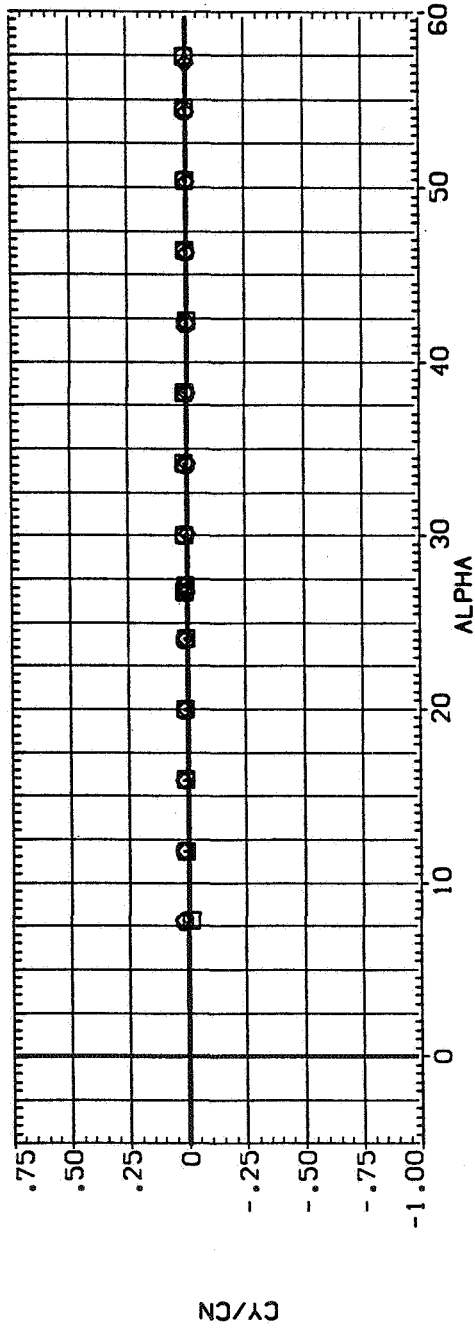
SYMBOL CONFIGURATION DESCRIPTION
 NI C1 S
 N2 C1 S
 N4 C1 S



(a) x_{acN}/d and C_N versus α .

Figure 11.— Effect of nose tip rounding; $M = 1.5$, $Re = 3.8 \times 10^5$.

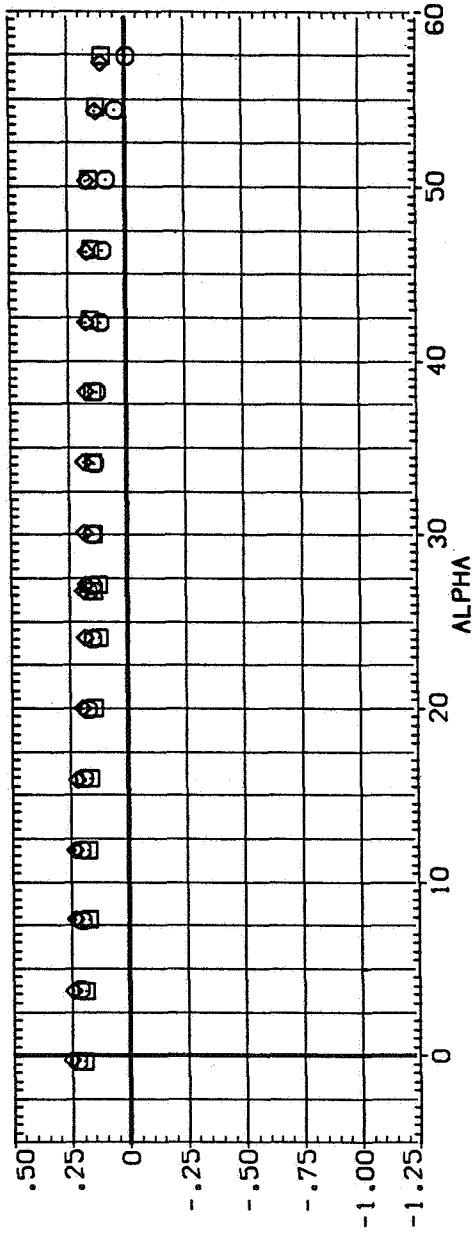
SYMBOL CONFIGURATION DESCRIPTION
 N1 C1 S
 N2 C1 S
 N4 C1 S



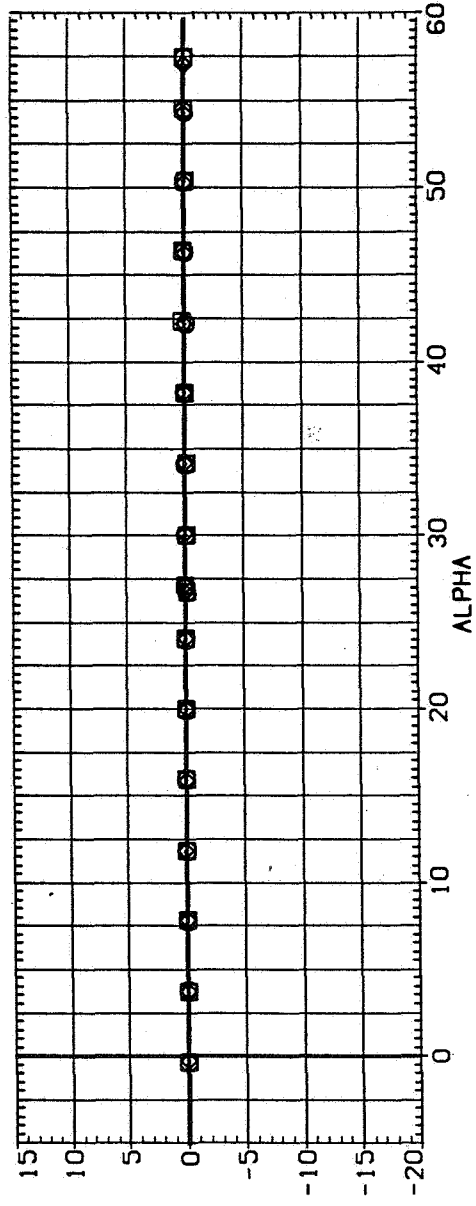
(b) C_Y/C_N and C_Y versus α .

Figure 11.— Continued.

SYMBOL CONFIGURATION DESCRIPTION
 N1 C1 S
 N2 C1 S
 N4 C1 S



CA



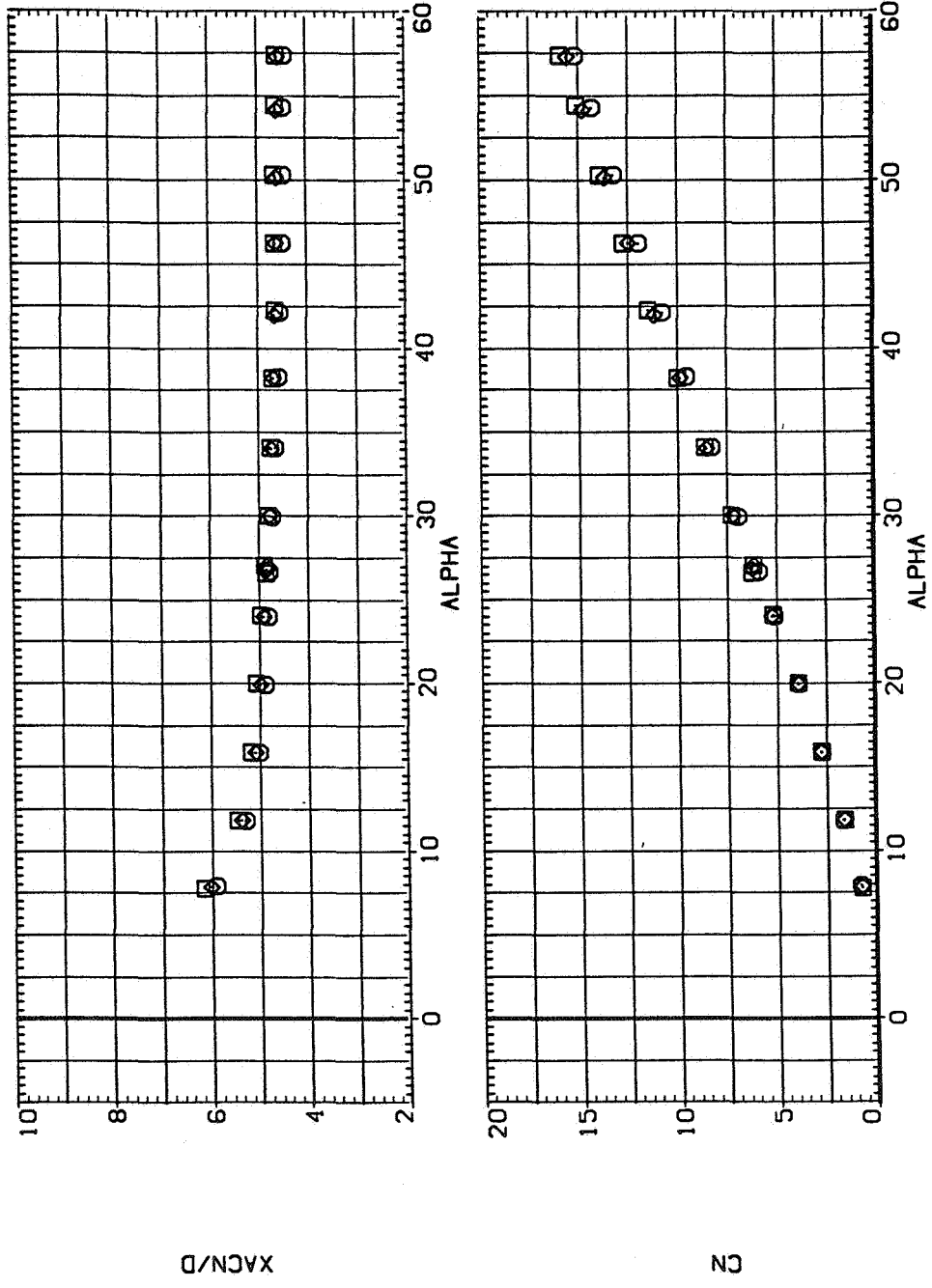
CYN

(c) C_A and C_n versus α .

Figure 11.— Concluded.

SYMBOL CONFIGURATION DESCRIPTION




- N1 C1 S
- N2 C1 S
- N4 C1 S

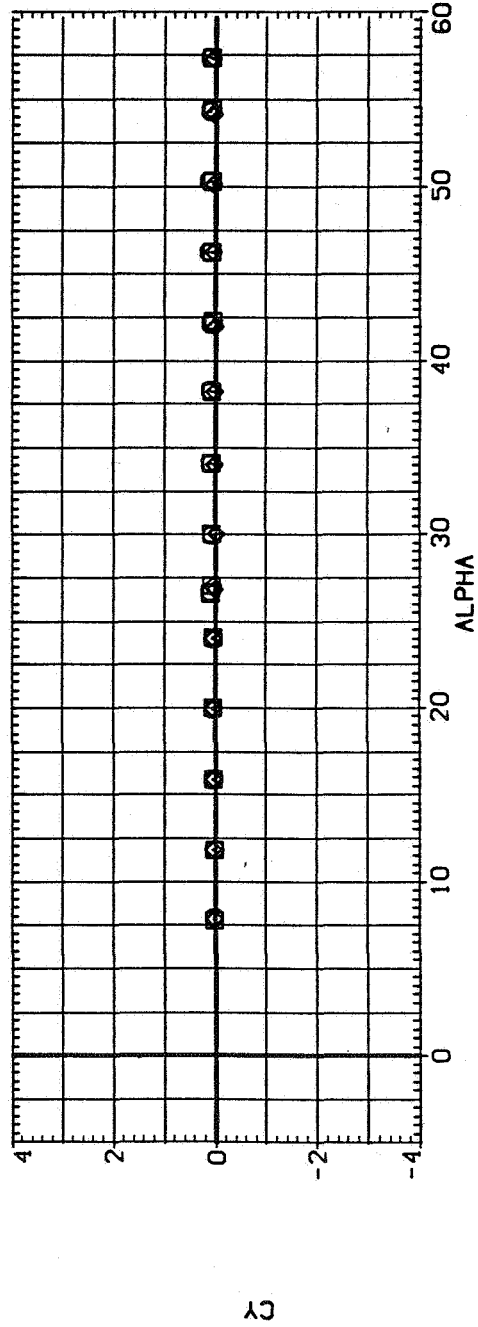
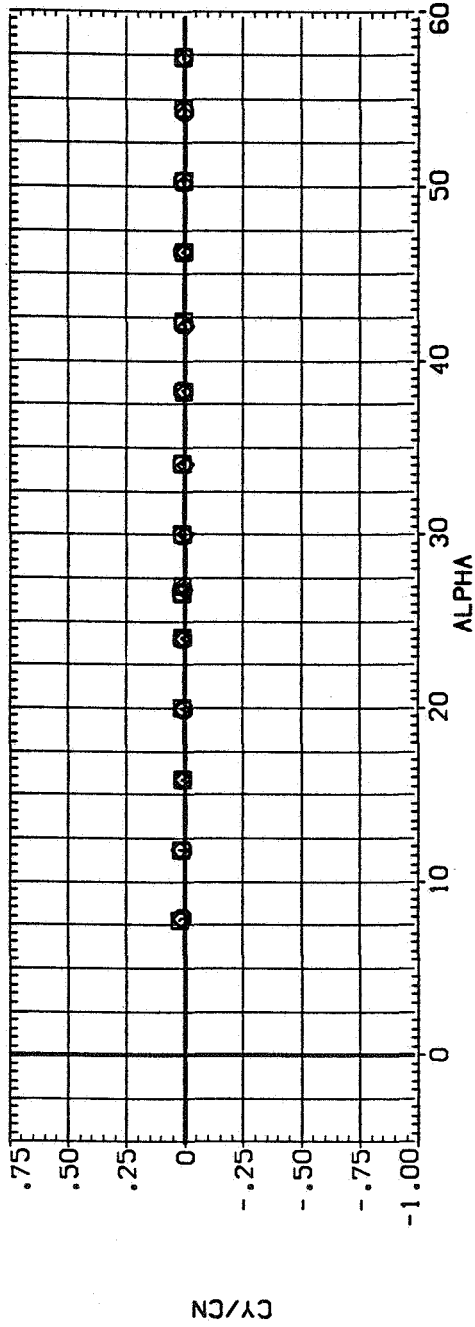


(a) x_{acN}/d and C_N versus α .

Figure 12.— Effect of nose tip rounding, $M = 2.0$, $Re = 3.8 \times 10^5$.

SYMBOL CONFIGURATION DESCRIPTION

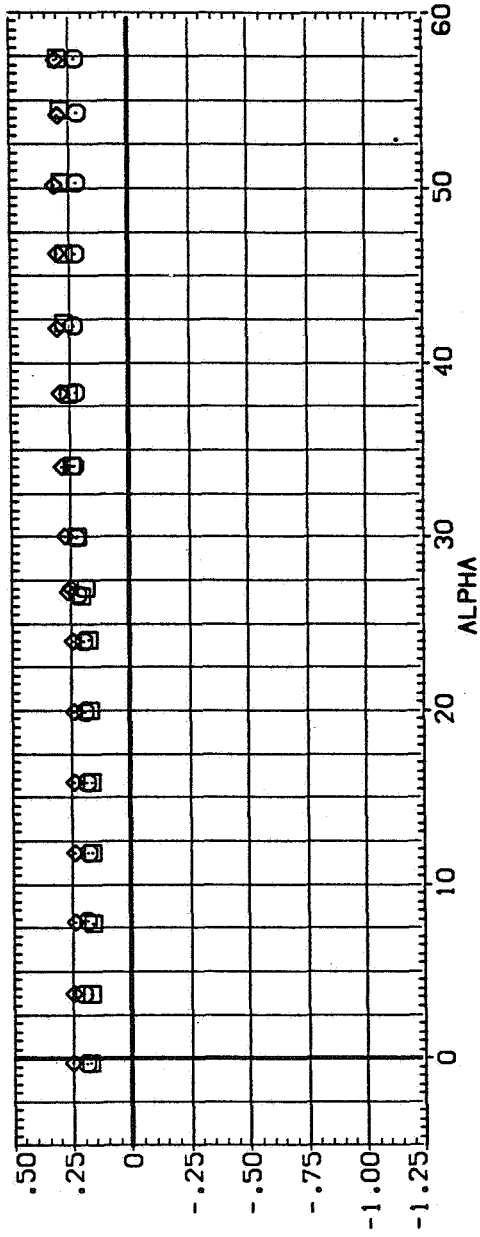
 N1 C1 S
 N2 C1 S
 N4 C1 S



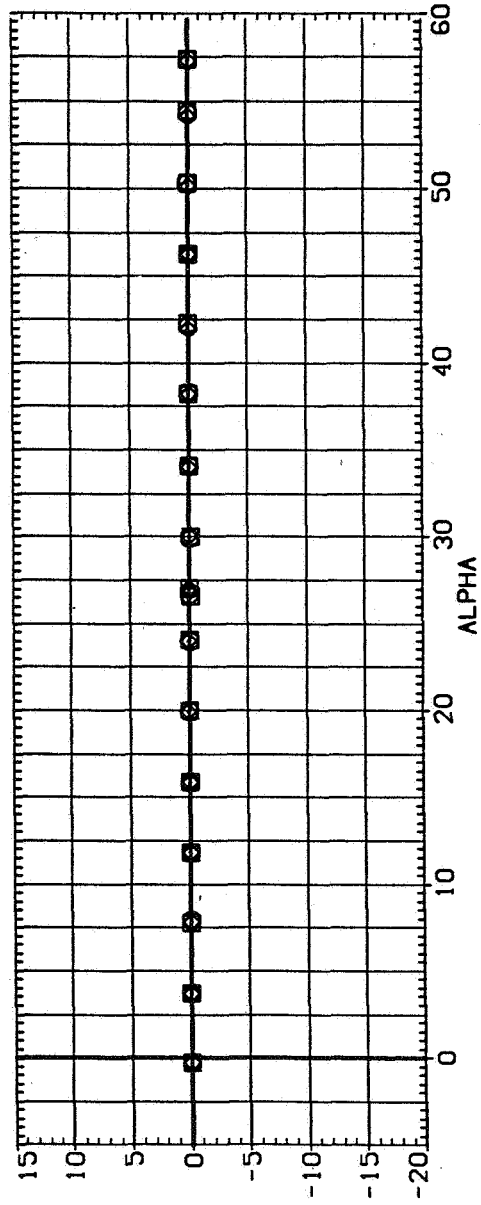
(b) C_Y/C_N and C_Y versus α .

Figure 12.— Continued.

SYMBOL CONFIGURATION DESCRIPTION
 NI CI S
 N2 CI S
 NA CI S



CN

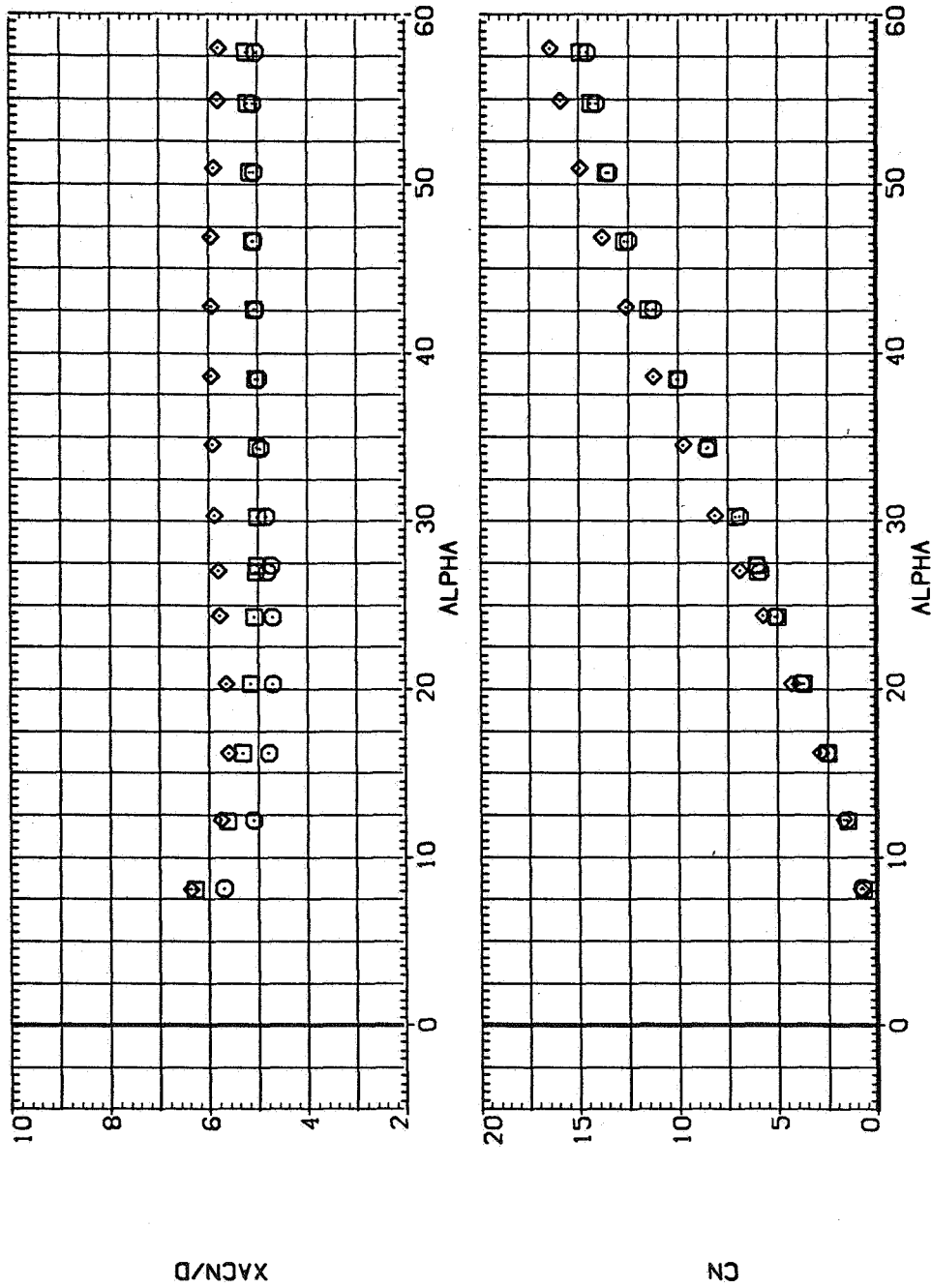


CN

(c) C_A and C_n versus α .

Figure 12.— Concluded.

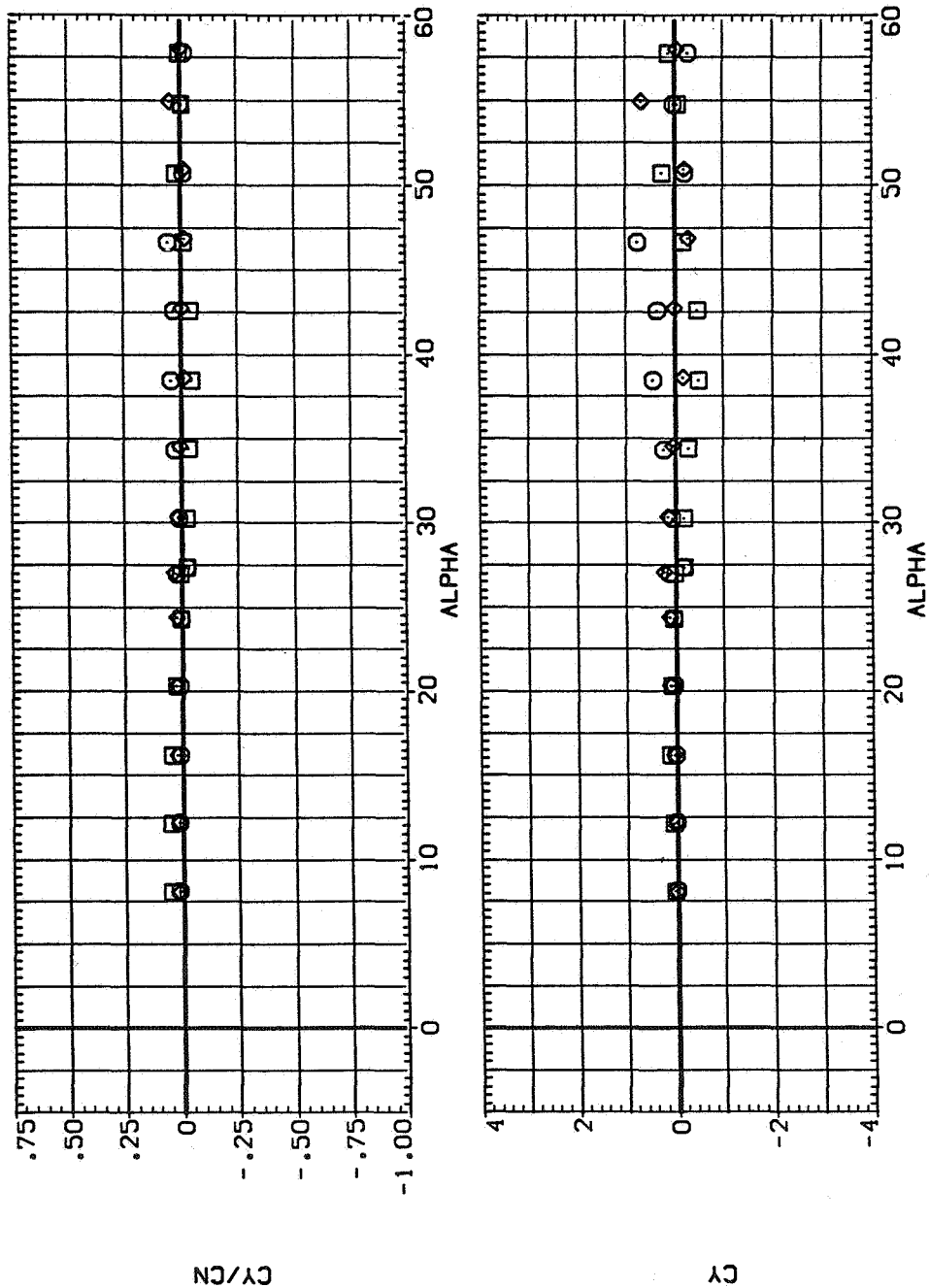
SYMBOL CONFIGURATION DESCRIPTION
 NI CI S
 NS CI S
 NS CI S



(a) x_{acN}/d and C_N versus α .

Figure 13.— Effect of nose strokes; $M = 0.6$, $Re = 6.5 \times 10^5$.

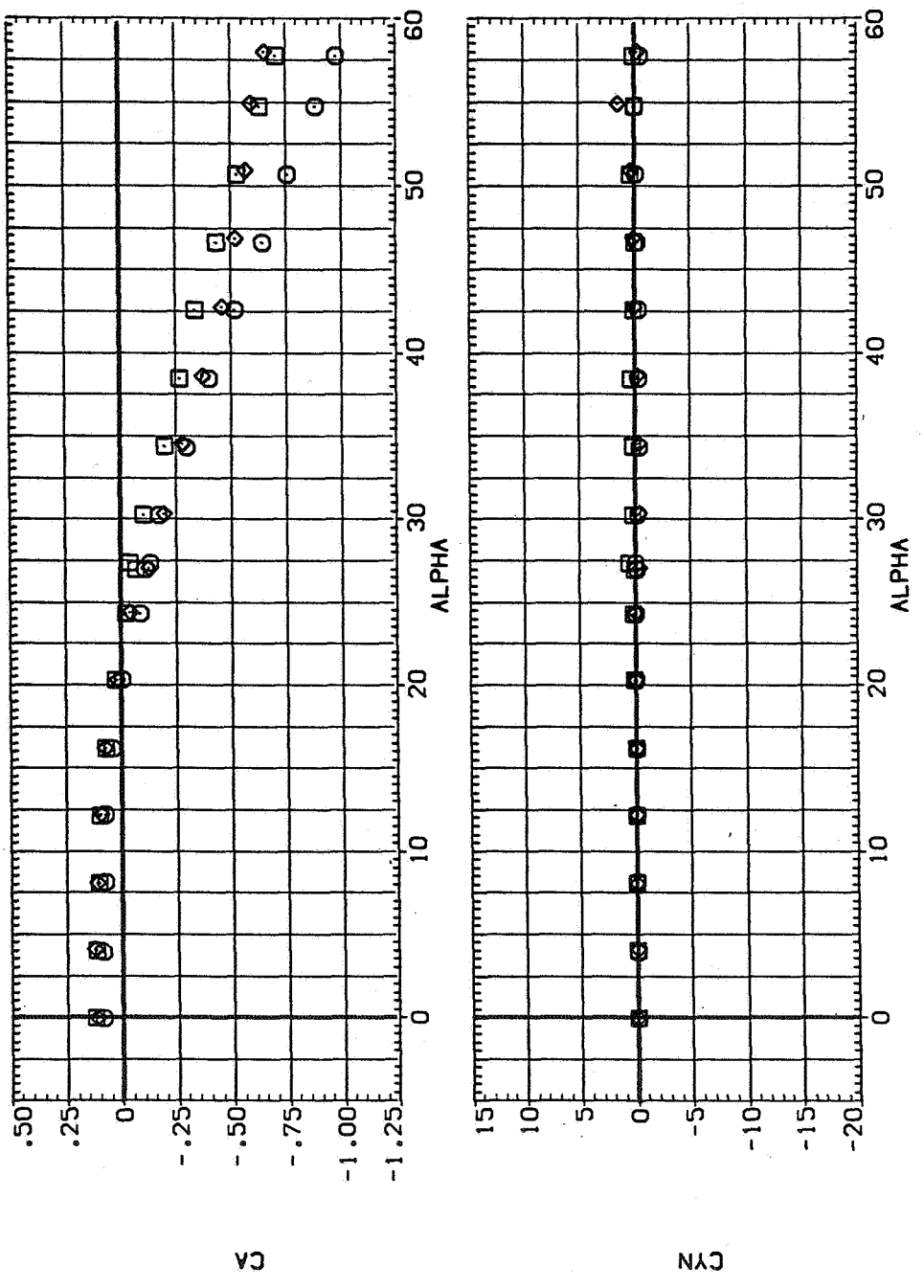
SYMBOL CONFIGURATION DESCRIPTION
 NI CI S S
 NS CI S S
 NS CI S S



(b) C_Y/C_N and C_Y versus α .

Figure 13.— Continued.

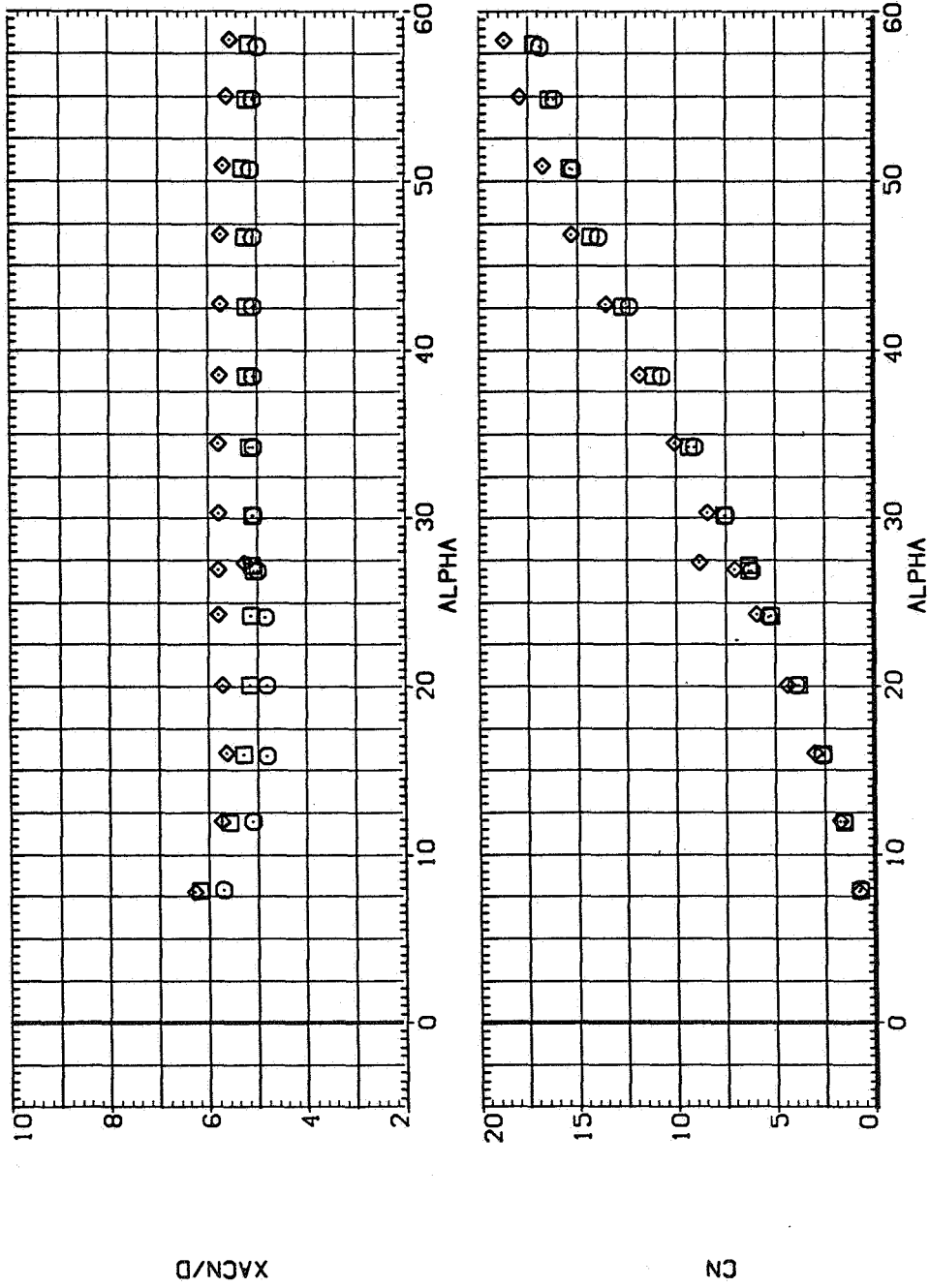
SYMBOL CONFIGURATION DESCRIPTION
 NI CI S
 NS CI S
 NS CI S



(c) C_A and C_n versus α .

Figure 13.— Concluded.

SYMBOL CONFIGURATION DESCRIPTION
 NI CI S
 NS CI S
 NS CI S

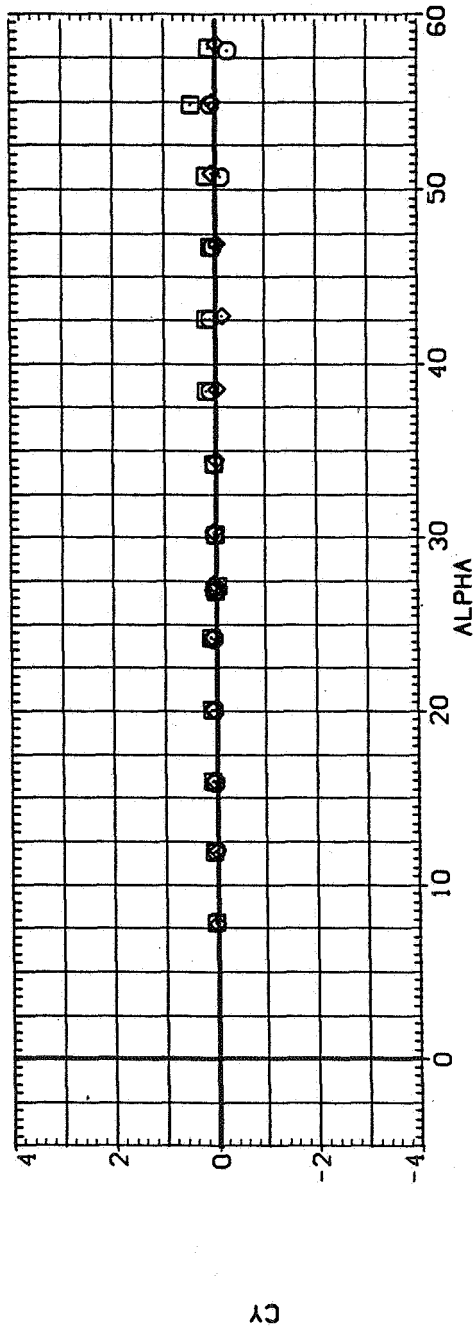
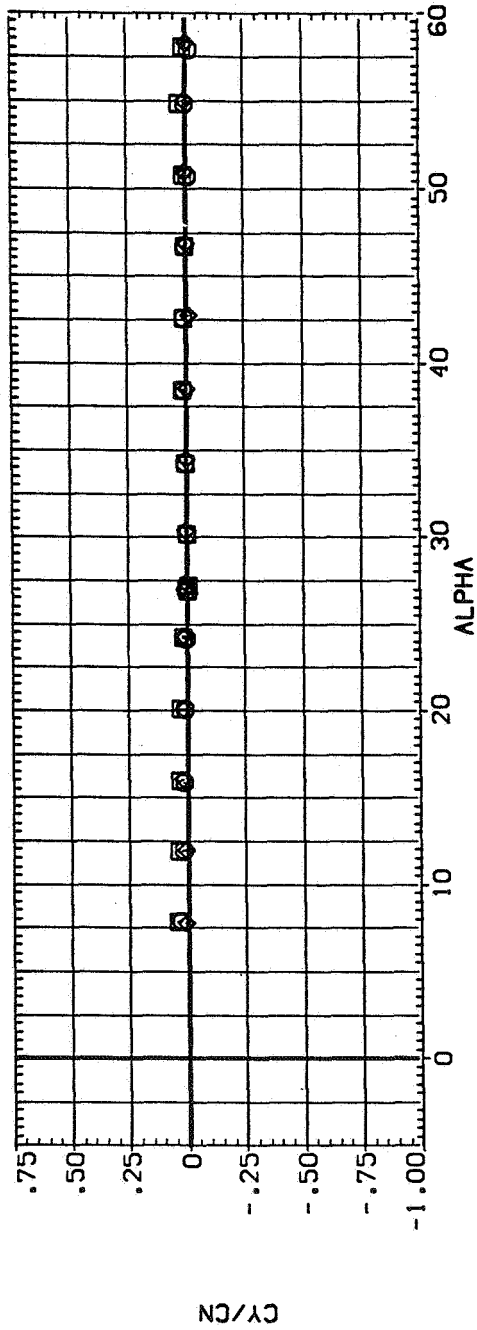


(a) x_{acN}/d and C_N versus α .

Figure 14.— Effect of nose strokes; $M = 0.9$, $Re = 6.5 \times 10^5$.

SYMBOL CONFIGURATION DESCRIPTION

NI CI S
NS CI S
NS CI S

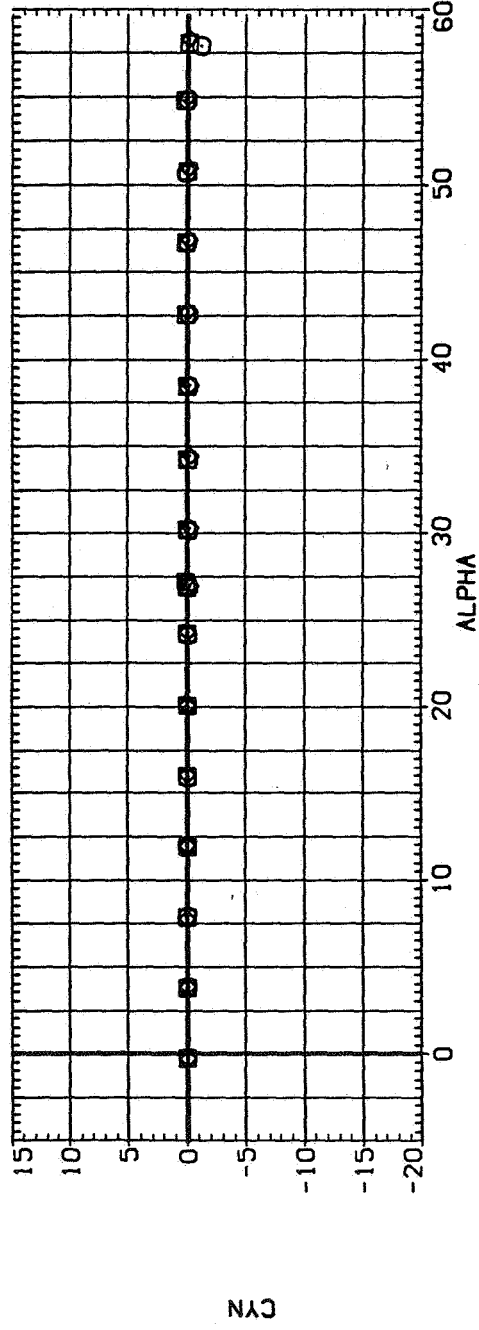
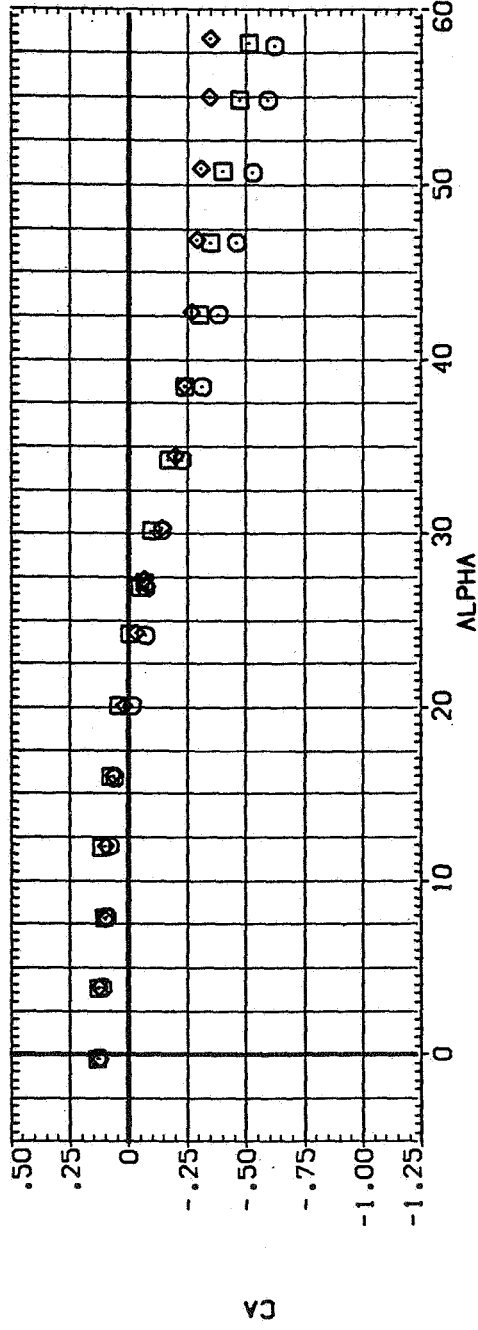


(b) C_Y/C_N and C_Y versus α .

Figure 14. - Continued.

SYMBOL CONFIGURATION DESCRIPTION

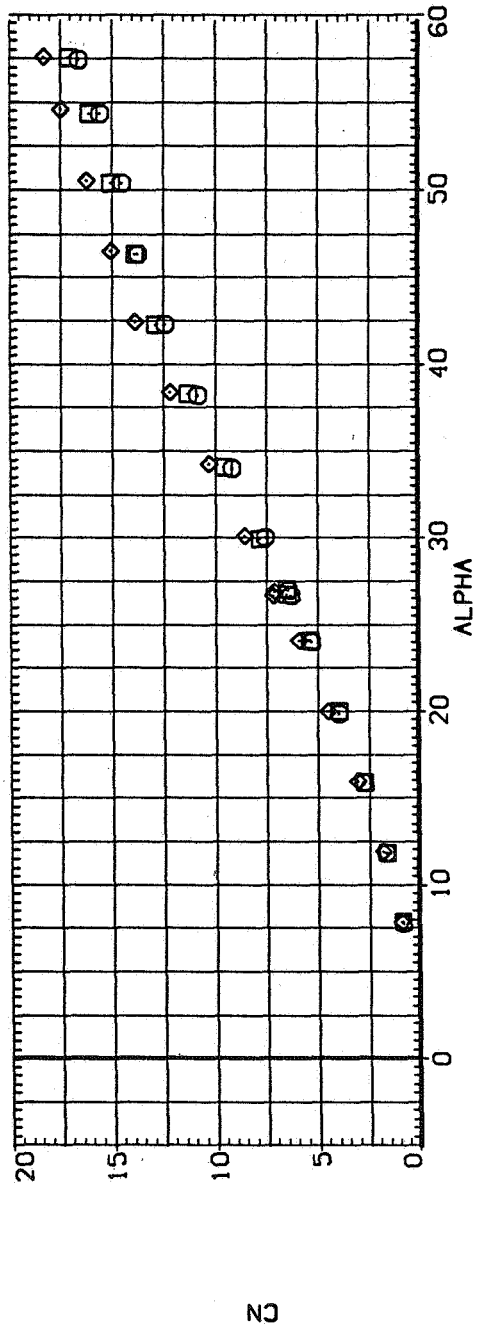
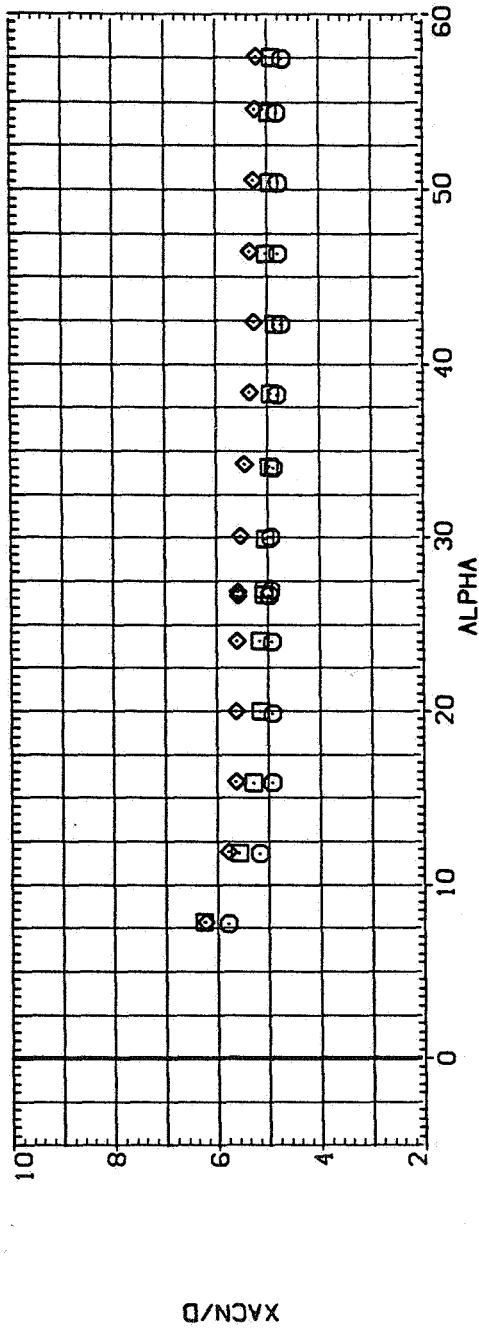
\square NI
 \square CI
 \square SS
 \square S
 \square NS
 \square NS
 \square CI
 \square CI
 \square S



(c) C_A and C_n versus α .

Figure 14.- Concluded.

SYMBOL CONFIGURATION DESCRIPTION
 NI CI S
 NS CI S

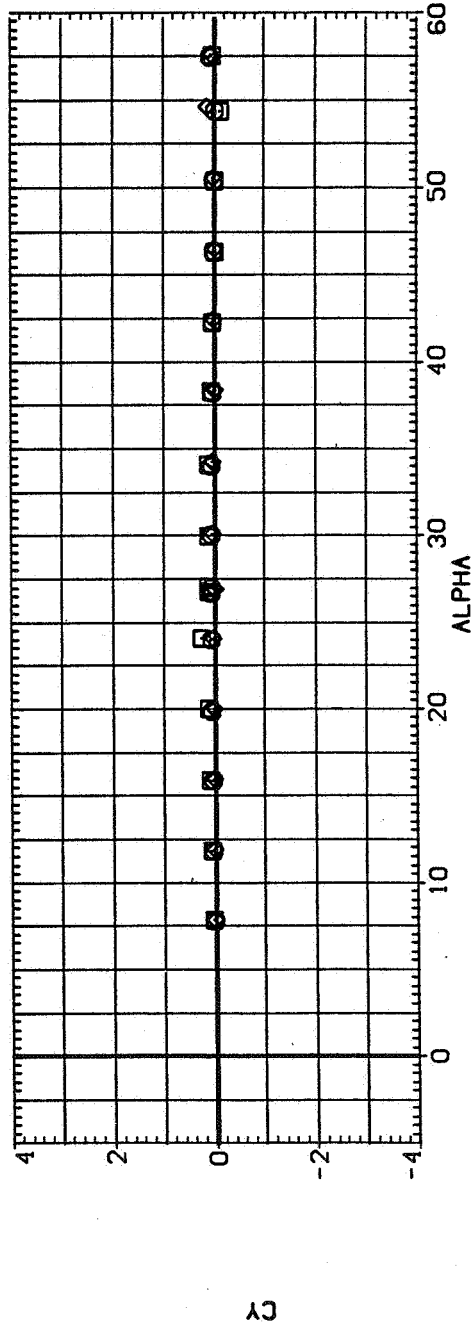
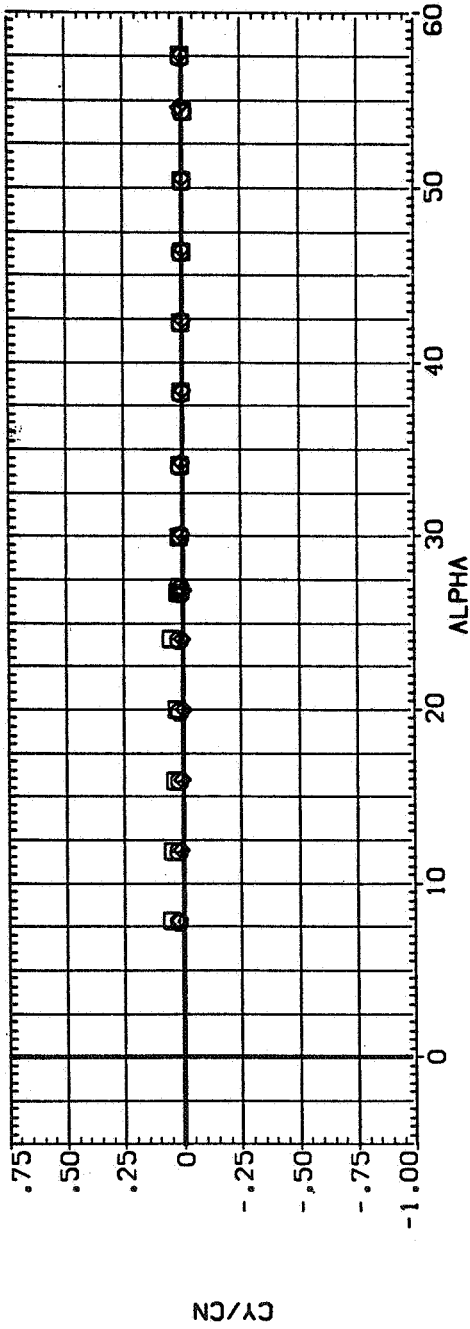


(a) x_{acN}/d and C_N versus α .

Figure 15.— Effect of nose strokes; $M = 1.2$, $Re = 3.8 \times 10^5$.

SYMBOL CONFIGURATION DESCRIPTION

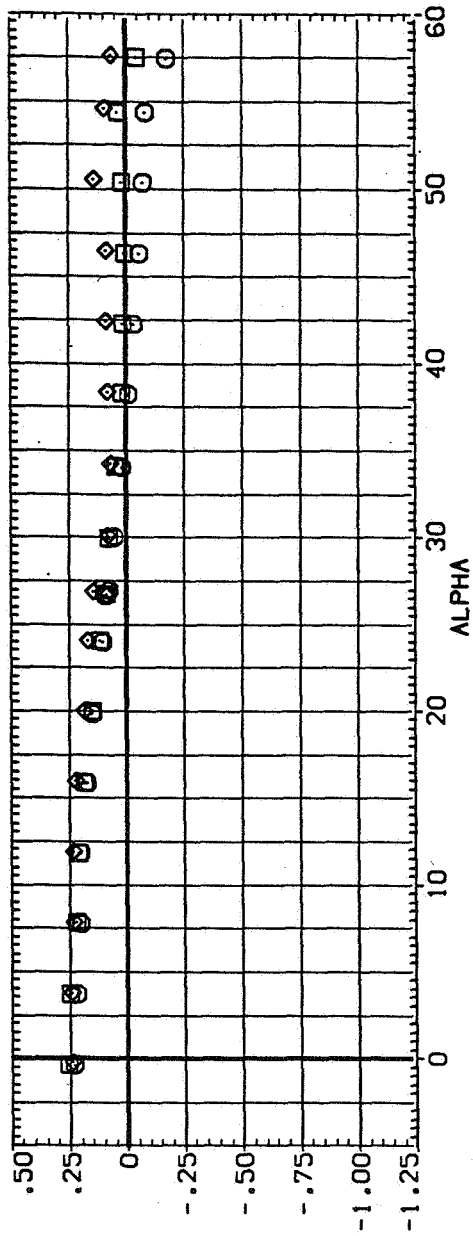
NI Cl S
NS Cl S
NS Cl S



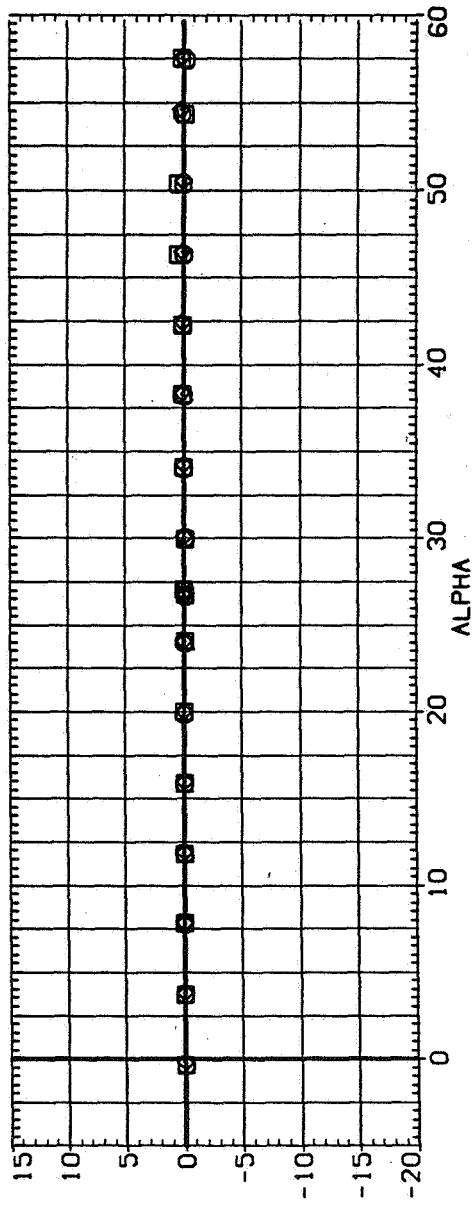
(b) C_Y/C_N and C_Y versus α .

Figure 15.— Continued.

SYMBOL CONFIGURATION DESCRIPTION
 NI Cl S S
 NS Cl S S
 NS Cl S S



CA









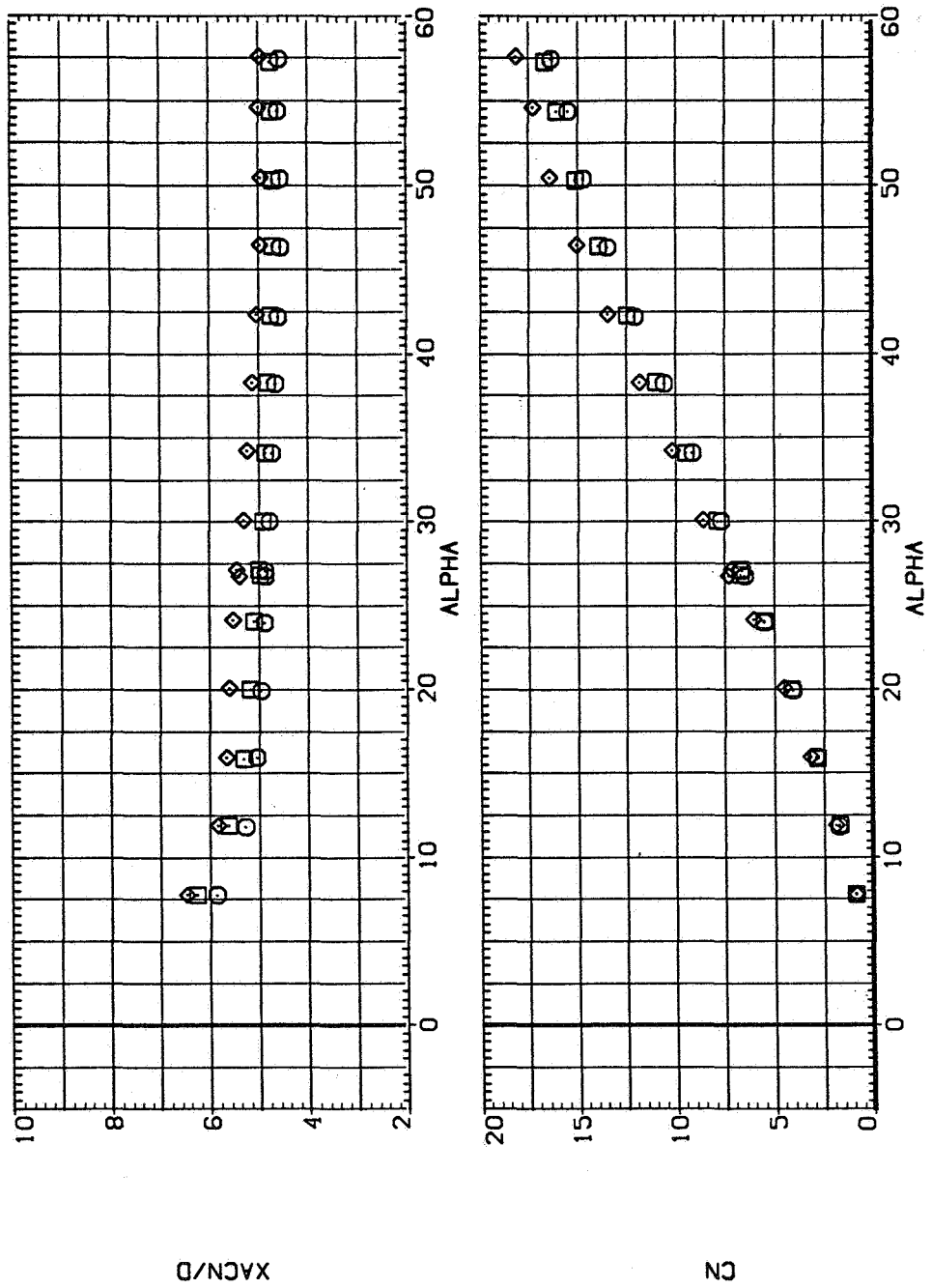
Cn

(c) C_A and C_n versus α .

Figure 15.— Concluded.

SYMBOL CONFIGURATION DESCRIPTION

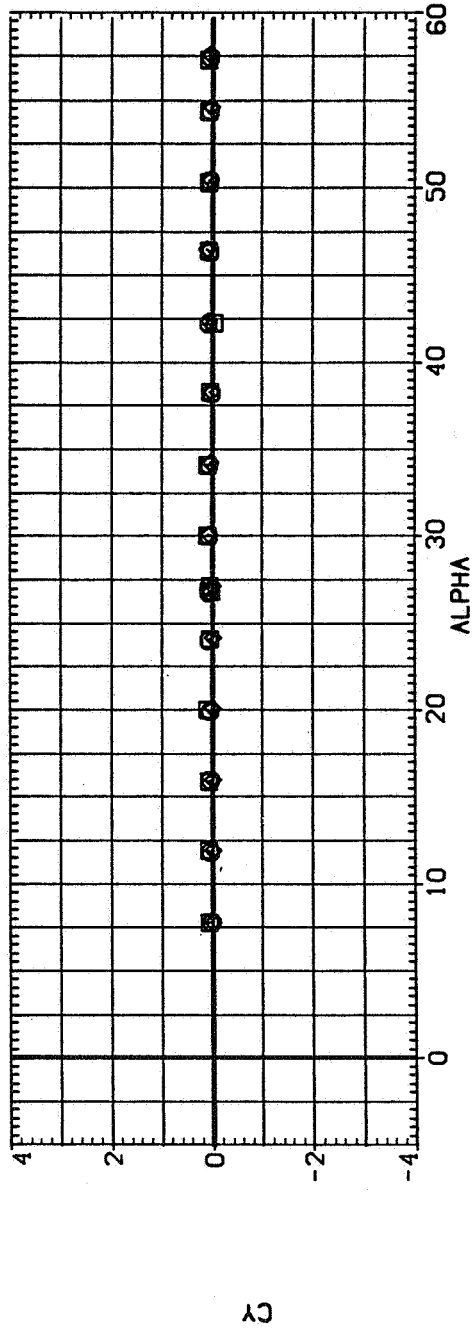
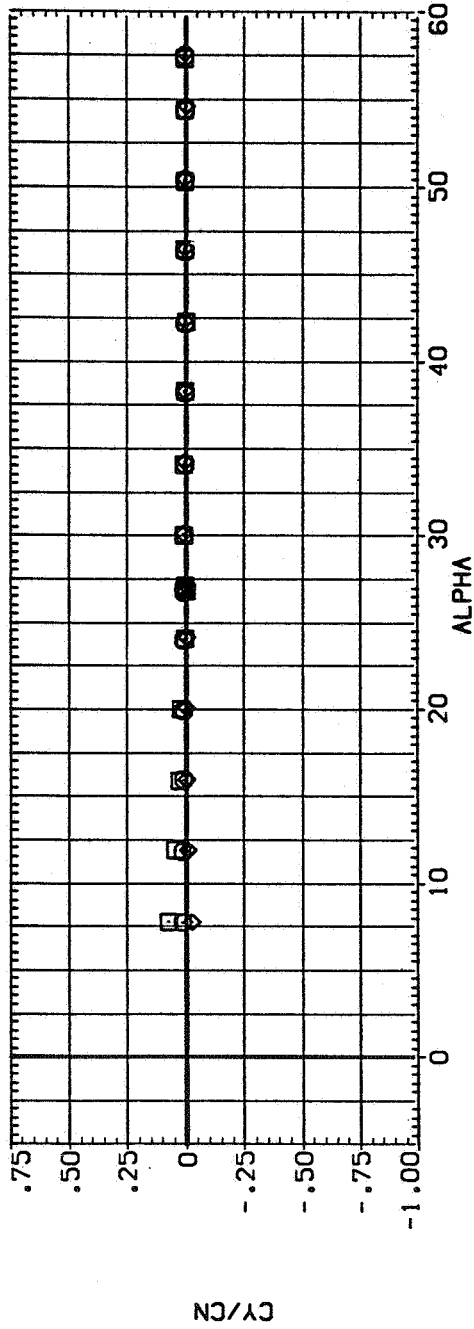
 N
 S
 S
 N
 S
 S



(a) x_{acN}/d and C_N versus α .

Figure 16.— Effect of nose strokes; $M = 1.5$, $Re = 3.8 \times 10^5$.

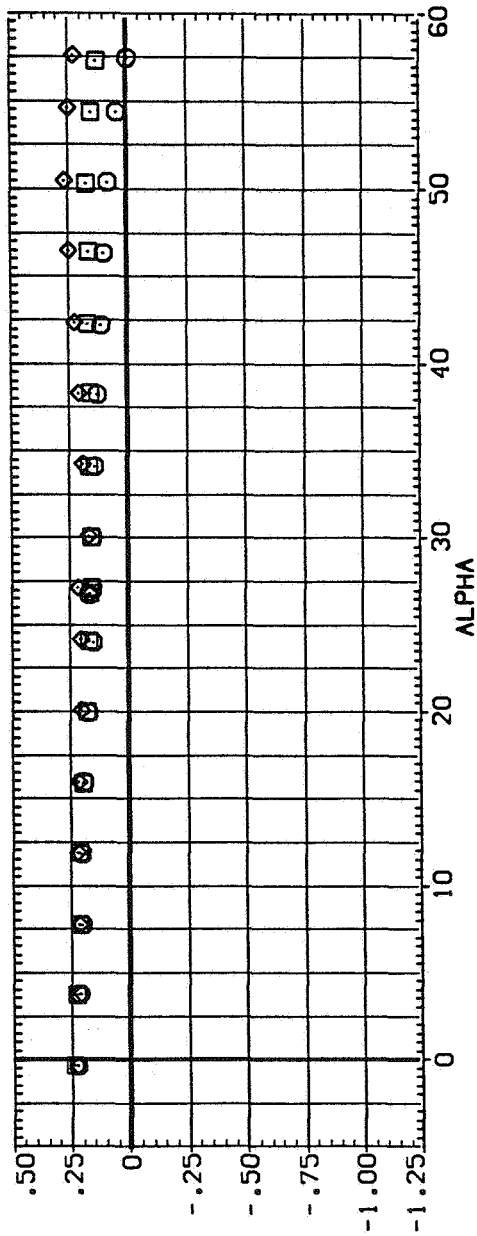
SYMBOL CONFIGURATION DESCRIPTION
 NI CI S
 NS CI S
 NS CI S



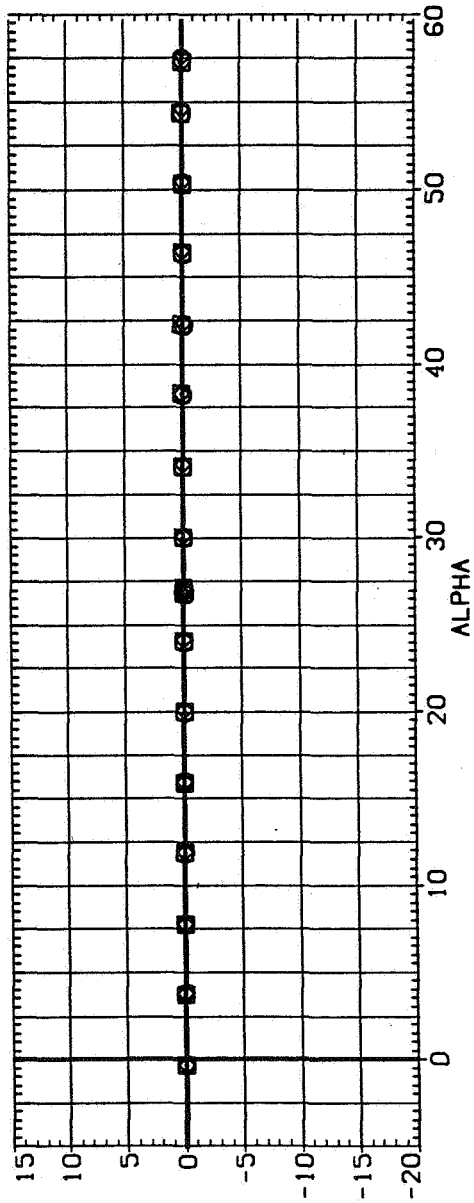
(b) C_Y/C_N and C_Y versus α .

Figure 16.— Continued.

SYMBOL CONFIGURATION DESCRIPTION
 NI CI S
 NS CI S
 NS CI S



CA

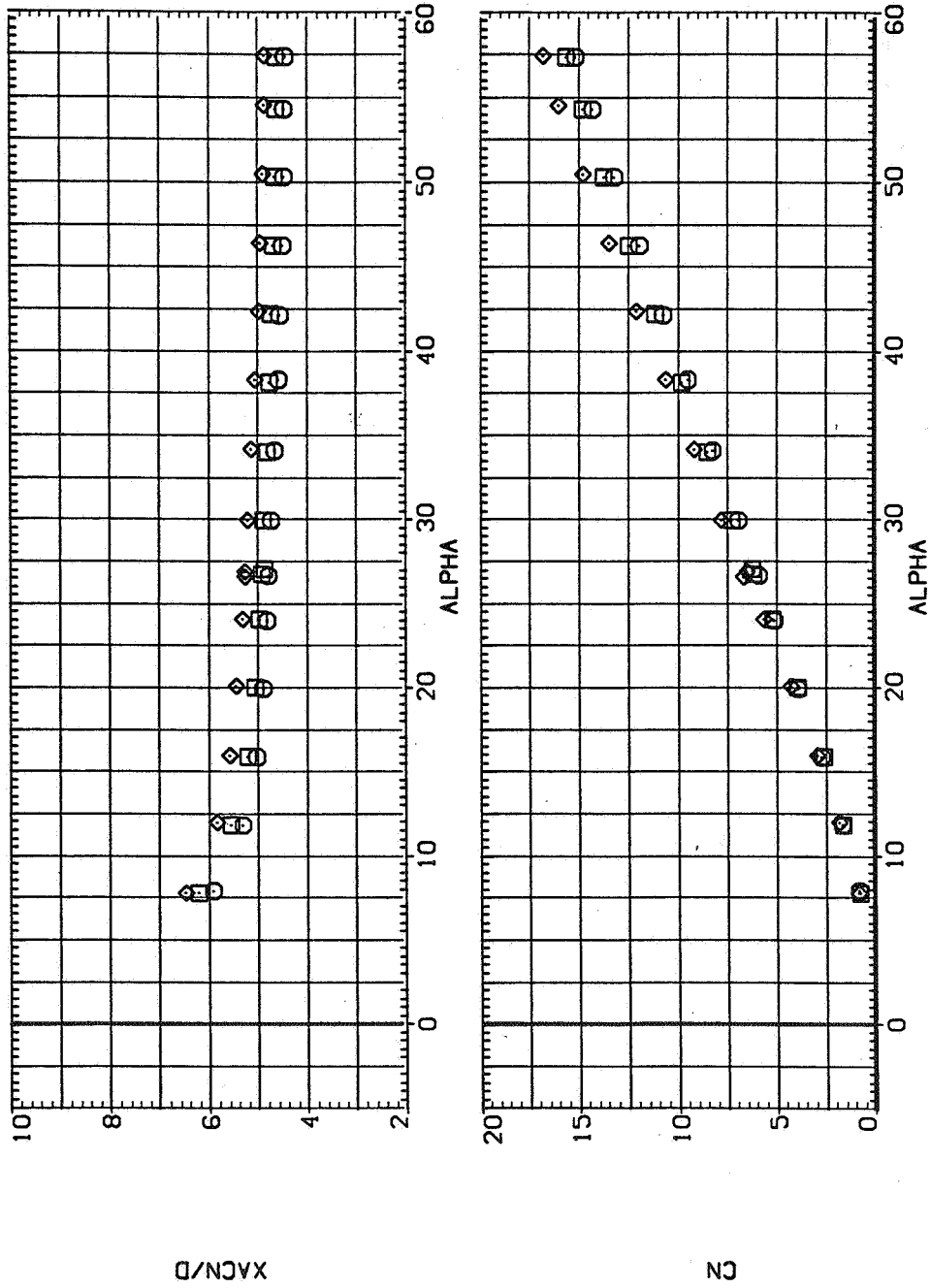


CYN

(c) C_A and C_n versus α .

Figure 16.— Concluded.

SYMBOL CONFIGURATION DESCRIPTION
 NI CI S
 NS CI S
 NS CI S

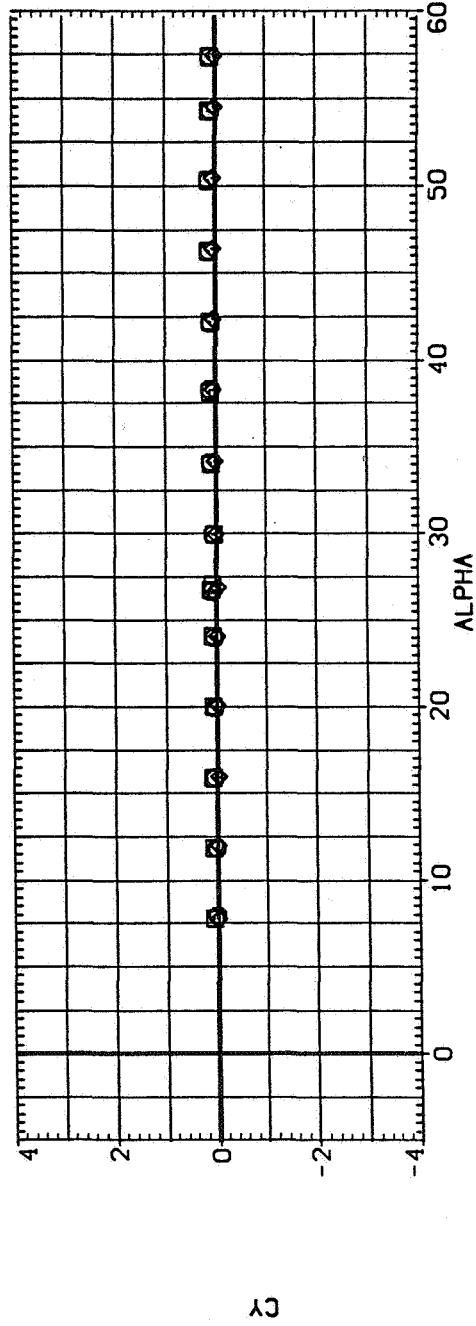
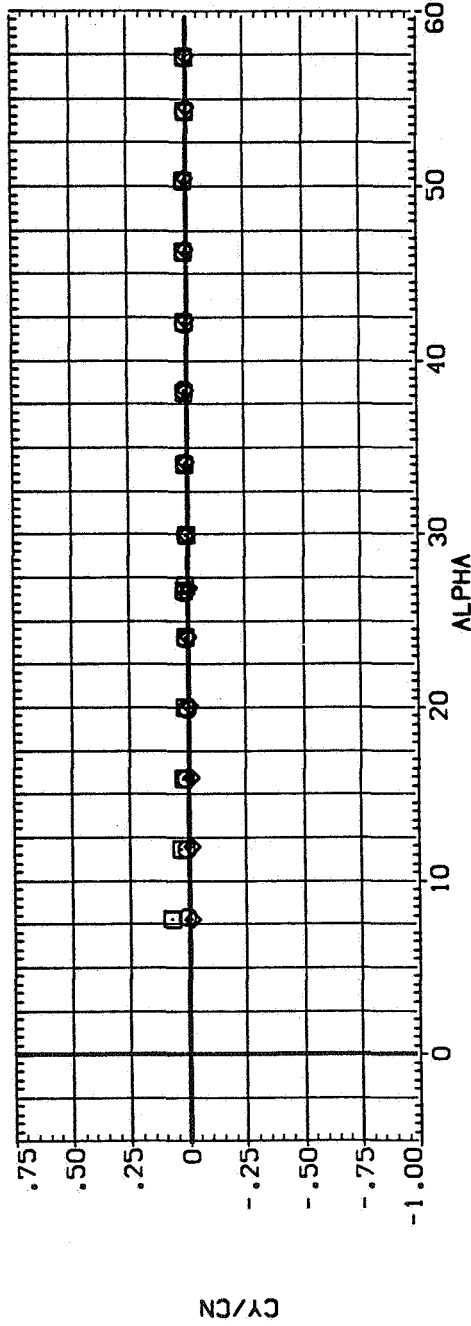


(a) x_{acN}/d and C_N versus α .

Figure 17.— Effect of nose strokes; $M = 2.0$, $Re = 3.8 \times 10^5$.

SYMBOL CONFIGURATION DESCRIPTION

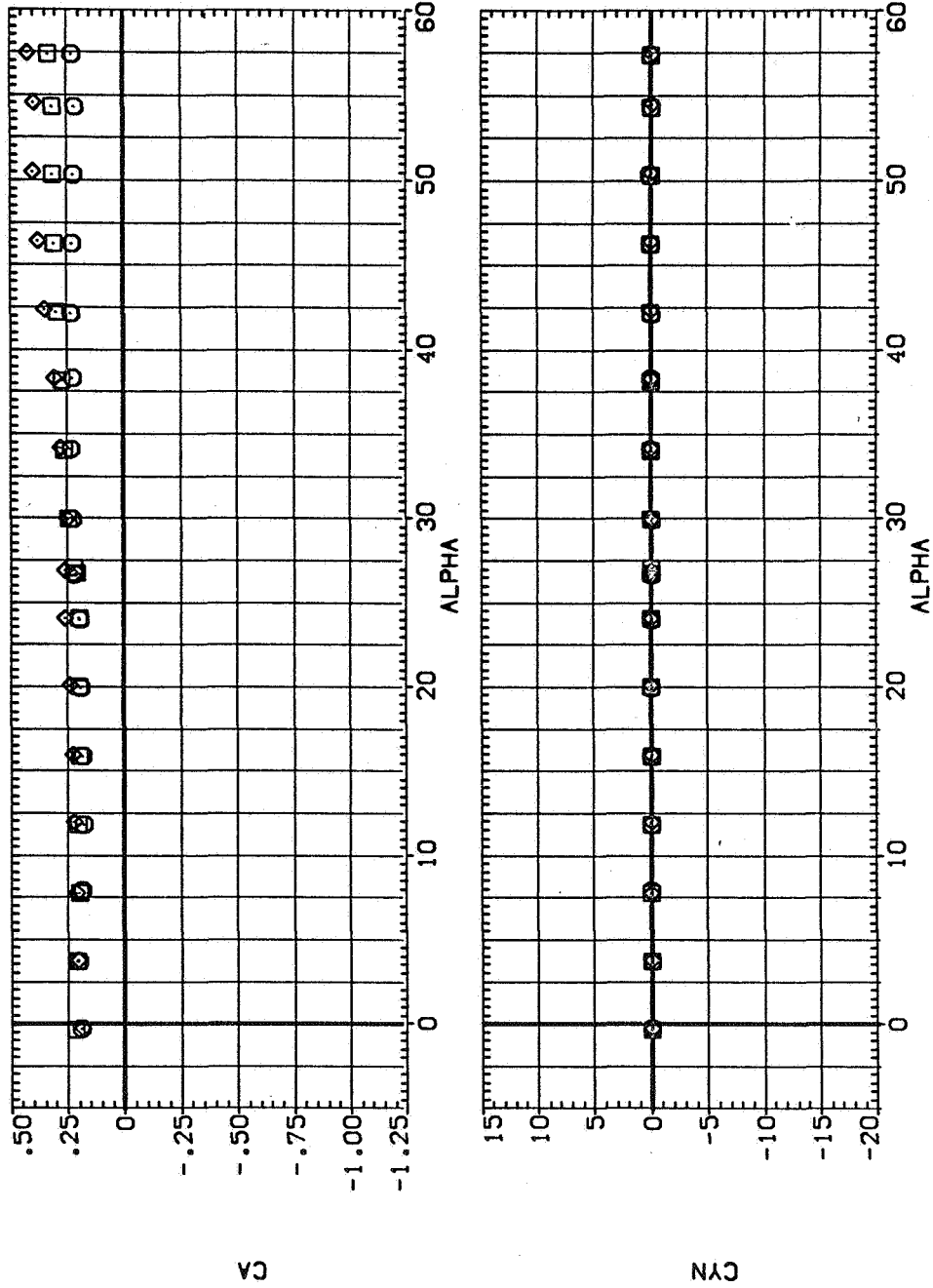
\square NI Cl S
 \diamond NS Cl S
 \circ NS Cl S



(b) C_Y/C_N and C_Y versus α .

Figure 17.— Continued.








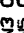
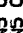
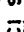
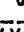
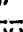
SYMBOL CONFIGURATION DESCRIPTION
 NI CI S
 NS CI S
 NS CI S

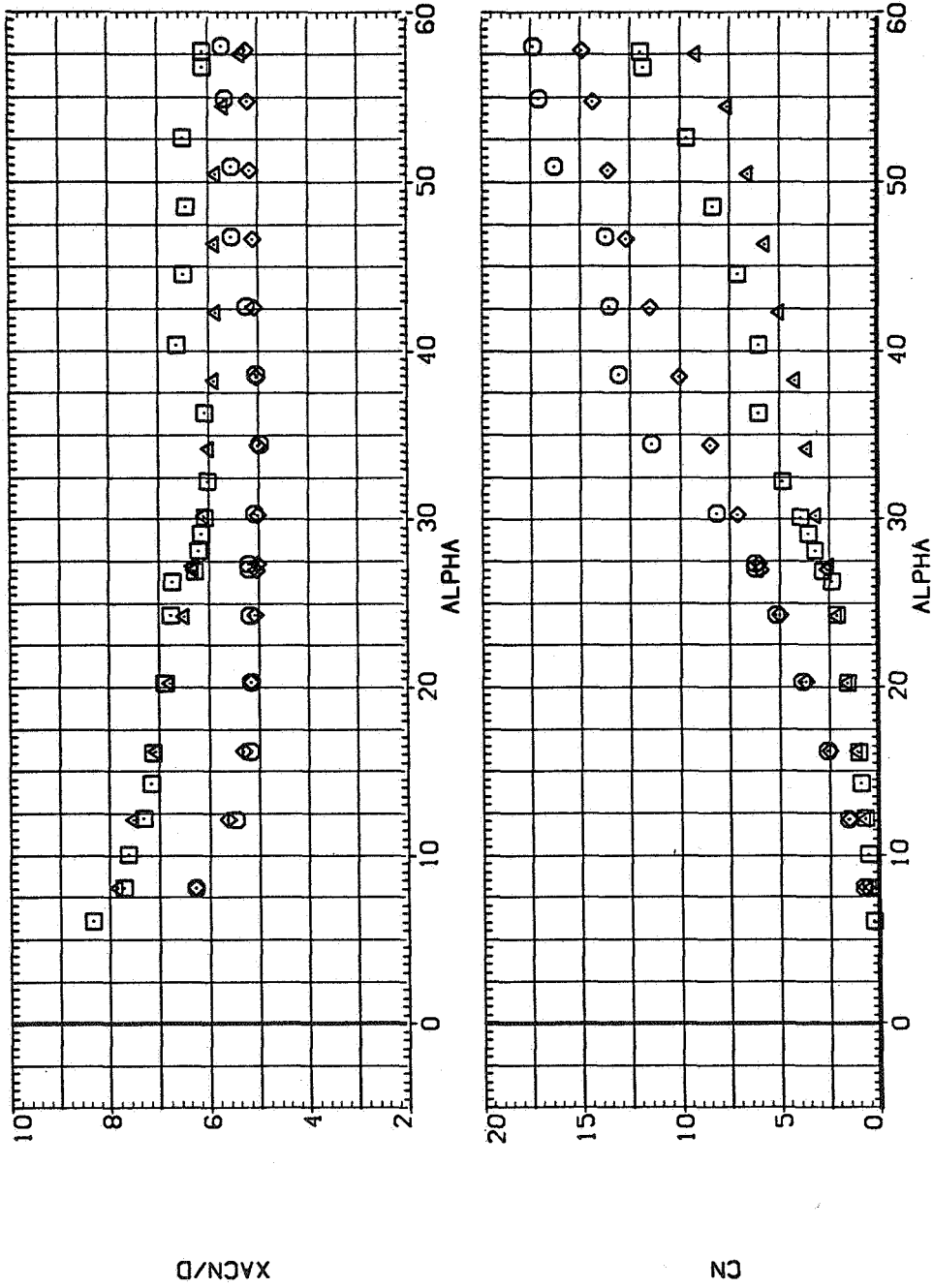


(c) C_A and C_η versus α .

Figure 17.— Concluded.

SYMBOL CONFIGURATION DESCRIPTION

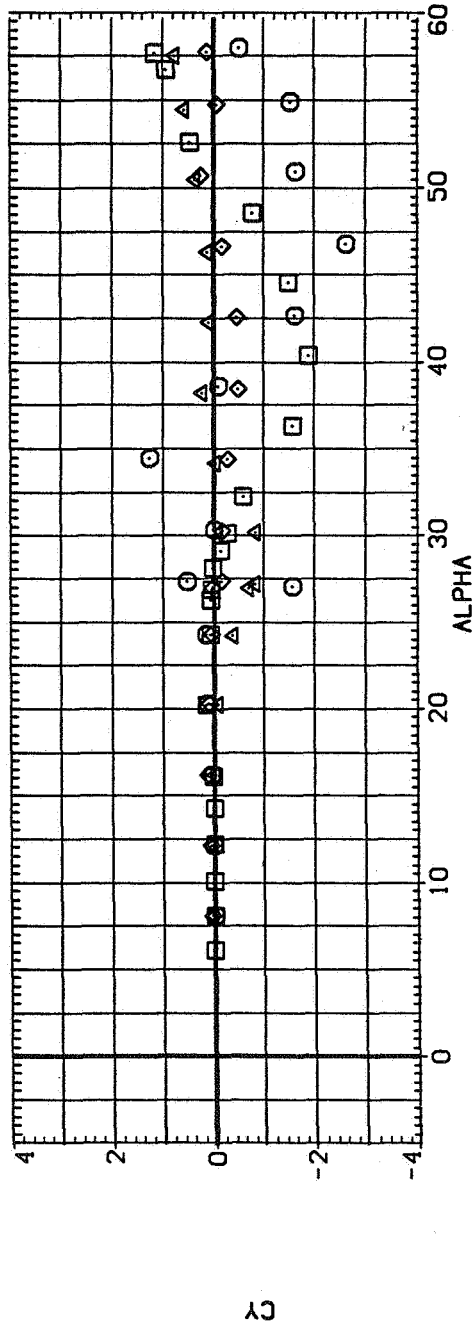
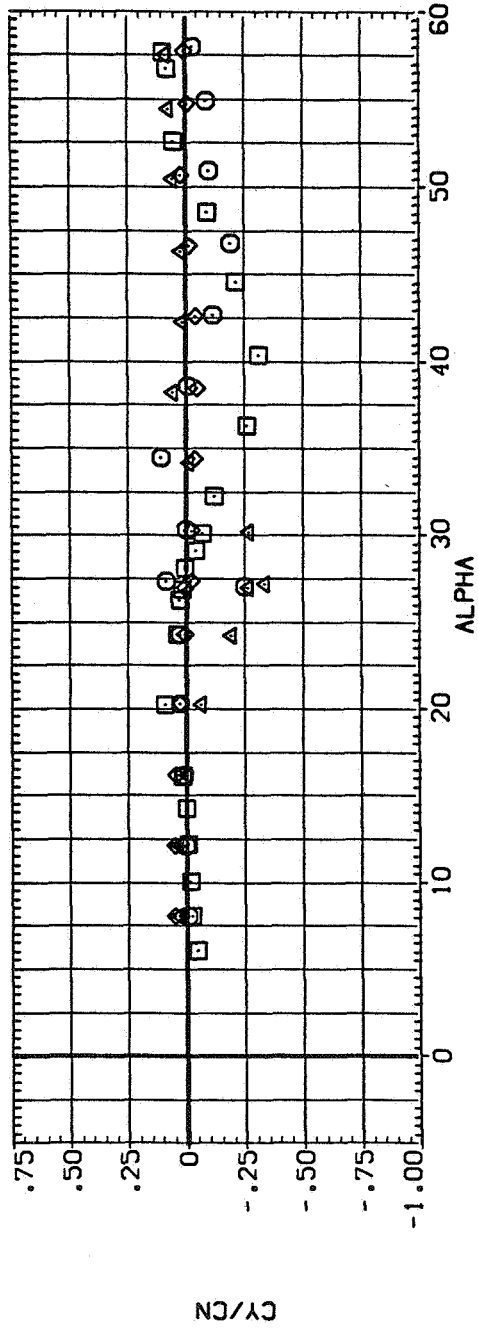
 NS
 CI
 S
 NS
 CI
 S
 NS
 CI
 S
 NS
 CI
 S



(a) x_{acN}/d and C_N versus α .

Figure 18.— Effect of removing strakes from body, $M = 0.6$, $Re = 6.5 \times 10^5$.

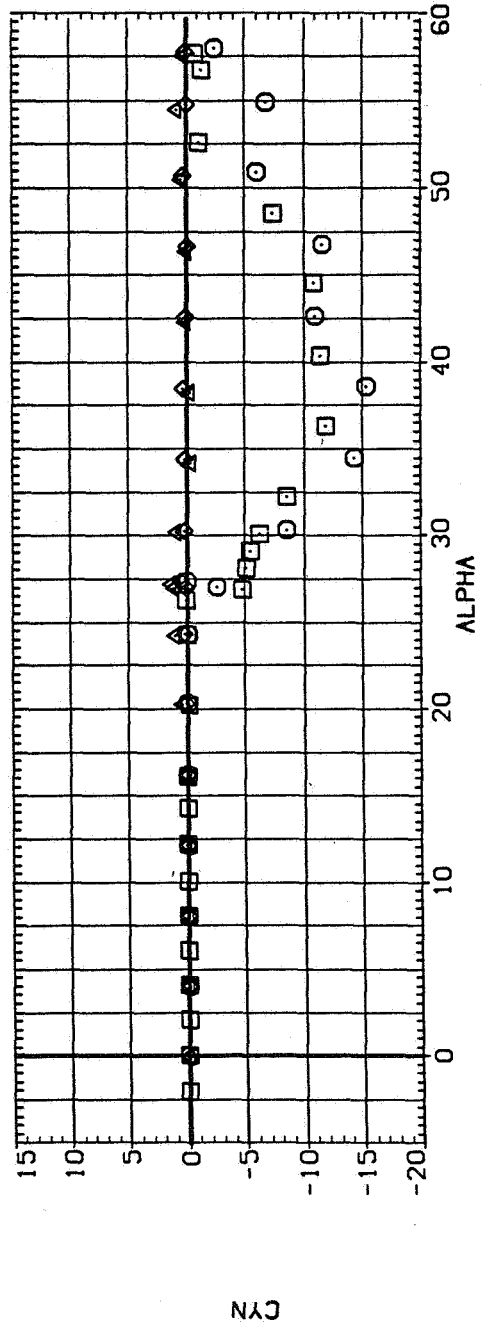
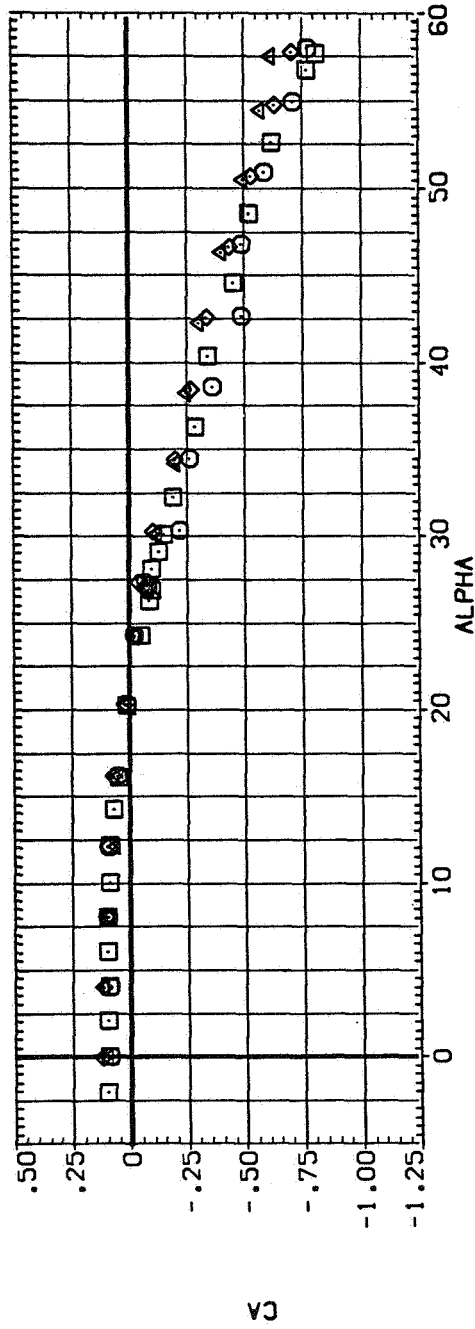
SYMBOL CONFIGURATION DESCRIPTION
 ○ N3 C1 S
 □ N3 C1 S
 △ N5 C1 S
 ⊗ N5 C1 S



(b) C_Y/C_N and C_Y versus α .

Figure 18.— Continued.

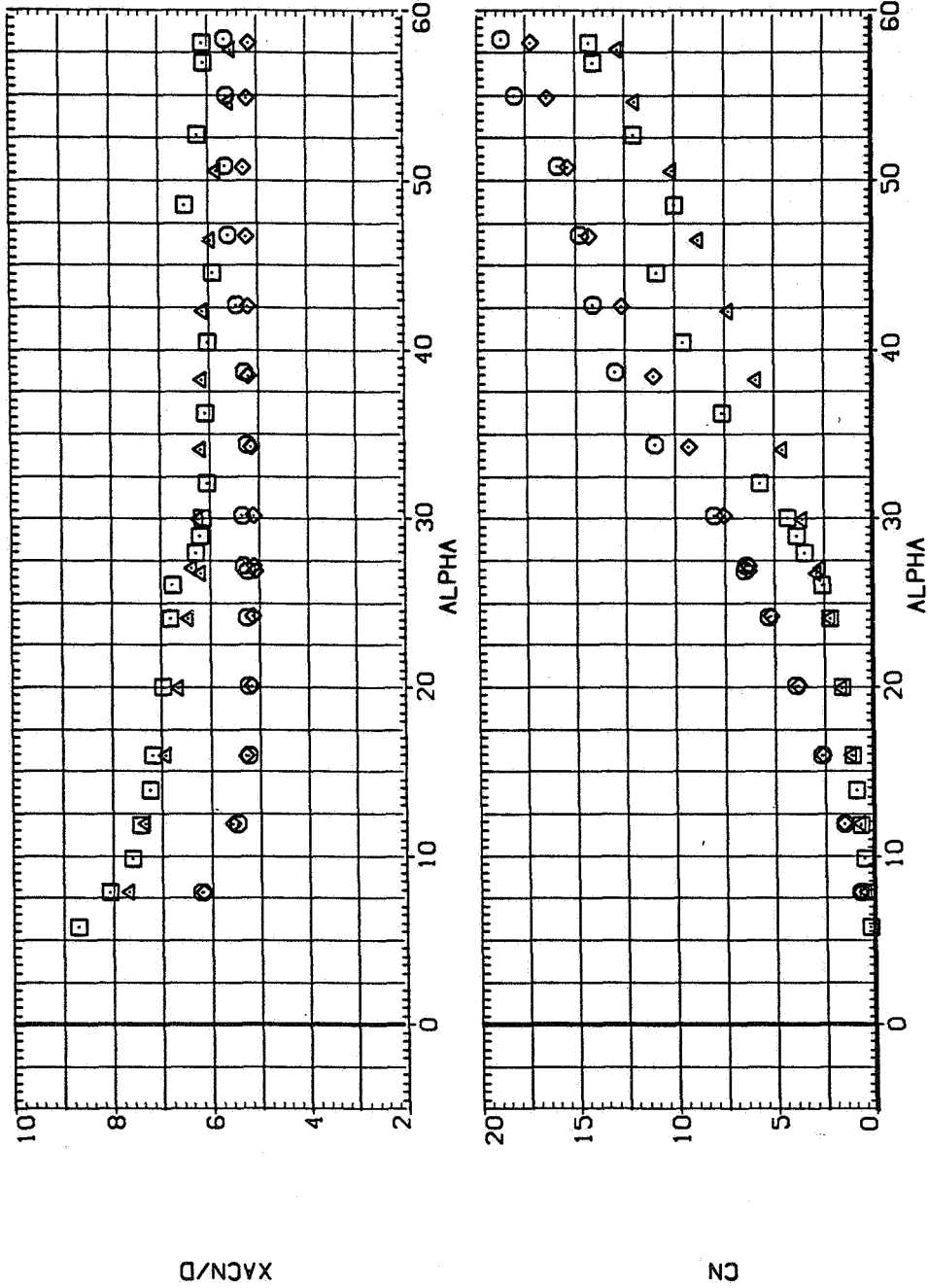
SYMBOL CONFIGURATION DESCRIPTION
 □ N3 C1 S
 ○ N3 C1 S
 △ N5 C1 S
 ◇ N5 C1



(c) C_A and C_n versus α .

Figure 18.— Concluded.

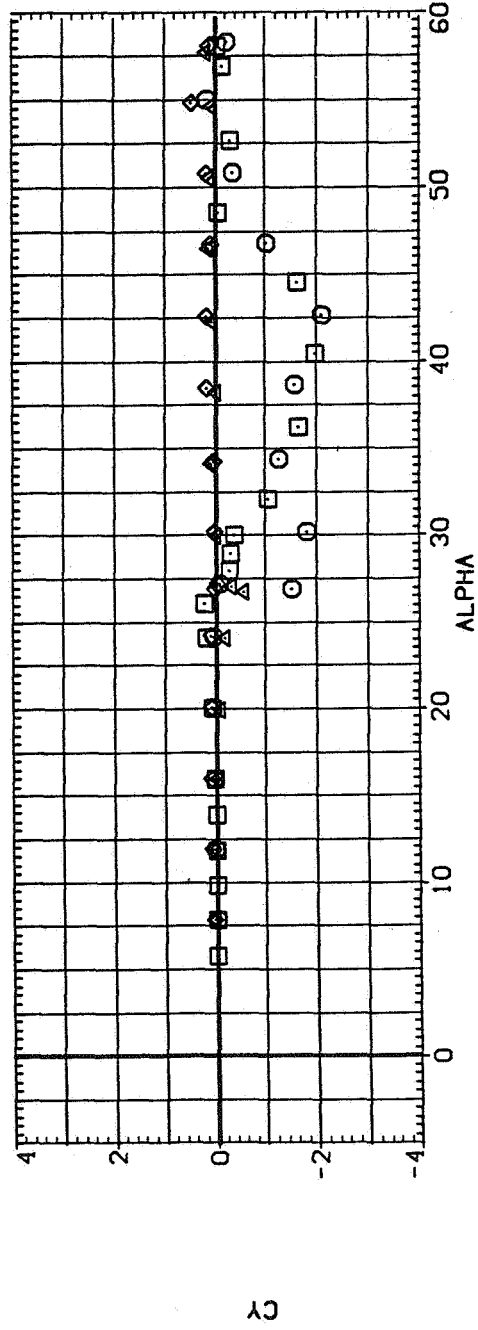
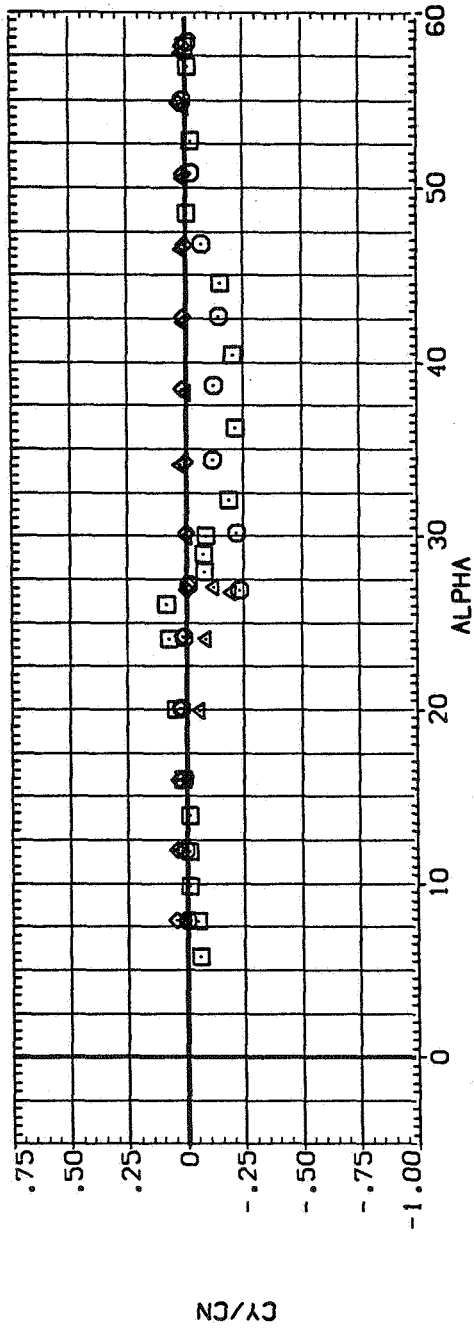
SYMBOL CONFIGURATION DESCRIPTION
 □ N3 CI S
 △ N3 CI S
 ○ N5 CI S
 ⊗ N5 CI



(a) x_{acN}/d and C_N versus α .

Figure 19.— Effect of removing strakes from body; $M = 0.9$, $Re = 6.5 \times 10^5$.

SYMBOL CONFIGURATION DESCRIPTION
 □ N3 C1 S
 ○ N3 C1 S
 △ N6 C1 S
 × N6 C1 S

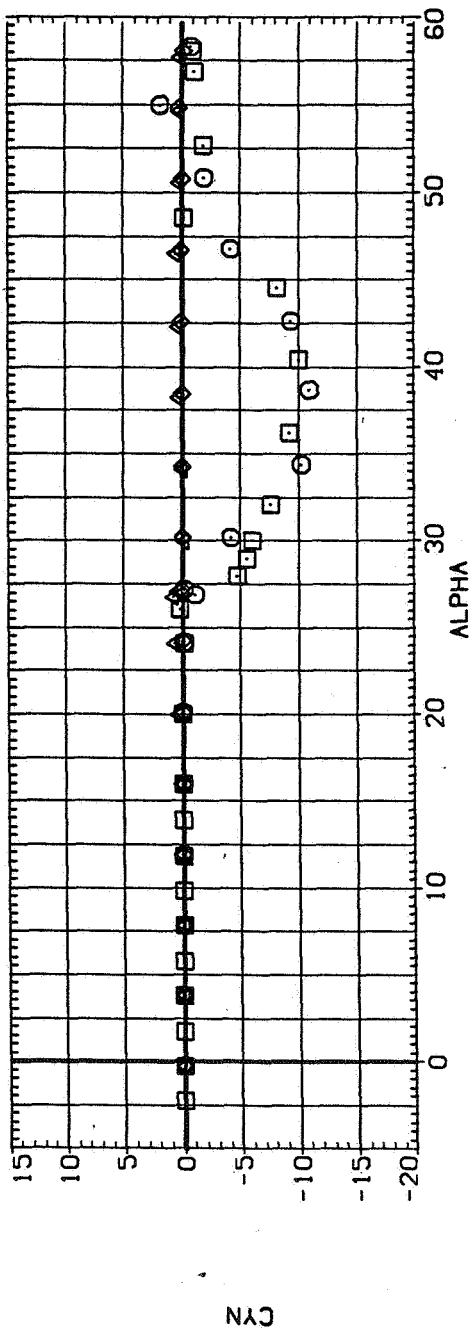
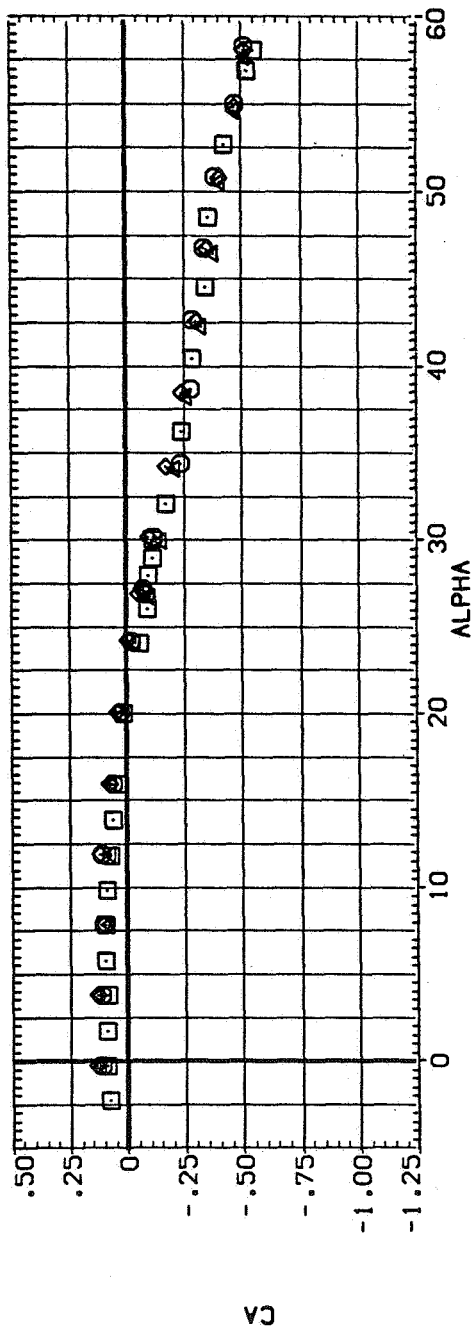


(b) C_Y/C_N and C_Y versus α .

Figure 19.— Continued.

SYMBOL CONFIGURATION DESCRIPTION

\square N3 Cl S
 \circ N3 Cl S
 \triangle N5 Cl S
 \times N5 Cl S

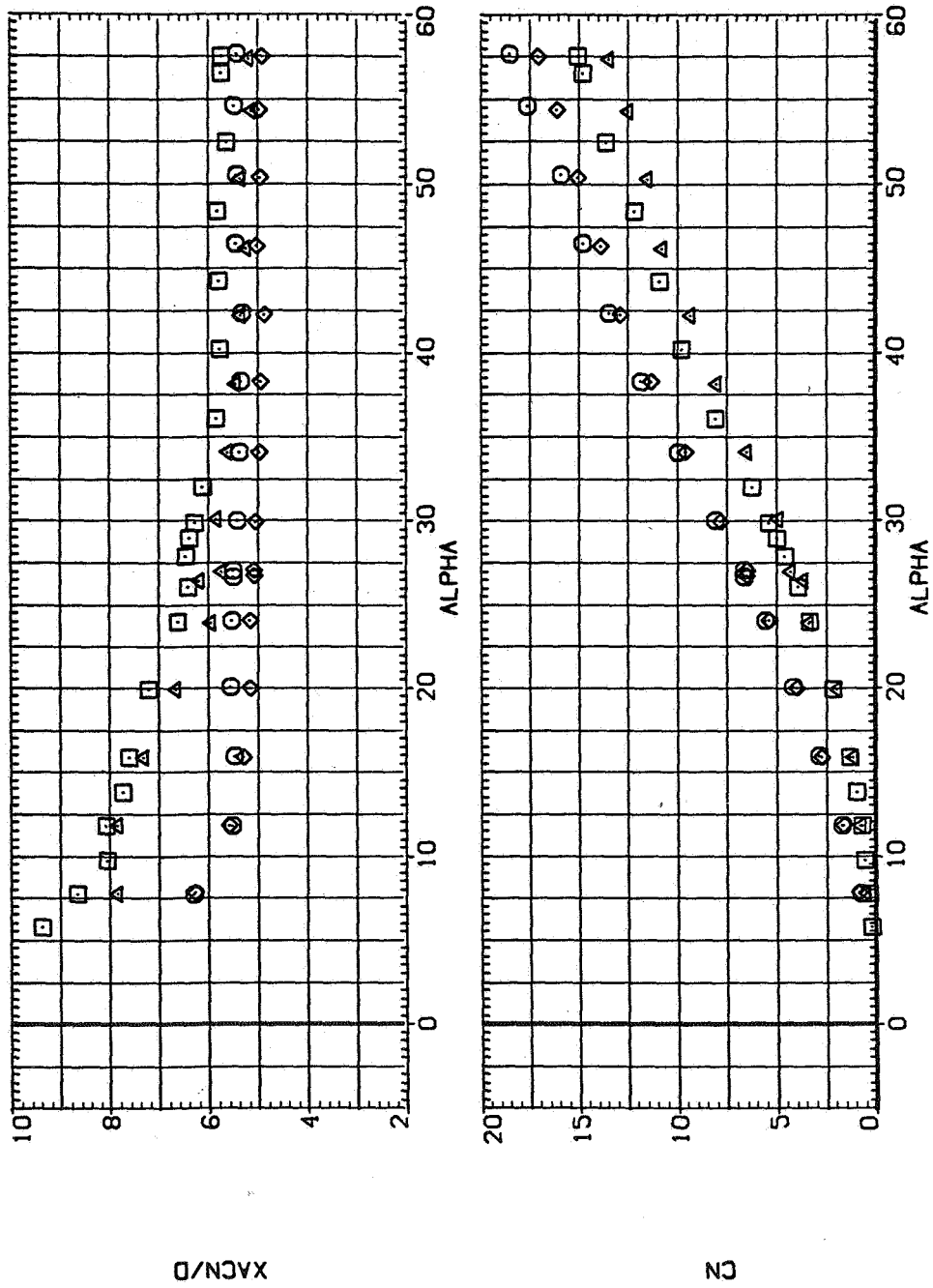


(c) C_A and C_{η} versus α .

Figure 19.— Concluded.

SYMBOL CONFIGURATION DESCRIPTION

\square N3 C1 S
 \triangle N3 C1 S
 \circ N5 C1 S
 \diamond N5 C1

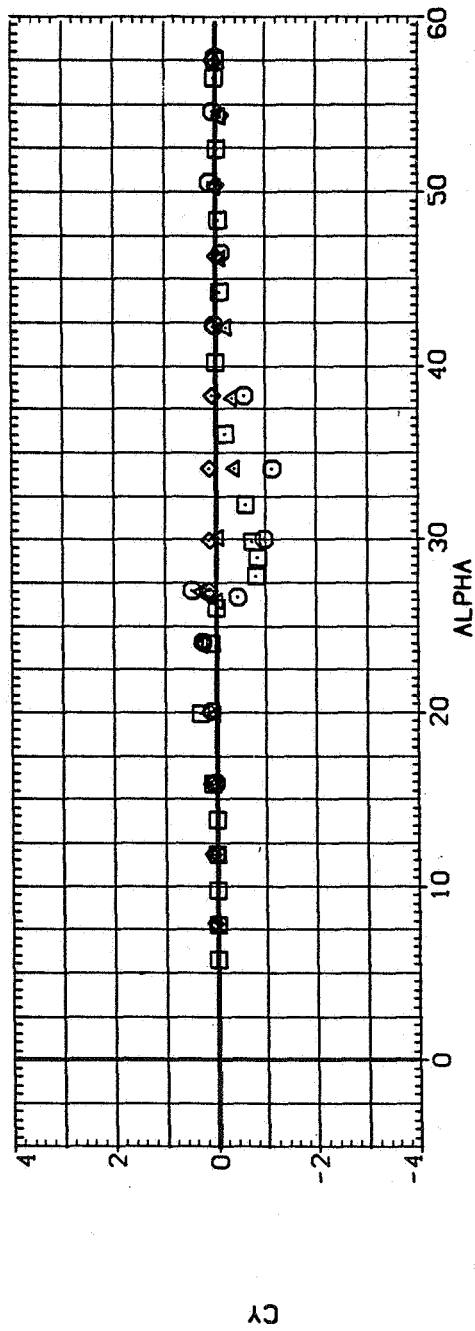
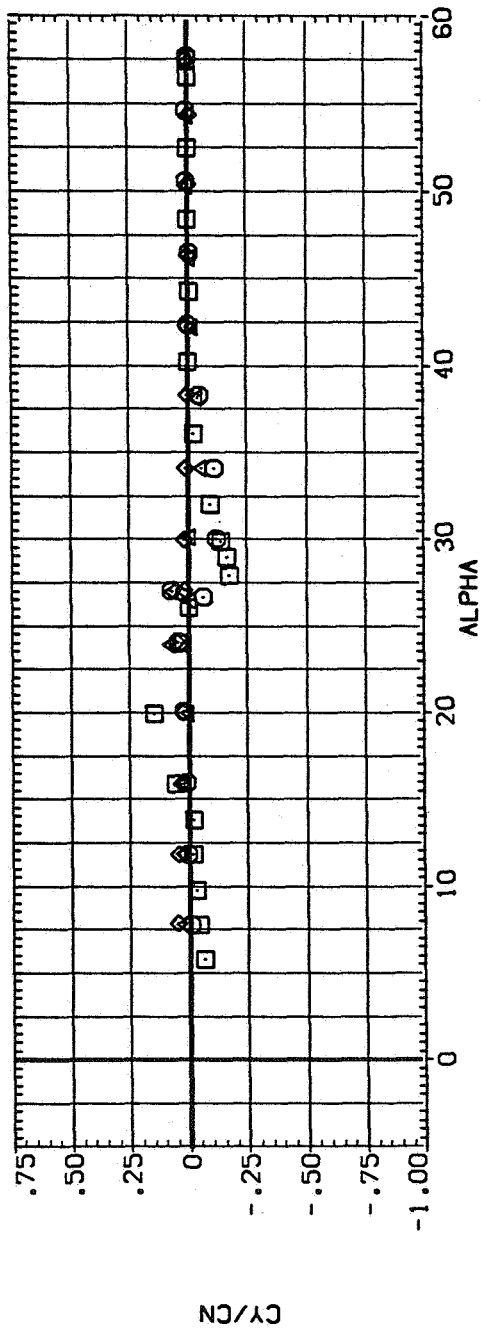


(a) x_{acN}/d and C_N versus α .

Figure 20.— Effect of removing strakes from body; $M = 1.2, Re = 3.8 \times 10^5$.

SYMBOL CONFIGURATION DESCRIPTION

○ N3 CI S
□ N3 CI S
△ N3 CI S
◇ N3 CI S

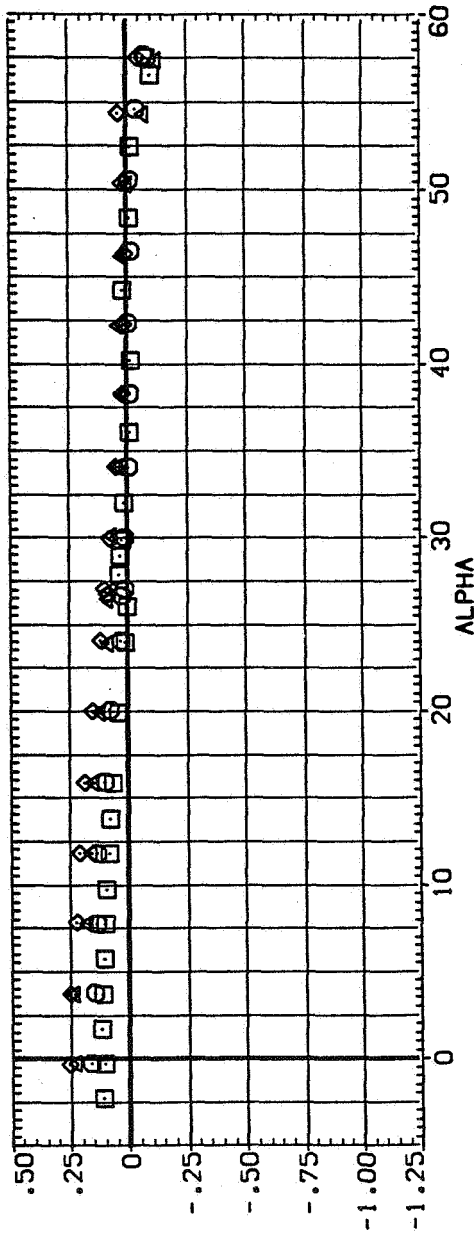


(b) C_Y/C_N and C_Y versus α .

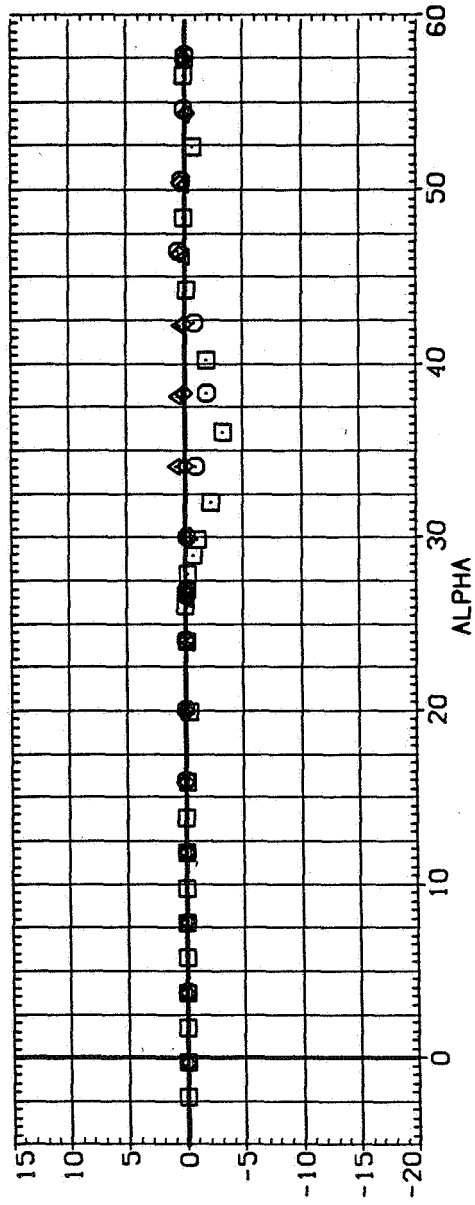
Figure 20. - Continued.

SYMBOL CONFIGURATION DESCRIPTION

- N3 C1 S
- N3 C1 S
- N5 C1 S
- N5 C1 S



CA



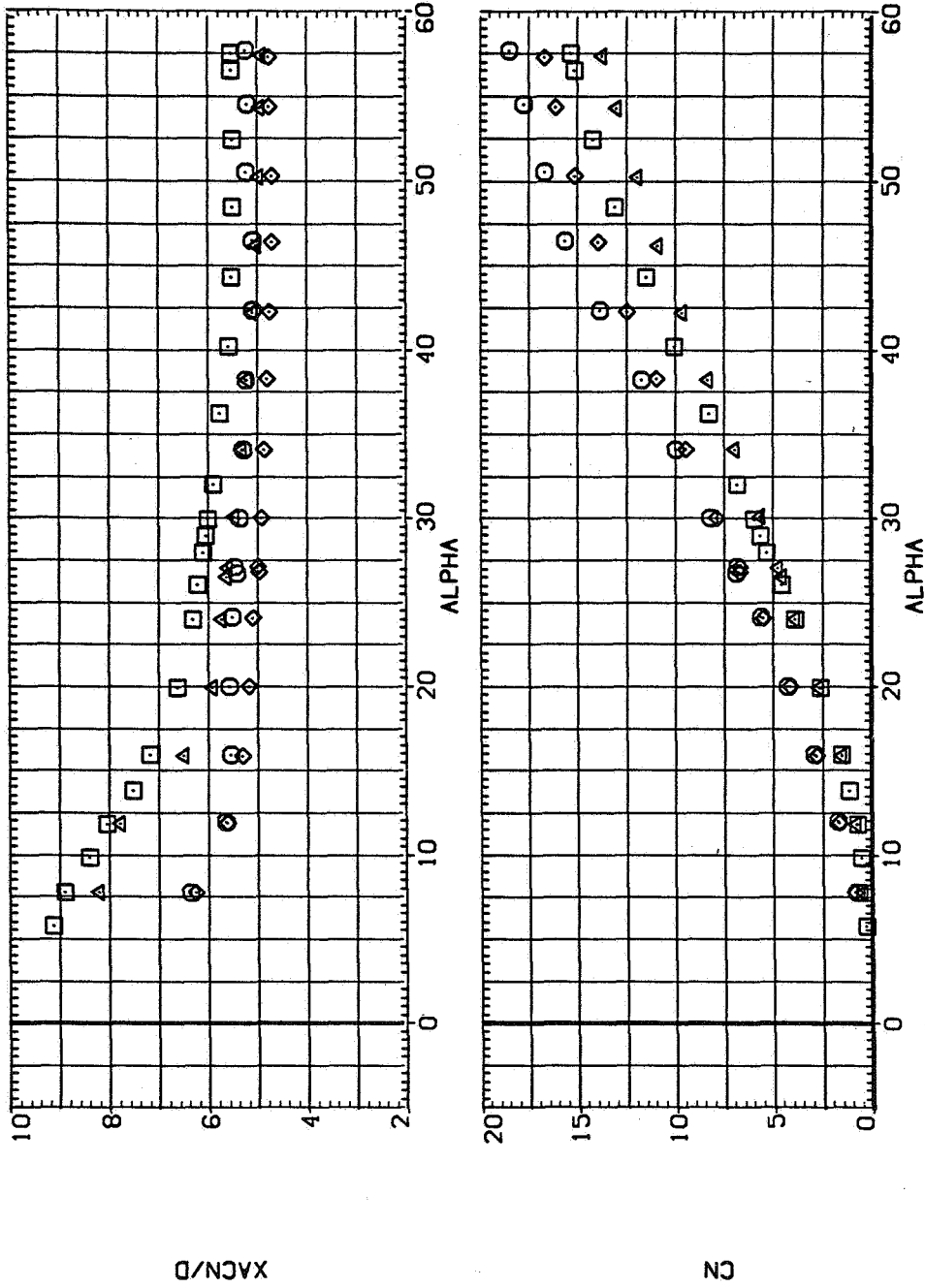
CYN

(c) C_A and C_n versus α .

Figure 20.- Concluded.

SYMBOL CONFIGURATION DESCRIPTION

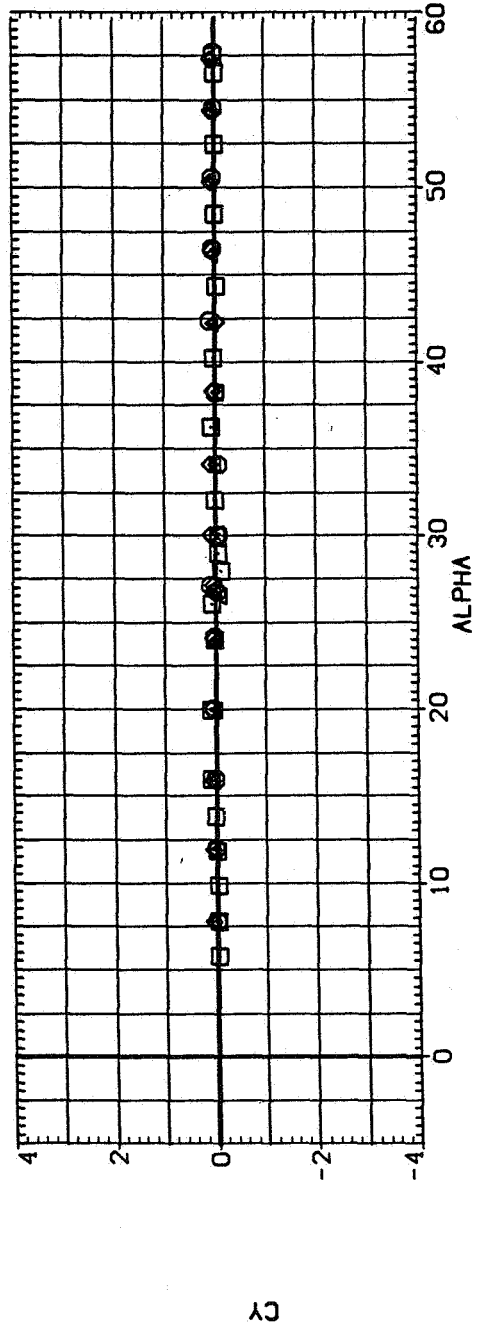
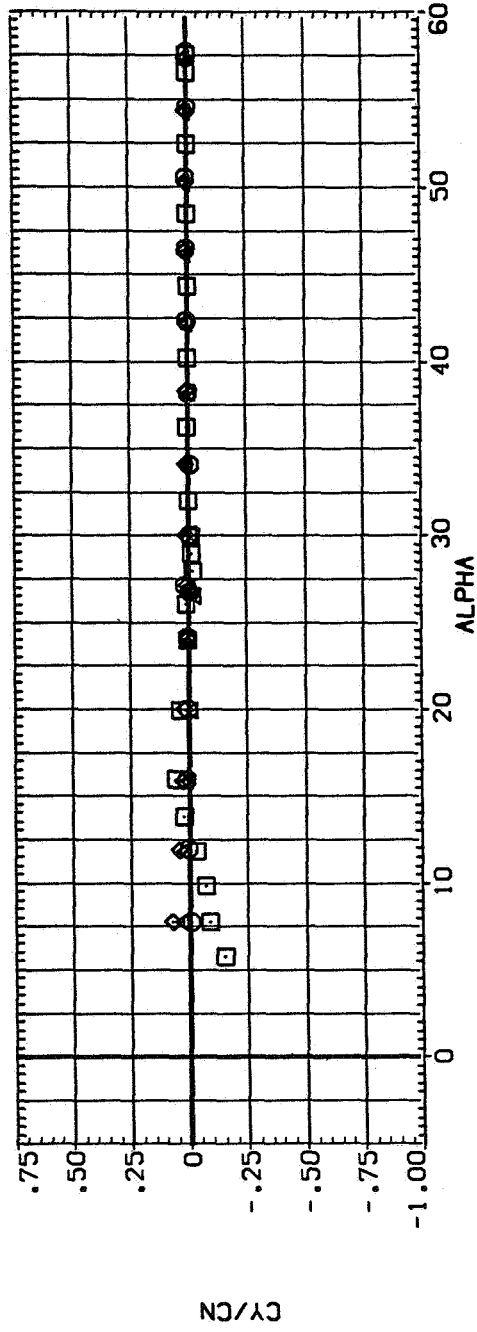
\square N3 CI S
 \triangle N3 CI S
 \circ N5 CI S
 \diamond N5 CI S



(a) x_{ac_N}/d and C_N versus α .

Figure 21.— Effect of removing strakes from body; $M = 1.5$, $Re = 3.8 \times 10^5$.

SYMBOL CONFIGURATION DESCRIPTION
 □ N3 C1 S
 ○ N2 C1 S
 ⊗ N2 C1 S
 ⊙ N2 C1 S

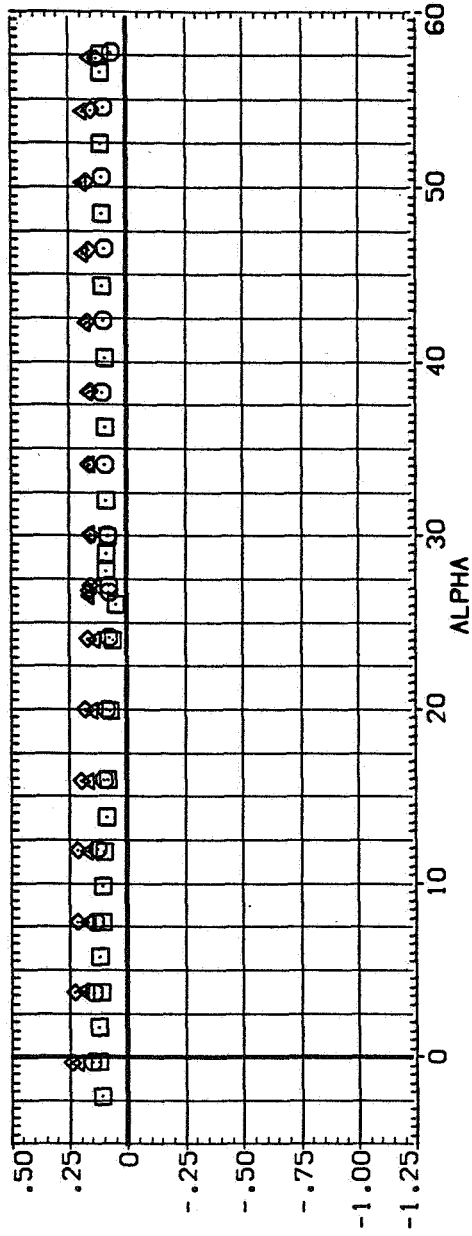


(b) C_Y/C_N and C_Y versus α .

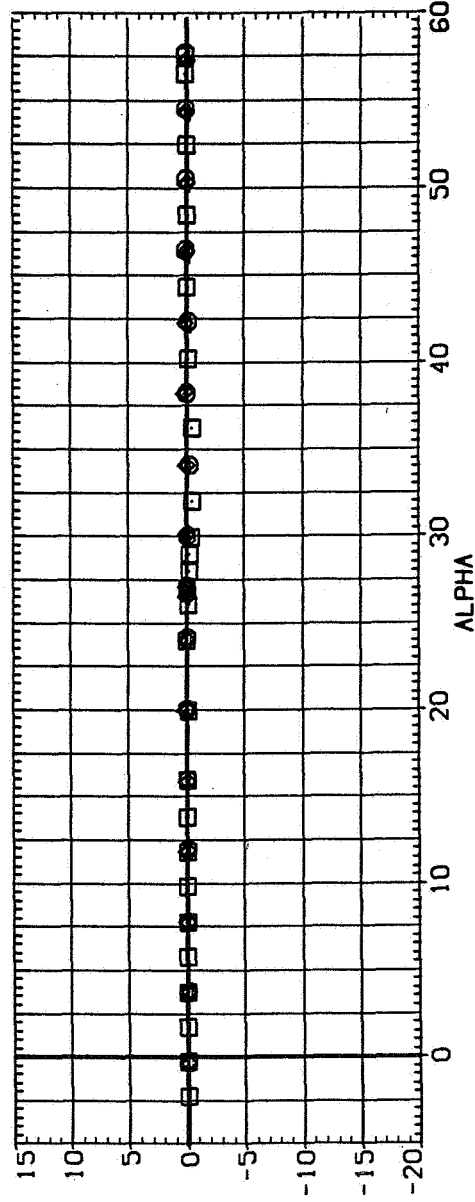
Figure 21.— Continued.

SYMBOL CONFIGURATION DESCRIPTION

 N3 Cl S
 N3 Cl
 N5 Cl S
 N5 Cl



CA

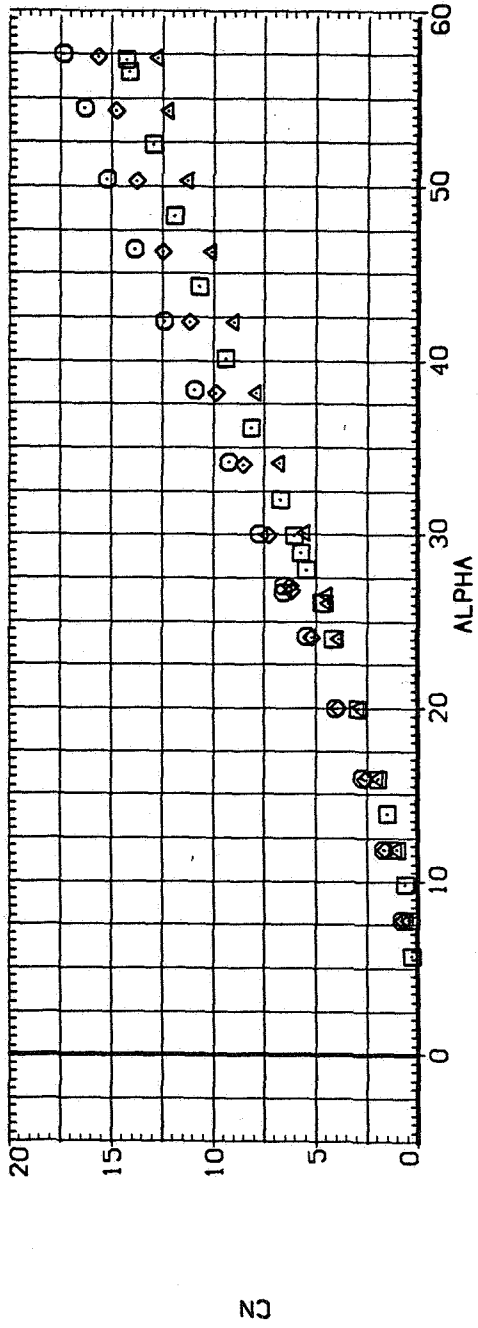
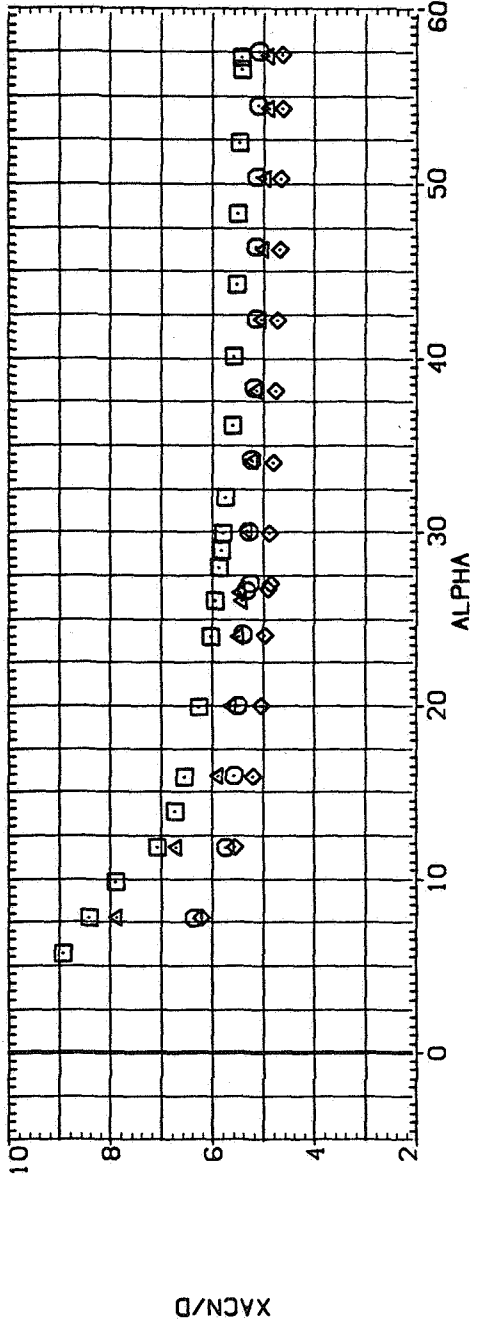


CYN

(c) C_A and C_n versus α .

Figure 21.- Concluded.

SYMBOL CONFIGURATION DESCRIPTION
 □ NS C I S
 ○ NS C I S
 △ NS C I S
 ◇ NS C I S

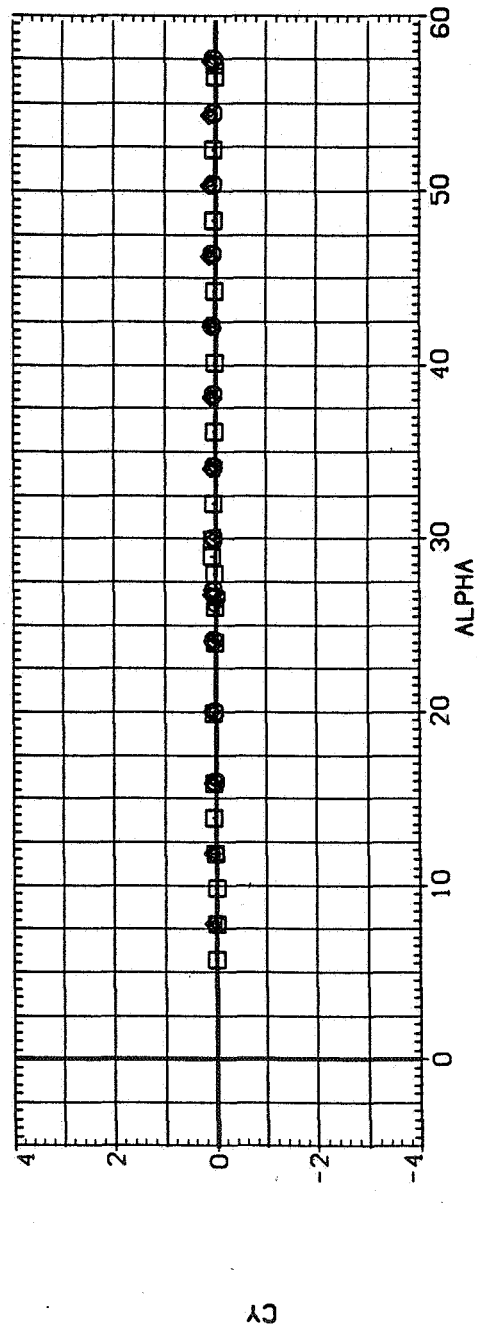
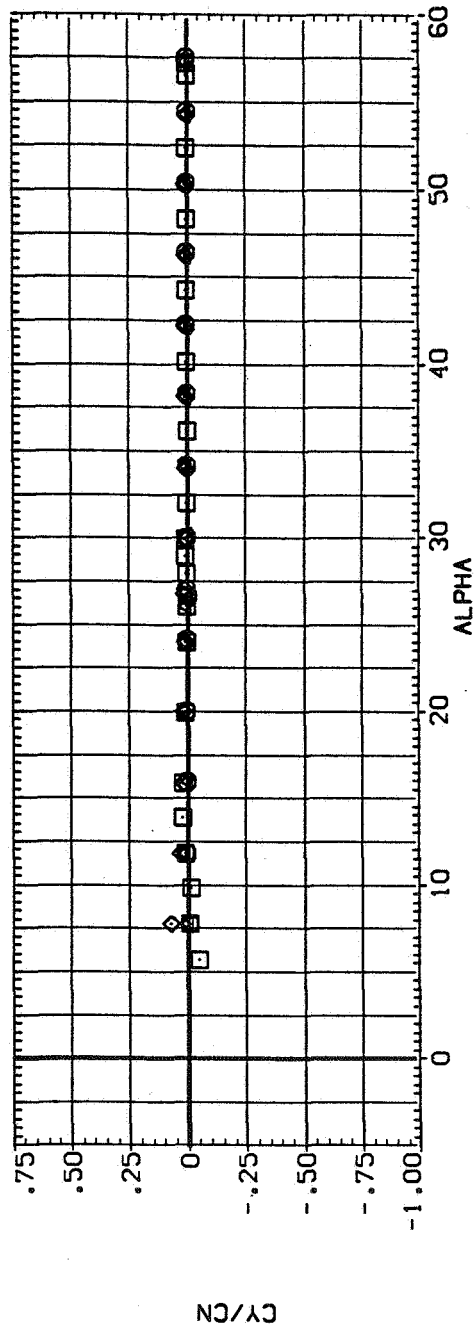


(a) x_{acN}/d and C_N versus α .

Figure 22.— Effect of removing strakes from body; $M = 2.0$, $Re = 3.8 \times 10^5$.

SYMBOL CONFIGURATION DESCRIPTION

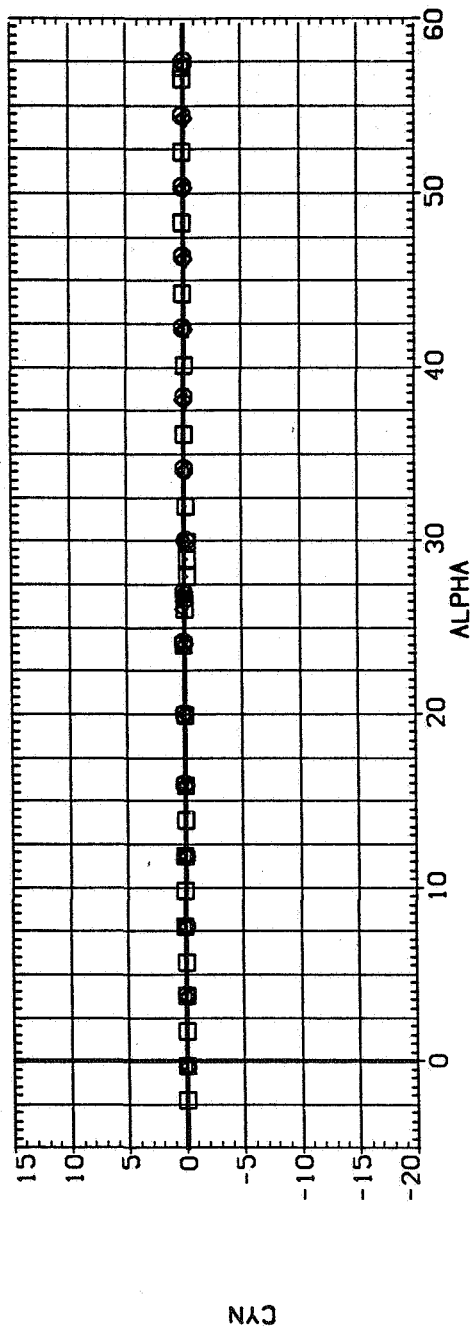
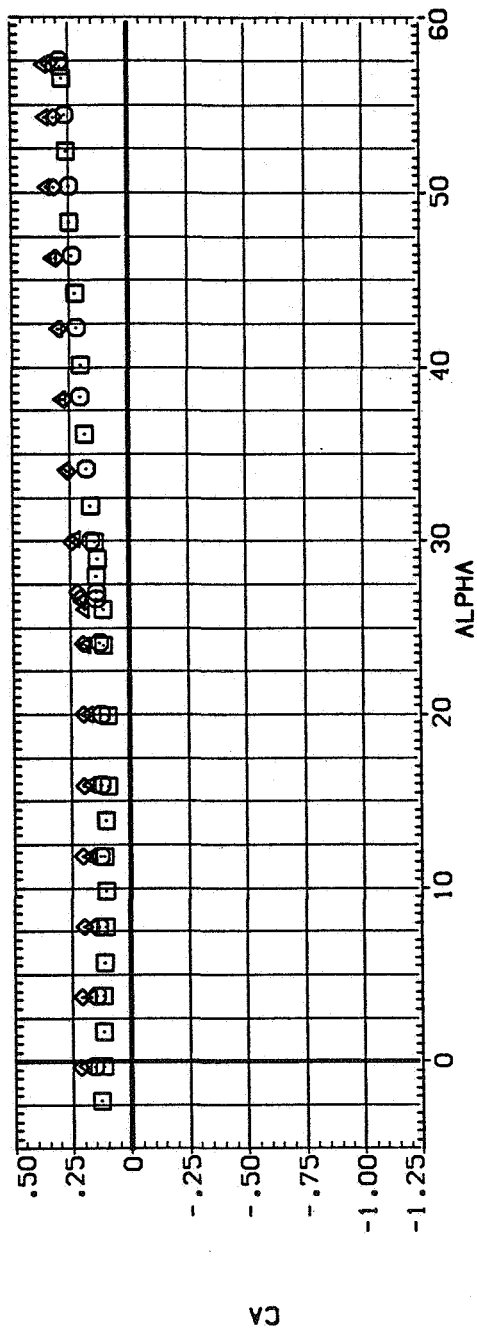
\square NS CI S
 \circ NS CI S
 \times NS CI S



(b) C_Y/C_N and C_Y versus α .

Figure 22.— Continued.

SYMBOL. CONFIGURATION DESCRIPTION
 □ NS CI S
 ○ NS CI S
 ⊗ NS CI S
 ⊙ NS CI S



(c) C_A and C_n versus α .

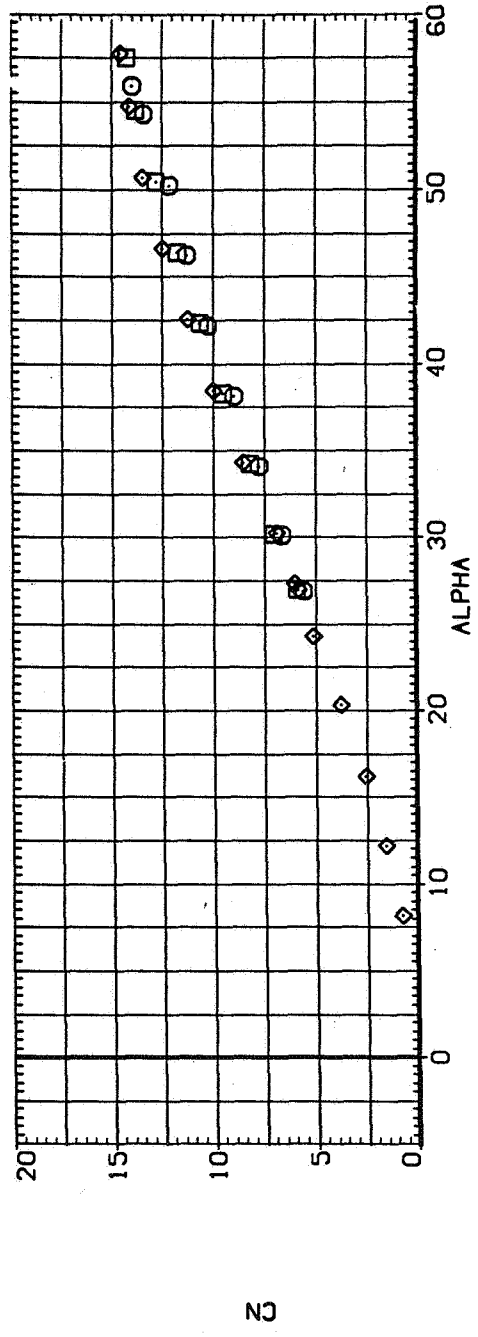
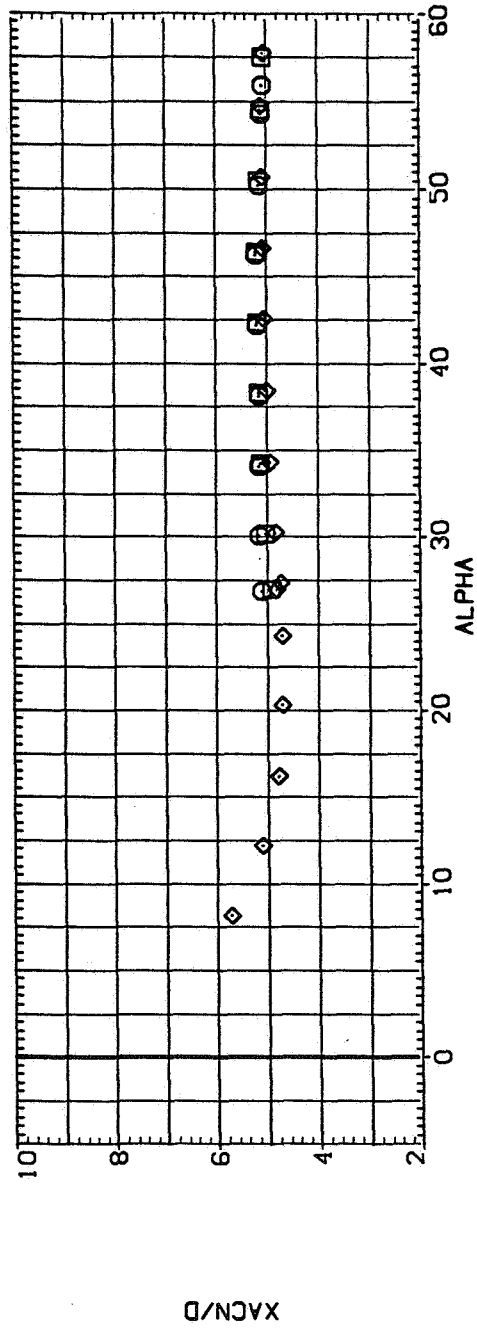
Figure 22. — Concluded.

SYMBOL CONFIGURATION DESCRIPTION

RE 2,200
4,300
6,500

NI CI S
NI CI S
NI CI S

◇
◇
◇

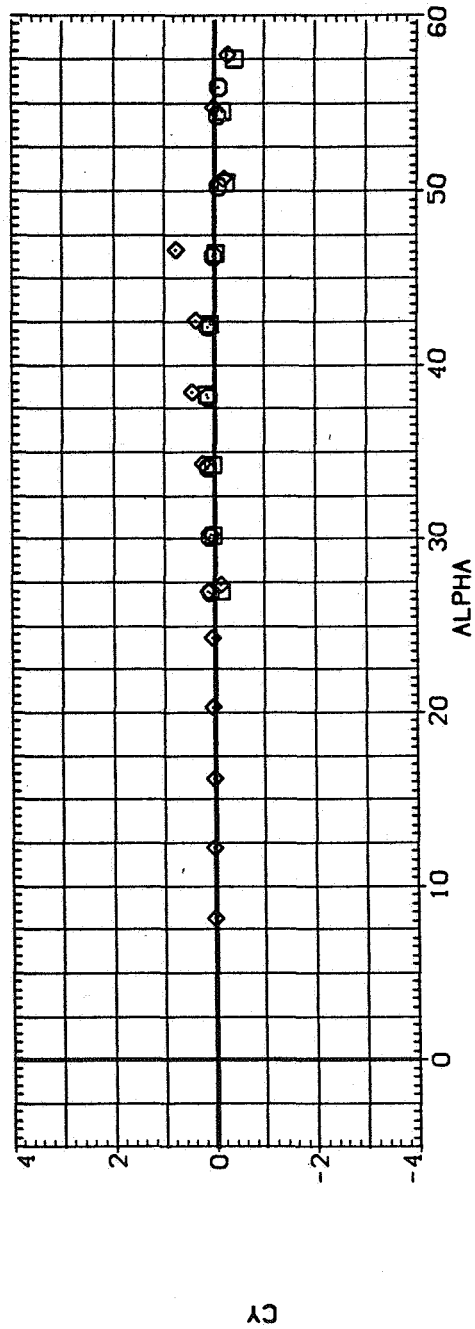
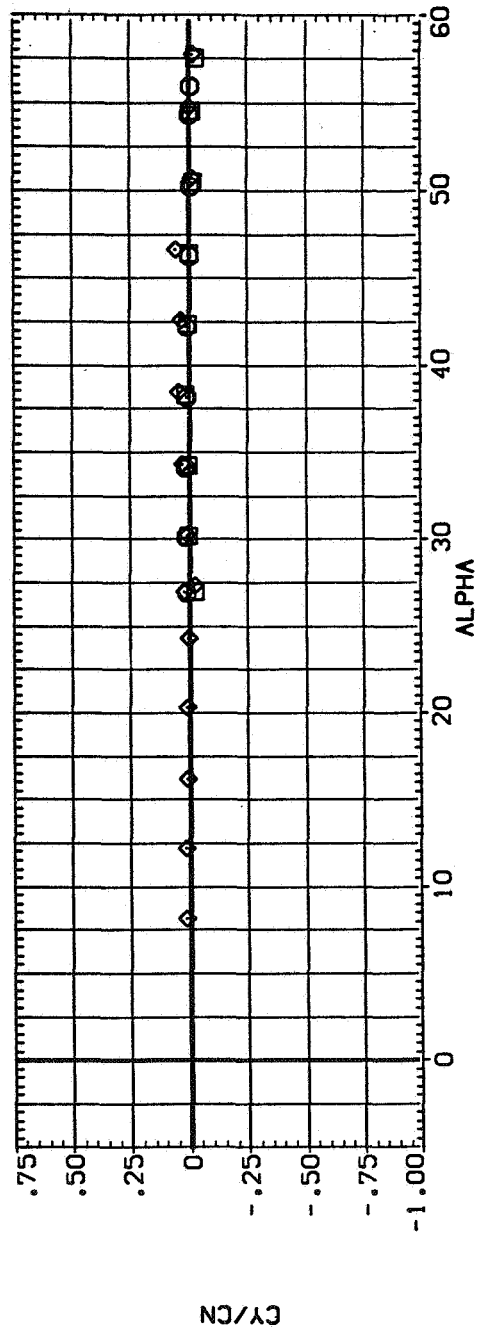


(a) x_{acN}/d and C_N versus α .

Figure 23.— Effect of Reynolds number for $N_1 C_1 S; M = 0.6$.

SYMBOL CONFIGURATION DESCRIPTION
 NI CI S
 NI CI S
 NI CI S

RE 2.200
 4.300
 6.500

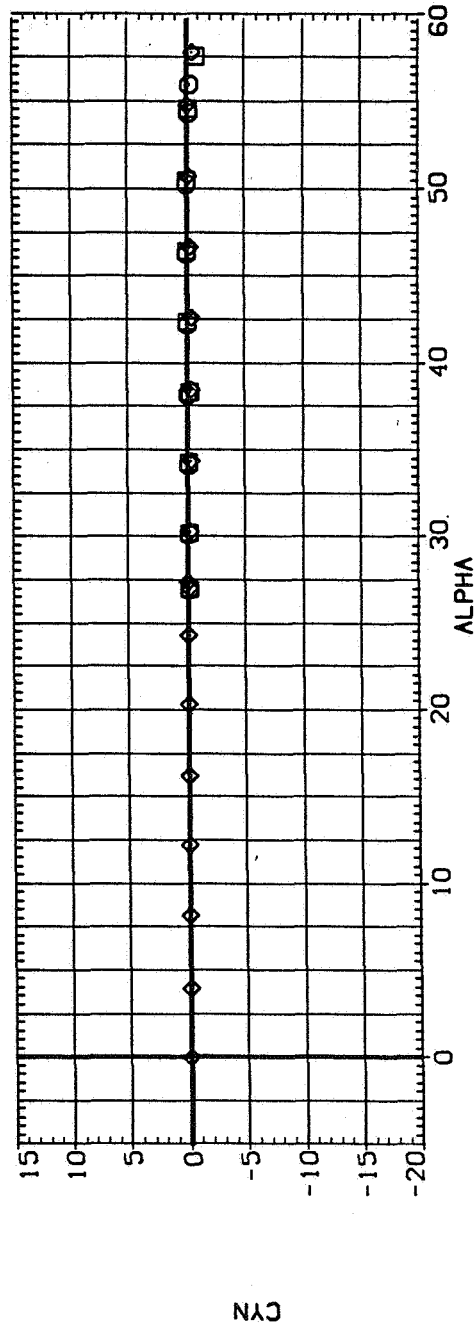
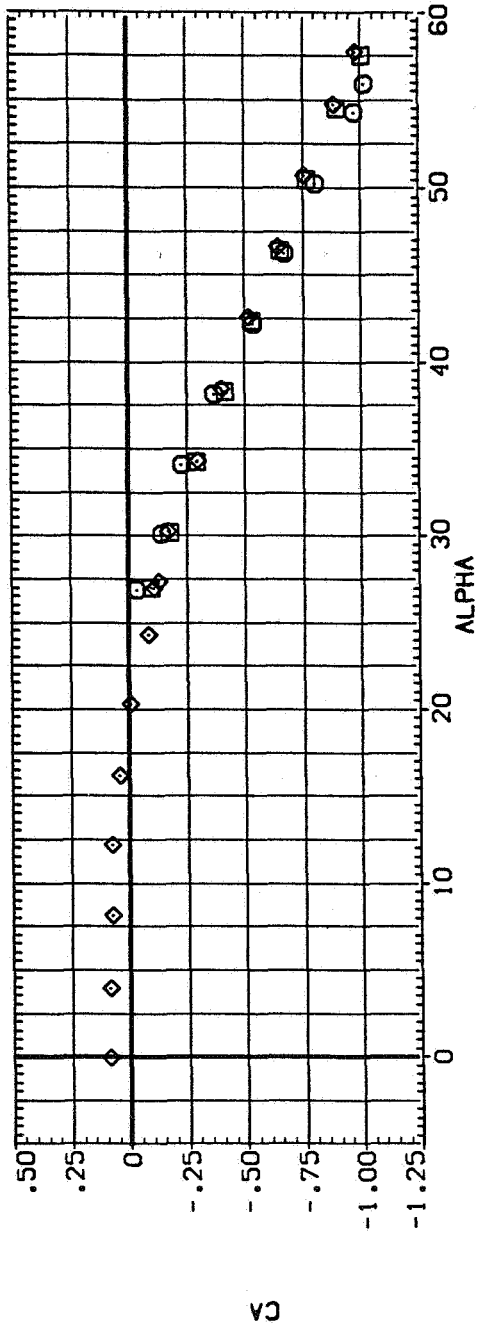


(b) C_Y/C_N and C_Y versus α .

Figure 23. - Continued.

SYMBOL CONFIGURATION DESCRIPTION RE

○	NI CI S	2.200
◊	NI CI S	4.300
◻	NI CI S	6.500



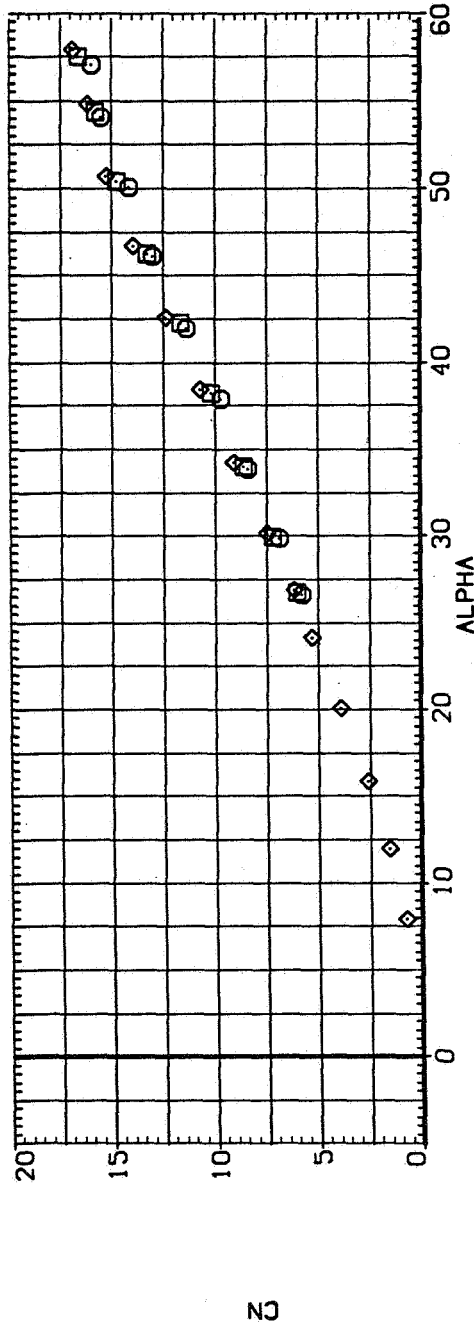
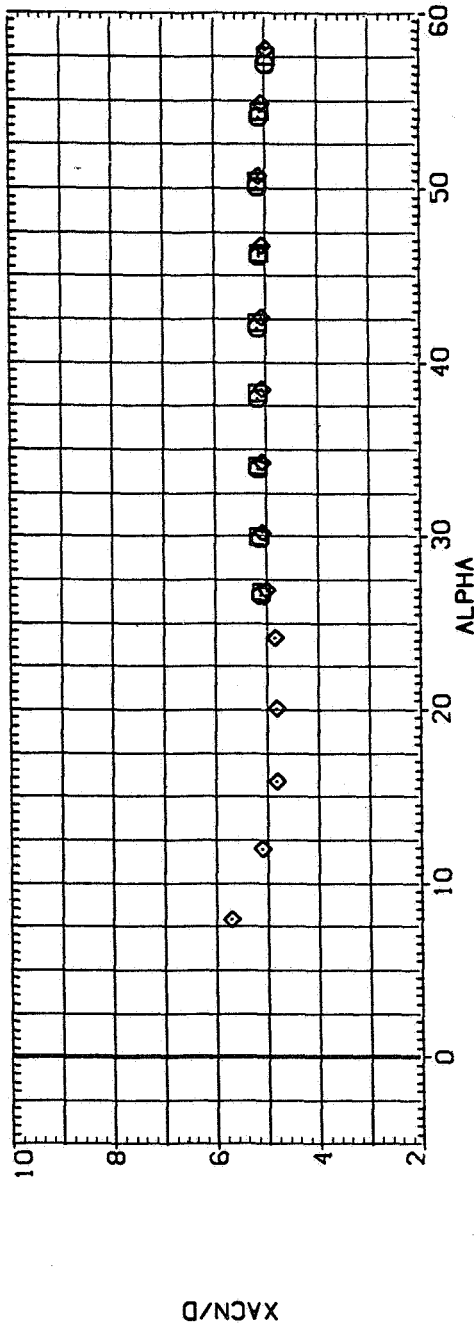
(c) C_A and C_n versus α .

Figure 23.— Concluded.

SYMBOL CONFIGURATION DESCRIPTION

RE 2,200
4,500
6,500

○ NI C1 S
◇ NI C1 S



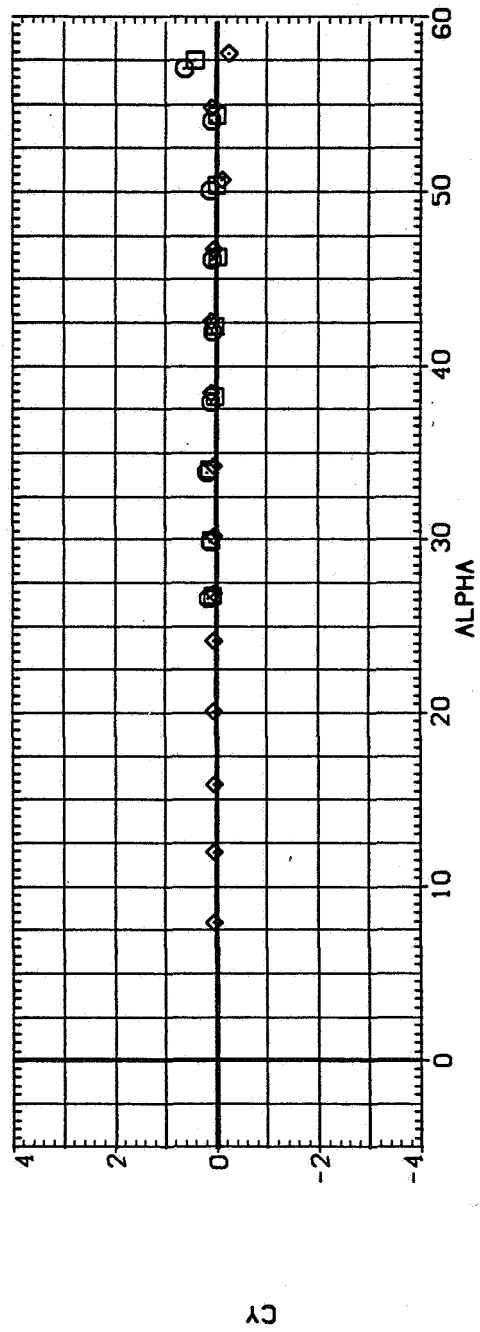
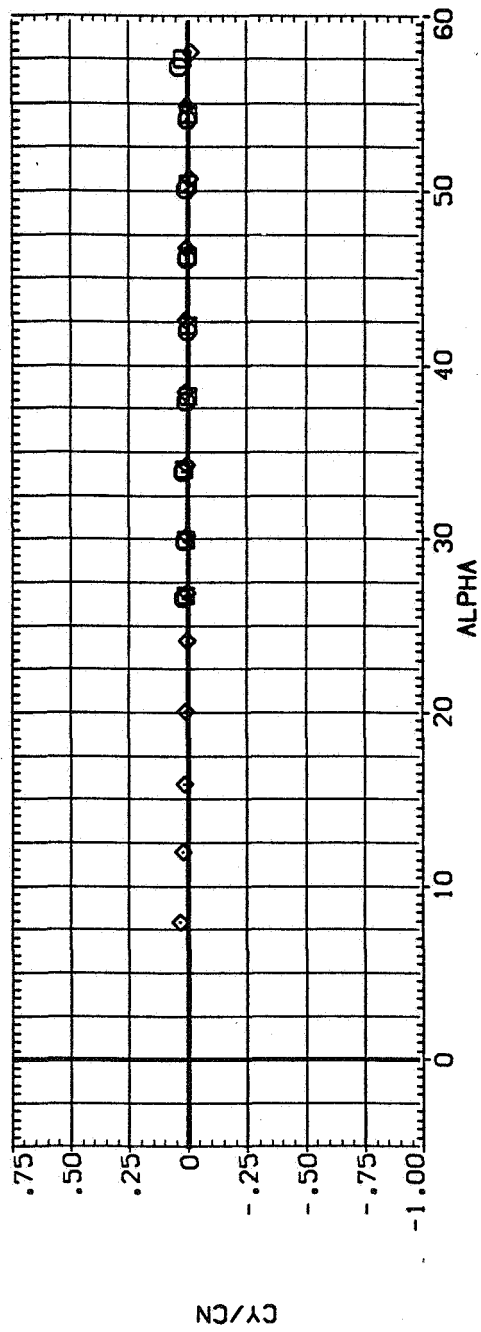
(a) x_{acN}/d and C_N versus α .

Figure 24.— Effect of Reynolds number for $N_1 C_1 S; M = 0.9$.

SYMBOL CONFIGURATION DESCRIPTION

NI CI S
 NI CI S
 NI CI S

RE 2,200
 4,300
 6,500

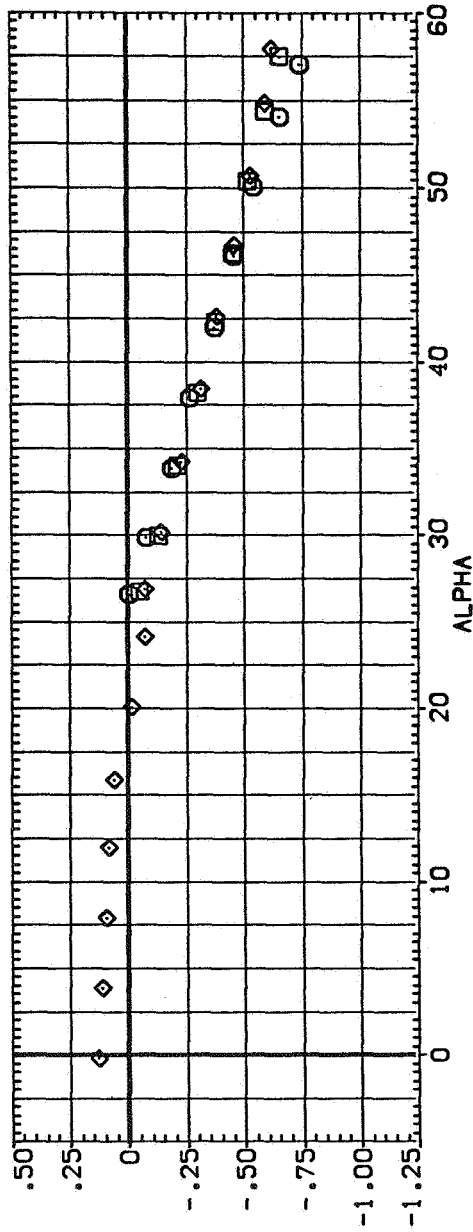


(b) C_Y/C_N and C_Y versus α .

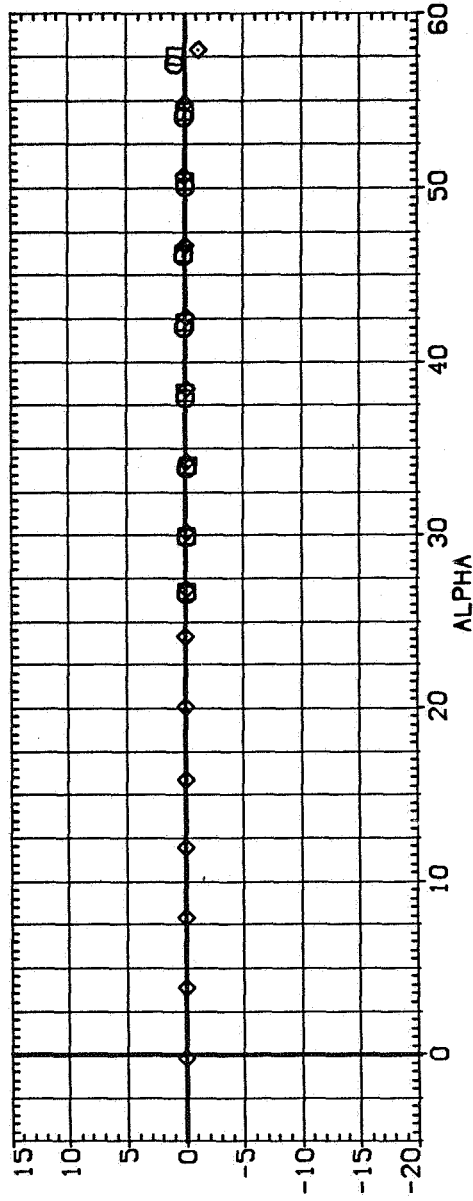
Figure 24.— Continued.

SYMBOL CONFIGURATION DESCRIPTION
 ○ NI Cl₃S
 ◇ NI Cl₂S

RE 2:200
 4:300
 6:500



CA



CYN

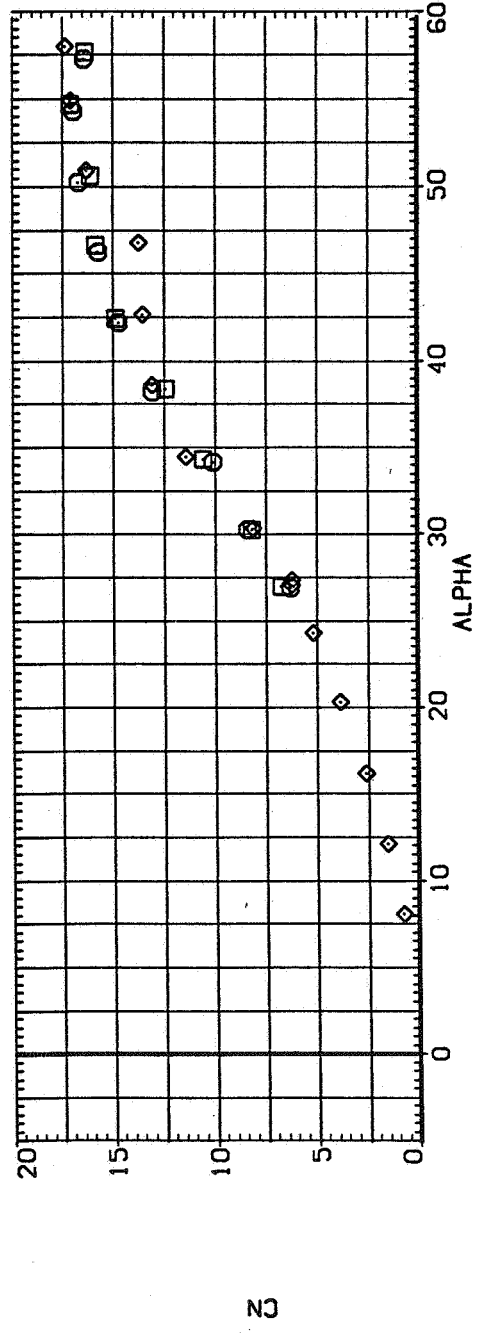
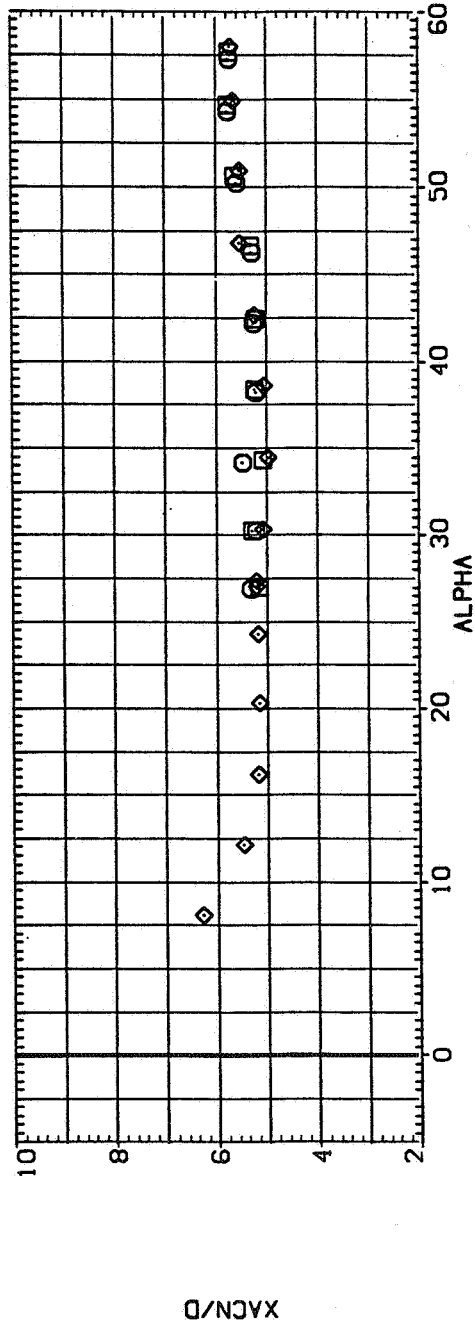
(c) C_A and C_n versus α .

Figure 24.— Concluded.

SYMBOL CONFIGURATION DESCRIPTION

□ N3 C1 S
 ○ N3 C1 S
 ◇ N3 C1 S

RE 2,200
 4,300
 6,500



(a) x_{acN}/d and C_N versus α .

Figure 25.— Effect of Reynolds number for $N_3 C_1 S$; $M = 0.6$.

SYMBOL CONFIGURATION DESCRIPTION

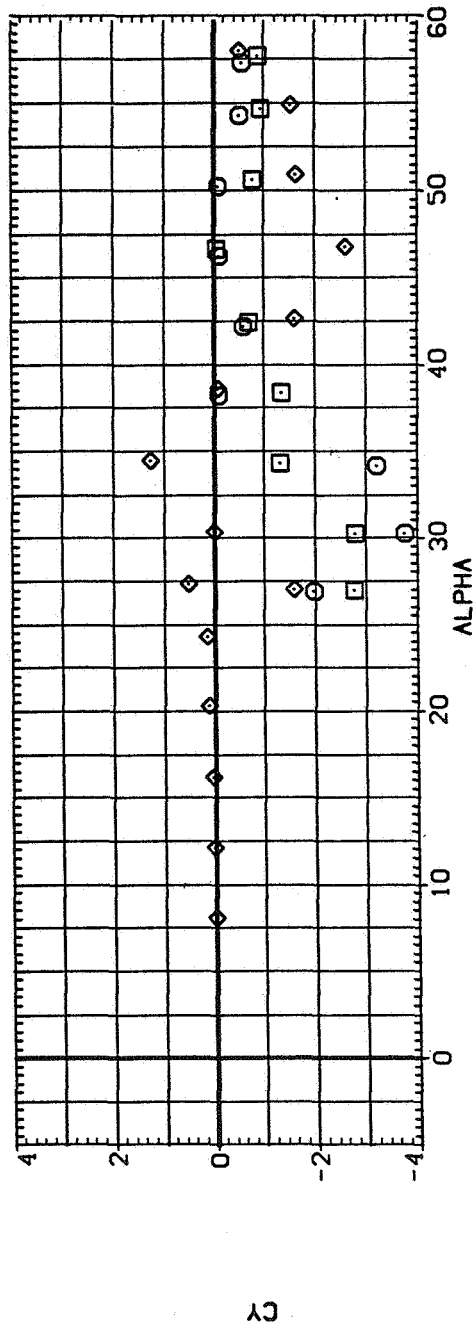
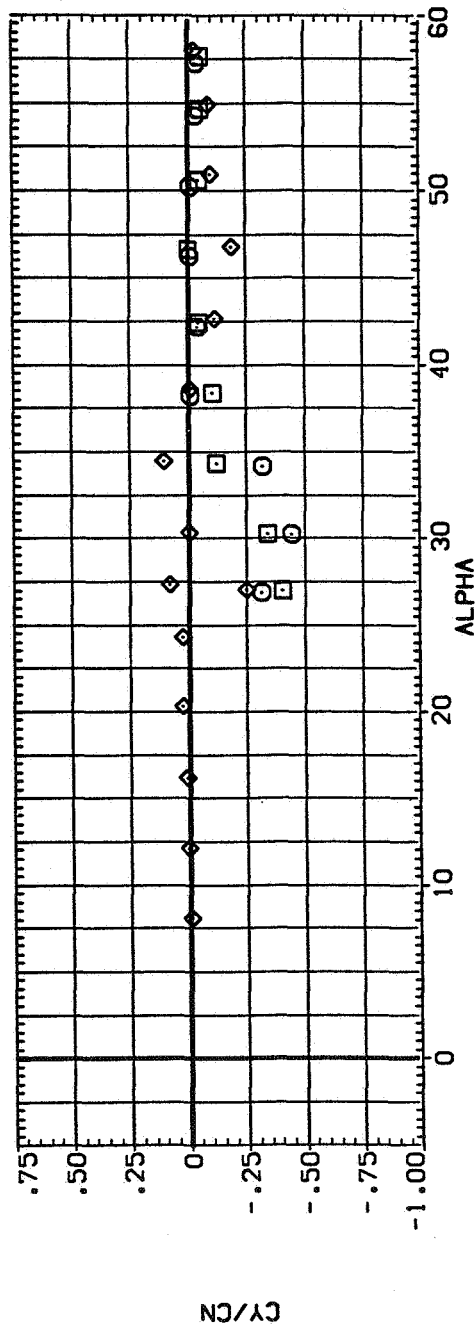
◇

N3 C1 S

N3 C1 S

N3 C1 S

RE 2.200
4.300
6.500



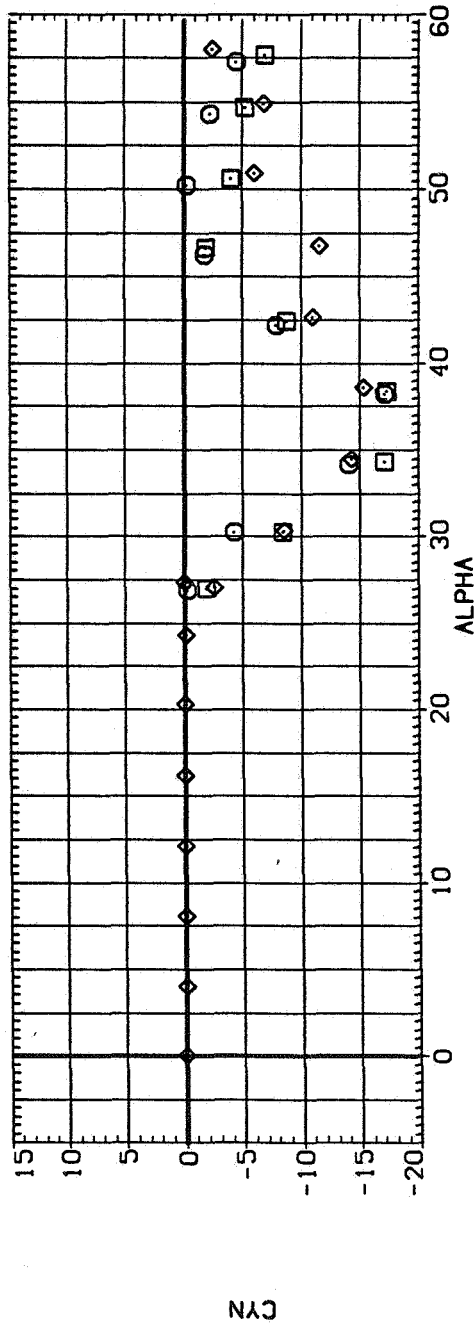
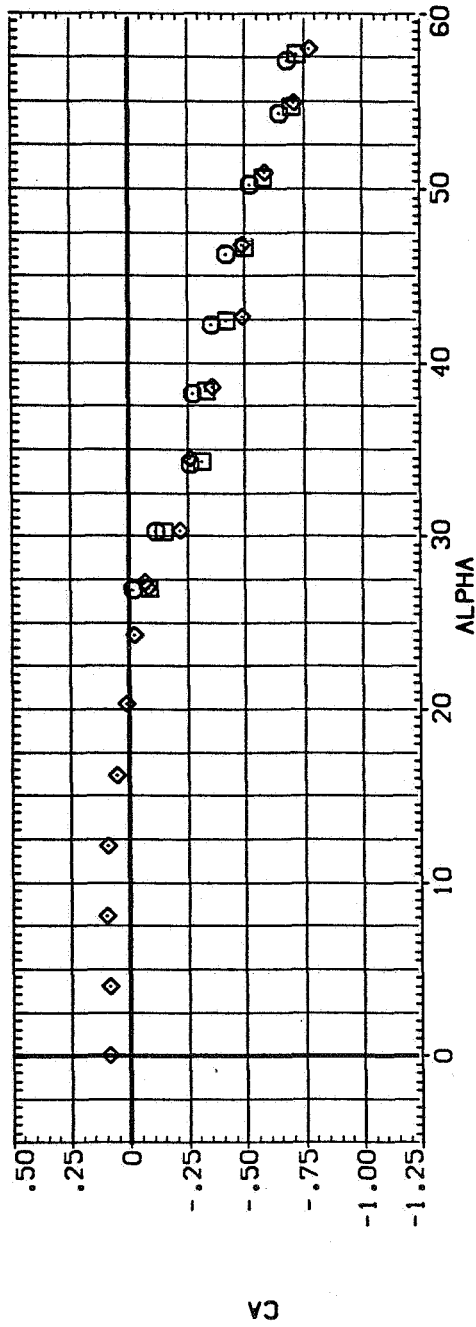
(b) CY/CN and CY versus α .

Figure 25.— Continued.

SYMBOL CONFIGURATION DESCRIPTION

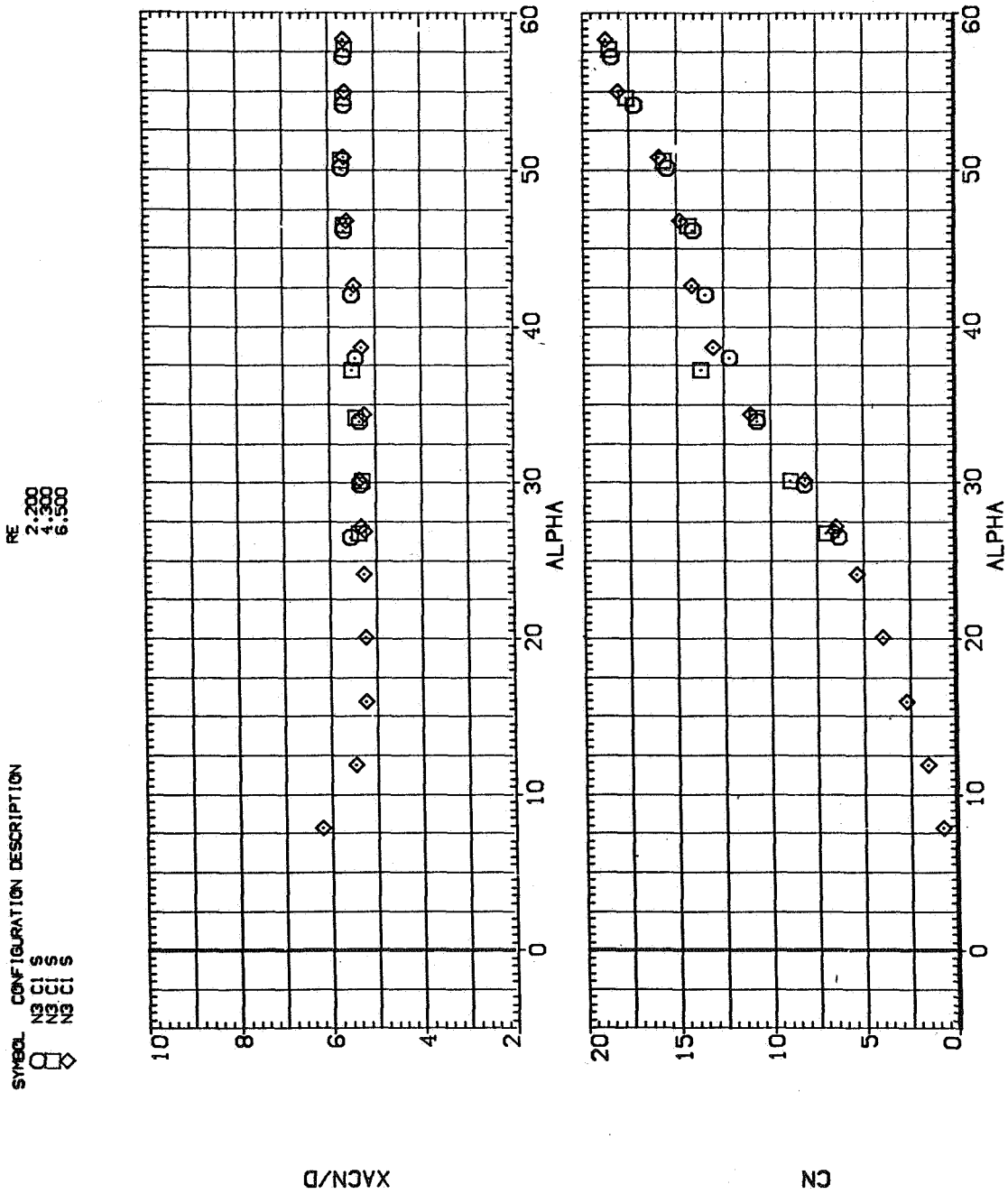
RE
2,200
4,300
6,500

□ □ □ □
○ ○ ○ ○
◇ ◇ ◇ ◇



(c) C_A and C_{η} versus α .

Figure 25.— Concluded.



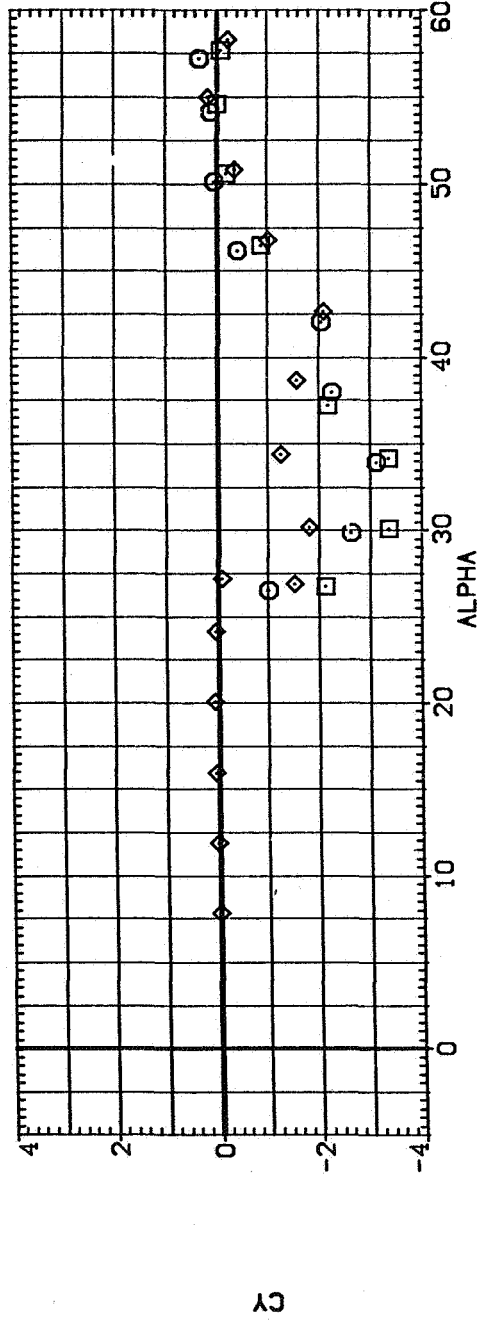
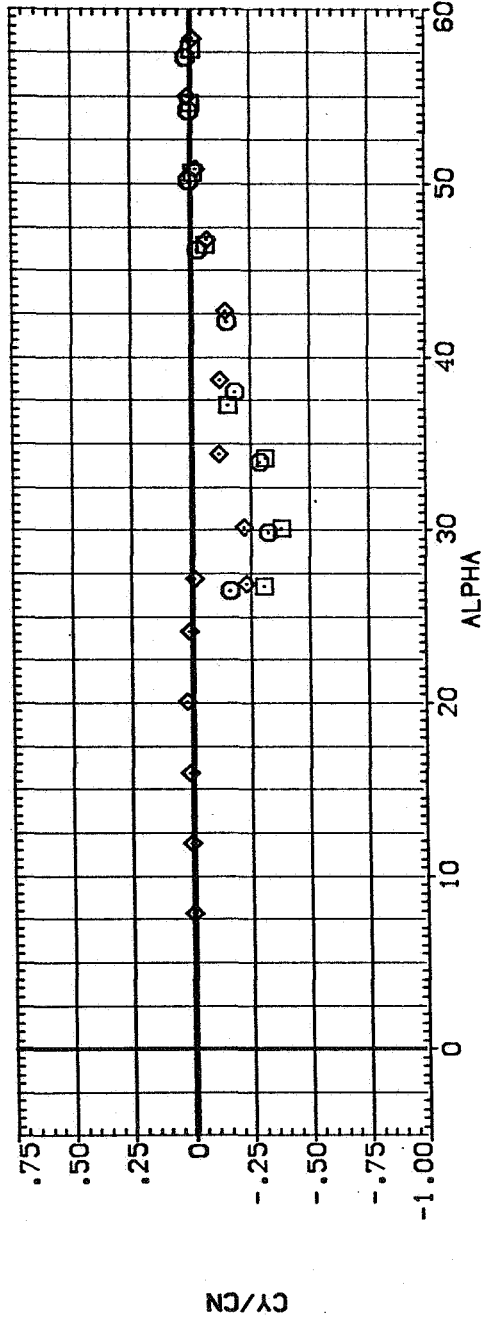
(a) x_{acN}/d and C_N versus α .

Figure 26.— Effect of Reynolds number for $N_3 C_1 S$; $M = 0.9$.

SYMBOL CONFIGURATION DESCRIPTION

RE 2,200
4,300
6,500

□ N3 C1 S
○ N3 C1 S
◇ N3 C1 S



(b) C_Y/C_N and C_Y versus α .

Figure 26. — Continued.

SYMBOL CONFIGURATION DESCRIPTION

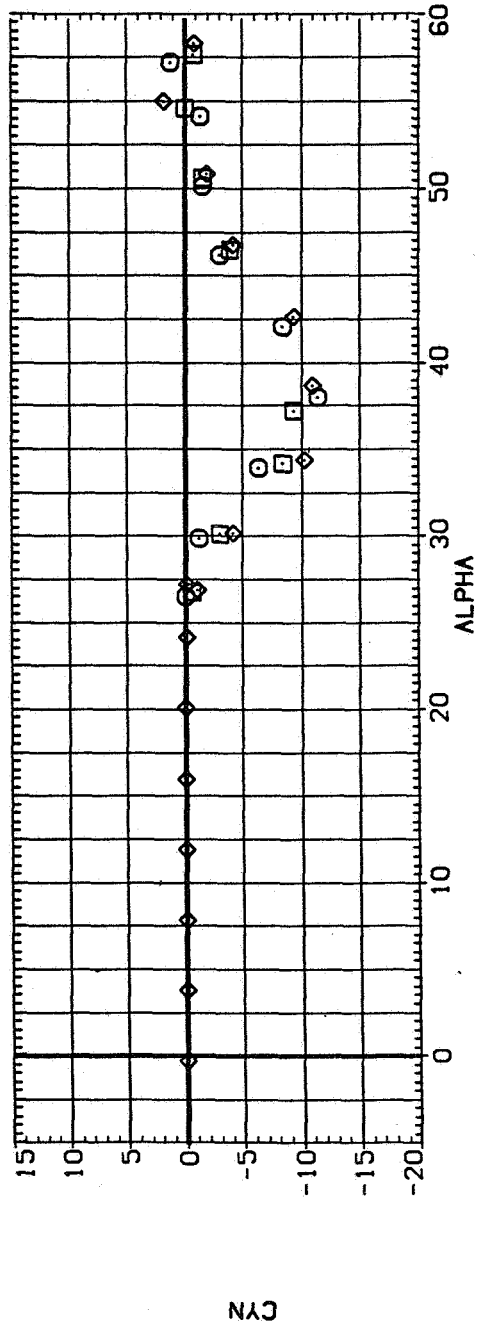
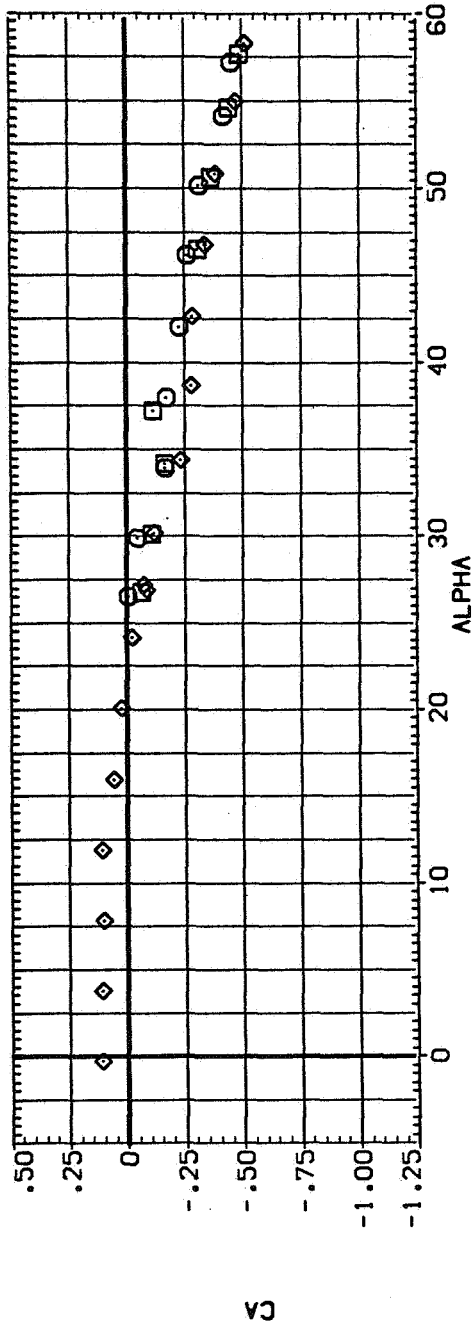
RE 2,200
4,300
6,500

○ □ ◇

N3 C1 S

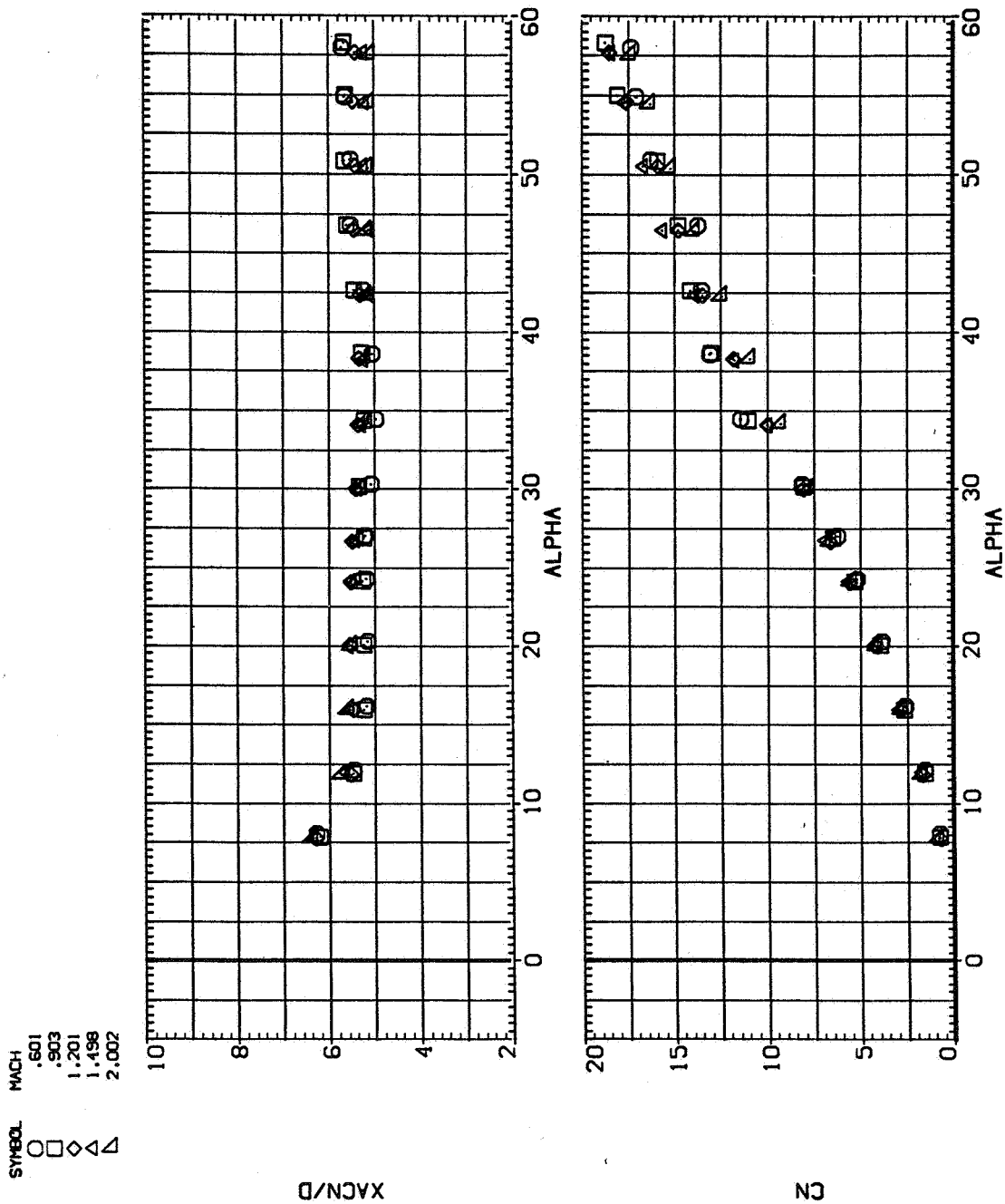
N3 C1 S

N3 C1 S



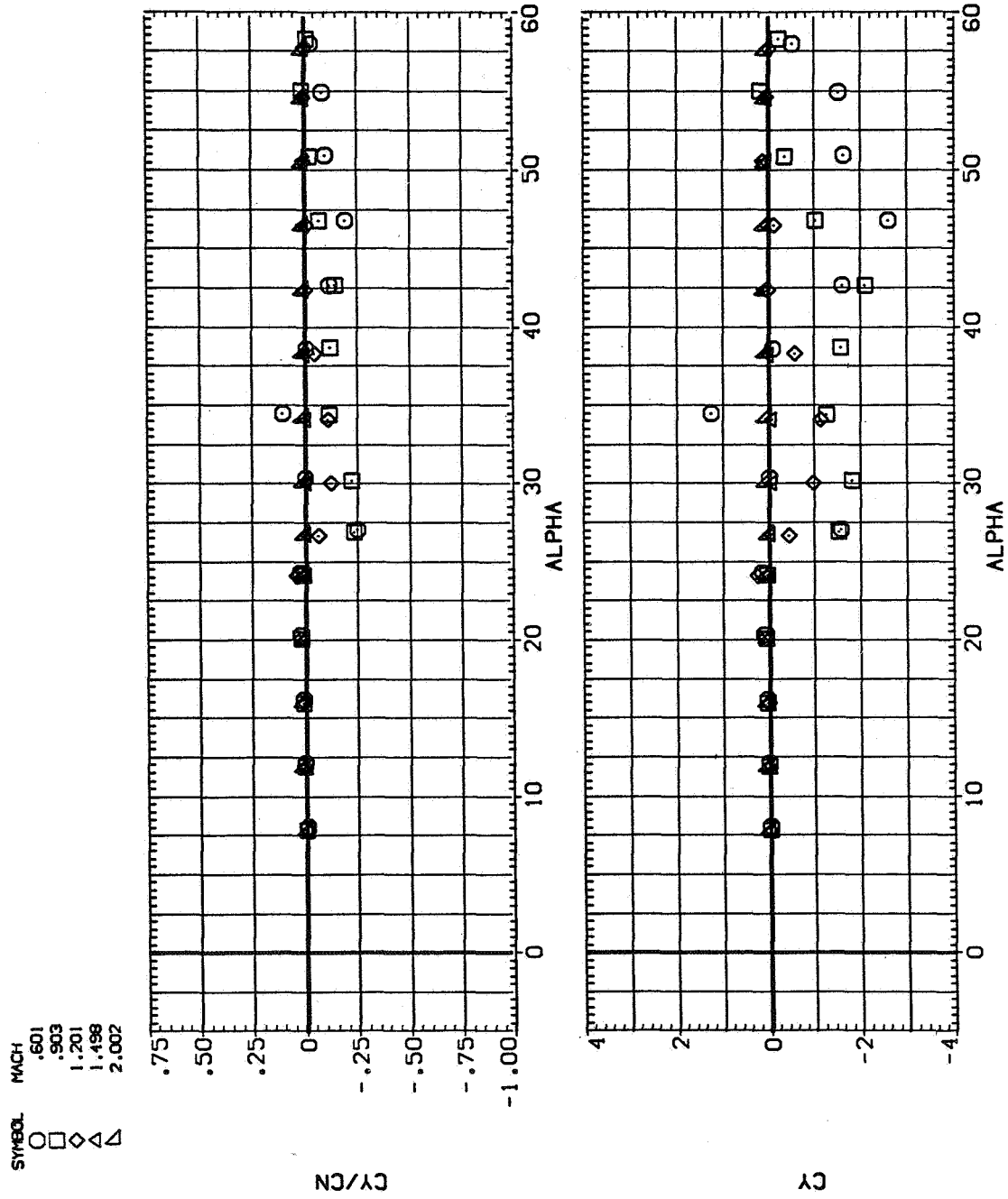
(c) C_A and C_n versus α .

Figure 26. — Concluded.



(a) x_{acN}/d and C_N versus α .

Figure 27.— Effect of Mach number for $N_3 C_1 S$.

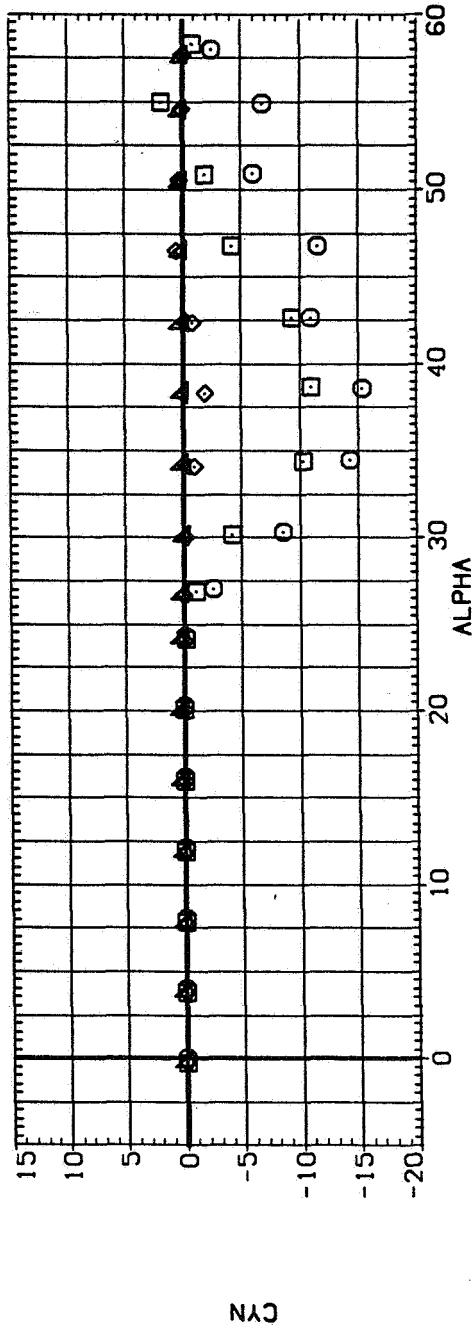
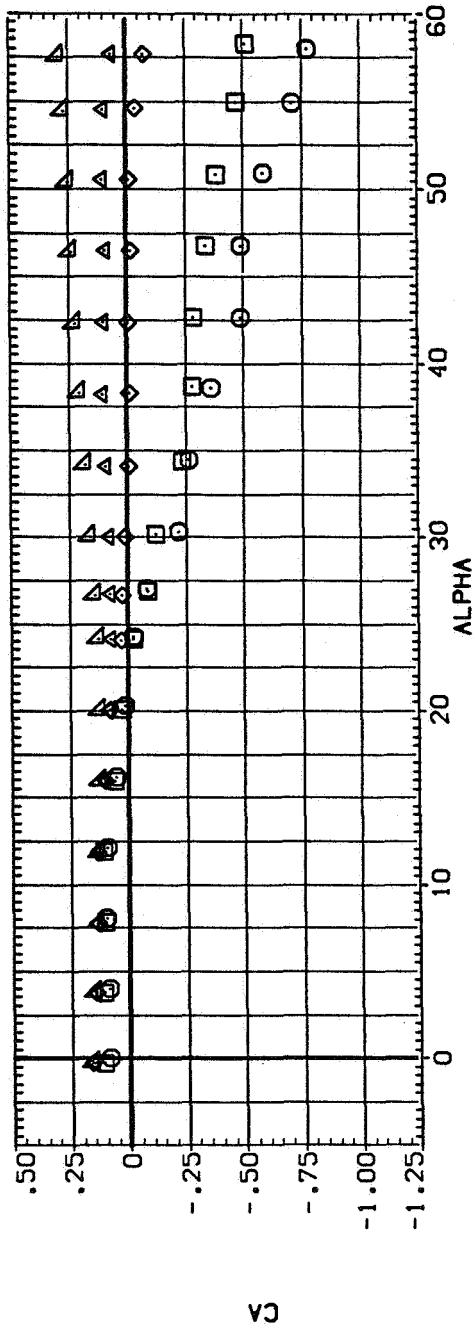


(b) C_Y/C_N and C_Y versus α .

Figure 27.— Continued.

SYMBOL
 ○ □ ◇ △

MACH
 .601
 .903
 1.201
 1.498
 2.002



(c) C_A and C_N versus α .

Figure 27.— Concluded.



POSTMASTER: If Undeliverable (Section 158
Postal Manual) Do Not Return

"The aeronautical and space activities of the United States shall be conducted so as to contribute . . . to the expansion of human knowledge of phenomena in the atmosphere and space. The Administration shall provide for the widest practicable and appropriate dissemination of information concerning its activities and the results thereof."

—NATIONAL AERONAUTICS AND SPACE ACT OF 1958

NASA SCIENTIFIC AND TECHNICAL PUBLICATIONS

TECHNICAL REPORTS: Scientific and technical information considered important, complete, and a lasting contribution to existing knowledge.

TECHNICAL NOTES: Information less broad in scope but nevertheless of importance as a contribution to existing knowledge.

TECHNICAL MEMORANDUMS: Information receiving limited distribution because of preliminary data, security classification, or other reasons. Also includes conference proceedings with either limited or unlimited distribution.

CONTRACTOR REPORTS: Scientific and technical information generated under a NASA contract or grant and considered an important contribution to existing knowledge.

TECHNICAL TRANSLATIONS: Information published in a foreign language considered to merit NASA distribution in English.

SPECIAL PUBLICATIONS: Information derived from or of value to NASA activities. Publications include final reports of major projects, monographs, data compilations, handbooks, sourcebooks, and special bibliographies.

TECHNOLOGY UTILIZATION PUBLICATIONS: Information on technology used by NASA that may be of particular interest in commercial and other non-aerospace applications. Publications include Tech Briefs, Technology Utilization Reports and Technology Surveys.

Details on the availability of these publications may be obtained from:

**SCIENTIFIC AND TECHNICAL INFORMATION OFFICE
NATIONAL AERONAUTICS AND SPACE ADMINISTRATION
Washington, D.C. 20546**